QUANTUM CHAOS IN VIBRATING BILLIARD SYSTEMS

A Dissertation

Presented to the Faculty of the Graduate School

of Cornell University

in Partial Fulfillment of the Requirements for the Degree of

Doctor of Philosophy

by

Mason Alexander Porter

May 2002

QUANTUM CHAOS IN VIBRATING BILLIARD SYSTEMS

Mason Alexander Porter, Ph.D.

Cornell University 2002

The present work examines semiquantum chaos in vibrating quantum billiards, which may be used to explore nonadiabatic behavior in polyatomic molecules. A d-mode Galërkin expansion of a quantum billiard whose boundary has s mechanical degrees-of-freedom is interpreted physically as a molecule with s excited nuclear modes and a d-fold electronic near-degeneracy.

After introducing the problem, we consider in detail the derivation of semiquantum physics from the Born-Oppenheimer approximation, its application to molecular systems, and its relation to vibrating quantum billiards. We also review the notions of quantum chaos and quantum billiards to further connect this dissertation with the literature.

We then formulate the infinite-dimensional problem describing vibrating quantum billiards and consider its symmetries. Using Bloch variables for the quantum-mechanical degrees-of-freedom, we derive equations of motion for finite-dimensional truncations. We consider the cases $d = 1$, $d = 2$, and $d = 3$ in detail. We also analyze the radially vibrating spherical quantum billiard and vibrating rectangular quantum billiard as special cases.

Using an adiabatic action-angle formulation, which we prove to be equivalent to the Bloch formulation, we apply Melnikov's method to examine chaos and a priori unstable Arnold diffusion in this system analytically. We also study the relative facility of chaotic onset of the classical and quantum-mechanical degrees-of-freedom when perturbing from an integrable configuration.

Finally, we summarize the present work and conclude with a discussion of future

research concerning vibrating quantum billiards, other semiquantum systems, and other areas of quantum chaos and Hamiltonian dynamics.

BIOGRAPHICAL SKETCH

Nothing defines humans better than their willingness to do irrational things in the pursuit of phenomenally unlikely payoffs. This is the principle behind lotteries, dating, and religion.

— Scott Adams

If you laugh at yourself often enough, you might make the world think you understand its private joke.

— Mason Porter

When you come to a fork in the road, take it.

— Yogi Berra

Mason Porter was born February 10, 1976 in Los Angeles, California. He has an older brother (Adam), a younger sister (Tammy), and several wonderful stuffed animals. His father (Samuel) practices obstectrics and gynecology; his mother (Judith) helps his father and has a few projects of her own. Mason graduated from Temple Emmanuel Nursery School in 1981, Hawthorne Elementary School in 1990, and Beverly Hills High School in 1994. (He was the Salutatorian of his class at Beverly High.)

In 1994, Mason enrolled at Caltech, where he was soon initiated as a member of Lloyd House. His activities at "Tech" included one year as co-editor of Caltech's weekly newspaper (*The California Tech*), four years as a writer for this newspaper, and two years as co-editor of Caltech's literary magazine (*The Totem*). Mason's misadventures with the school newspaper legendary. Additionally, he was jokingly named "Terrorist of the Week" by *The California Tech* during final's week of his senior year for his crimes against humanity and baseball. He is justafiably proud of this accomplishment.

Mason's escapades, a few of which will be mentioned in passing, were not limited to his involvement with *The Tech*. (As you may have already guessed, Mason was a fairly stereotypical Techer.) He played a minor role in a few pranks, including organizing the infamous junior Lloydie Ditch Day prank that was a complete flop. He also participated in three Lloyd movies and played an instrumental role in several Airband skits. He hosted a radio show on Lloyd radio, specializing in 80's music. As part of his radio show, Mason held several "All Cynical and Depressing Song Specials"–including one on Valentine's Day 1998 that began with "Black Celebration" and ended with "Blow Your Brains Out" (or whatever that song is actually called). Mason and his primary group of friends, now known collectively as "The Usual Bastards," constructed a stack for Ditch Day, perhaps Caltech's most precious tradition. Their theme was The Pink Panther, and Mason had the opportunity to play Inspector Clouseau. While at Caltech, The Usual Bastards logged myriad hours playing Mario Kart and frequented Carrow's for late-night dinners. Additionally, Mason was an enthusiastic participant in playing "The Ride of the Valkyries" (followed by "Ride Chasers") at 7 am every day of every finals week.

As a member (and UCC for two thirds of the year) of Kaos Alley his Senior year, he instituted table takeover night. (Valhalla was the primary target.) He helped synergize the Kaos residents' natural obnoxiousness by encouraging them to exhaust the dinner supply of chocolate milk. He also helped start a couple traditions without trying to do so. (He thought other things were more memorable, but these are the ones that are probably going to survive the longest.) Nevertheless, Mason will perhaps be remembered best by his fellow Lloydies for overplaying the song "Tarzan Boy" beyond acceptability.

Despite his misadventures at Caltech, Mason was an extremely dilligent stu-

dent. As a sophomore, he won Caltech's Zeigler award for math and applied math majors. The next year, he was awarded Caltech's Bell prize for mathematics research in recognition for his work under Jerrold Marsden. He won Caltech merit awards during both his Junior and Senior years and was nominated for Caltech's Froehlich award during his Junior year. He also served two years as a teacher's assistant in the math department. In June 1998, Mason earned his Bachelors of Science degree (with Honors) in Applied Mathematics with one of the top GPAs in that year's graduating class. Mason was also recognized at Caltech for his literary skill.

Armed with a Department of Defense (NDSEG) fellowship, Mason enrolled in Cornell University's Center for Applied Mathematics in August 1998. He soon started working for Richard Liboff on some problems in quantum chaos. The story of Mason's fascination with nonlinear dynamics and chaos is an interesting one. He first heard about fractals at Beverly High and wanted to find out more about them because of the beautiful pictures associated with them. These pictures, moreover, reminded him of the myriad doodles he used to produce as a child (which consisted mostly of fractal-like structures) as well as the intricate patterns he had occasionally seen while afflicted with migraine headaches. At Caltech, he had the opportunity to learn more about fractals and chaos throughout coursework, research, and independent reading. During this process, he somehow became more interested in continuous systems rather than discrete ones. He was particularly intrigued by how one could use nonlinear dynamics to model and explain natural (and man-made) phenomena. He chose to study quantum chaos for his dissertation because he wanted to discover how chaos manifested in the quantum regime. A devout pool player, Mason elected to use billiard systems to explore quantum chaos.

Still just 26, Mason has already presented his research (in the form of short talks and posters) at several international conferences. Two of his research articles constituted the cover story of the September 2001 issue of *International Journal of Bifurcation and Chaos*. Additionally, the November-December 2001 issue of *American Scientist* highlights one of his popular science articles as its cover story. Mason co-authored all three of these articles with Richard Liboff, his thesis advisor. Mason was one of three recipients of SIAM's 2001 Student Paper Prize. Additionally, he is a contributing editor for *Complexity Digest*, an online newsletter concerning complex systems.

Mason's interests outside academics are quite diverse. He is an avid baseball fan–he roots for the Los Angeles Dodgers as loudly and often as possible. He also enjoys Dungeons and Dragons (and other role-playing games), ping pong, pool, creative writing, fantasy novels, video games, ultimate frisbee, witticisms, satire, and myriad board games. He also enjoys booting his friends in the head.

Mason's future may not be so bright that he has to wear shades, but it isn't exactly murky either. At the very least, there is now a light at the end of the tunnel. Beginning August 2002, Mason will be a Visiting Assistant Professor of Mathematics and a Research Associate Member of the Center for Nonlinear Science (which is run by the School of Physics) at Georgia Institute of Technology. He will also be in residence at MSRI for their program on semiclassical analysis during the Spring 2003 semester.

Mason has promised to continue his misadventures and remain someone who is distinctive and easily-remembered (even if not always fondly so). Meanwhile, he plans to go outside and frolic.

To my friends, who have always been able to figure out when to boot me in the head. Honorable mention goes to the Los Angeles Dodgers.

ACKNOWLEDGEMENTS

Friends are those into whose souls you've looked, and therein glimpsed a oneness with yourself. They are a part of you, and you are a part of them. They own a piece of you.

— Harlan Ellison

Middle age is when you've met so many people that every new person you meet reminds you of someone else.

— Ogden Nash

Unfortunately, I cannot say that I enjoyed my four (academic) years at Cornell as I did my time at Caltech (which is a truly special place). I do not regret electing to come here for my Ph.D., as the academic environment proved to be an excellent fit for me. Nevertheless, most other facets of my life in Ithaca were quite disappointing.

On a more positive note, I would like to take this opportunity to ackowledge people who played a part in making my studies and my life more bearable. I suppose I am required to mention my family–especially my parents, without whom I would not have been born. Obviously, that event had a big impact on my life.

My advisor, Richard Liboff, was my primary collaborator. We worked together on numerous projects, and I think we made a pretty good team. Richard also wrote tons of letters of recommendation, for which I am indebted. Furthermore, he was far more accesible than I imagine is the case of most professors. He was often available even when I dropped by his office unnanounced (with some questions or yet another manuscript for him to read) and knocked on his door.

The other three members of my thesis committee (Greg Ezra, John Guckenheimer, and Steve Strogatz) have also been extraordinarily helpful. Greg Ezra

assisted my attempts to learn appropriate concepts from theoretical chemistry and read several drafts of my papers, providing useful advice and criticisms. He also guided me through the chemical physics literature and wrote nearly as many letters of recommendation as my advisor. John Guckenheimer was an invaluable source for answers to conceptual questions on nonlinear dynamics, guidance through the dynamical systems literature, assistance with DSTool when the program died on me, and two or three kicks-in-the-butt and wake-up calls that motivated me to work harder on certain aspects of my research. Steve Strogatz also provided reminders to make sure that my research was sufficiently connected with applications, as my work does tend to align itself with theoretical physics at least as much as applied math. (The advice he and John gave me led me to seek out Greg Ezra in order to learn some of the chemistry relevant to my research.) Additionally, Professor Strogatz supported and encouraged me when I founded CAM's Mathematical Sciences Graduate Student Seminar Series. He too wrote myriad letters of recommendation in support of my candidacy for various positions and fellowships.

Several other professors (from both Cornell and other institutions) have also been quite helpful. Carlos Castillo-Chavez wrote several letters of recommendations for me and was very encouraging. He and Steve Wirkus helped ease me into my role as a teacher's assistant in the MTBI program. They also helped me organize a minisymposium for the 2002 SIAM Annual Meeting, and Steve Wirkus also helped out when I had some thesis-related questions. Richard Rand provided encouragement and met with me a few times to discuss topics related to my research and job hunt. Paul Steen read several drafts of an early version of the component of my thesis devoted to bifurcation analysis, as that was my project in a course (ChE 753) he taught. Jerry Marsden answered conceptual questions by e-mail on a couple occasions and was one of my primary academic mentors during my

undergraduacy at Caltech. (He also wrote tons of letters of recommendation for me during that stage of my career.) Gottfried Mayer-Kress was a collaborator on a short paper about complex systems and whale culture and has been my editor at *Complexity Digest*. The members of the editorial team at *American Scientist* (especially Dave Schneider, Rosaline Reid, and Mike May) were extraordinarily patient and helpful during the production of my popular science article. Other people who helped me in some manner with my research the past few years–whether in person or via e-mail–include Sir Michael Berry, Eberhard Bodenschatz, Phil Boyland, Piet Brouwer, Alan Champneys, Greg Colyer, George Haller, Mark Levi, Paul McEuen, Ricardo Oliva, Donald Saari, and Bobby Schnabel. Tim Healey, my temporary advisor, gave me useful advice when I first got to Cornell as well as during my job hunt, and Richard Murray gave me useful advice when I was trying to decide where to go to graduate school. (It is interesting to be accepted into a program and simultaneously be advised by its head–not to mention others among its faculty–that I should go somewhere else for my own good.) Alhough not involved with my research, Joel Burdick and the inimitable Joel Franklin were two of my favorite professors at Caltech because of the time they were willing to commit to their students. Finally, Jane Wortman, one of my math teachers from Beverly Hills High School, sometimes let me divert my attention from her teaching in class so that I could instead work on things that were conceptually more challenging (like trying to figure out why a method for constructing parallel lines that I had inadvertently discovered during an exam my freshman year because I had forgotten the method we were taught was actually valid). Permitting such lapses of attention rather than holding me back–as most of my other high school teachers would have done–was greatly appreciated.

There are also numerous scientists upon whose work I have attempted to build.

I will not mention them here, as their identities are easy to determine by glancing at my bibliography and some of the names in the body of the thesis. (That's right; you'll have to read something other than the ackowledgements if you want to know this.) In the words of several famous mathematicians, this is left as an exercise for the reader. (Trust me; it's trivial.)

The first three years of my graduate studies were sponsored by an NDSEG (Department of Defense) fellowship. However, I don't think there's any danger of my dissertation research being for military purposes–despite any latent violent tendencies I may or may not have. It is deliciously ironic, however, that a couple of the scientists to whom I alluded in the preceeding paragraph were intimately involved in the establishment of nuclear-weapons technology.

I am also indebted to the people whose efforts make it possible for CAM to function on a daily basis. Eric Phipps and Jason Martin were excellent system administrators. Adrian Mariano taught me how to play Go and provided help with LaTeX and other computer issues on numerous occasions. Steve Vavasis, Steve Strogatz, and Terry Fine held the post of Director of Graduate Studies during my reign in CAM. Rini Bhattacharya, whose name I would never be able to spell without looking it up, and Stefanie Koch helped me advertise the seminar series I ran. Ellie Swartwood continually cleaned up after everybody in CAM until she retired. Dolores Pendell was CAM's überadministrator. In addition to ensuring that everything ran smoothly, she was the person to ask if one needed to be pointed in the proper direction to get something done.

There are several friends from my Cornell days (daze?) whom I'd like to thank for their role in preserving (what's left of) my sanity. Bill Dirks played games with me on several occasions. Kate Jenkins was also around for games, ice cream, and occasional attempts to cheer me up. Bill and Kate also get bonus points for having

the honor of listening to me rant (or reading my rants when they came by e-mail) more often than anyone else. Debra Goldberg was also witness to a number of my rants and provided help on a number of things. (She gave me access to her thesis documents, which is much appreciated.) Aaron Deever and Jesus Rodriguez were (and continue to be) the recipients of many of my baseball-related rants (of which there will always be many). Jason Martin was a worthy chess partner, though we both need to work on our concentration lapses. I played ultimate frisbee and Dungeons and Dragons with Varis Carey. Sean Carver went to several movies and plays with me, Prashant Mehta was around for discussions on academic subjects, and I remember a few really interesting philosophical coversations with Joel Ariaratnam. Prashant and Joel also provided encouragement while I was spazzing out during the couple weeks leading up to my thesis, and the former read and provided useful comments concerning Chapter 2 of version 1.xx of my thesis. Moreover, Prashtant, Joel, and Steve Wirkus read and commented on portions of some of the drafts of version 2.0 of my thesis. Friends outside of CAM included Eric Hwang (with whom I went to a lot of movies), Mike Winston (a fellow Beverly High alum), Leslie Ng (one of those crazy TAM people), Connie Chang (who spent a couple years at Caltech but whom I didn't meet until I came to Cornell) and Annie Lee (a token undergraduate). I mooched countless rides from several of the people I've mentioned in this paragraph. Some other people at Cornell were nice to me as well.

Although I have some friends at Cornell, my closest friends entered my life before I relocated to the barren wastelands of Ithaca, NY. My best friend since perhaps age 4 is Danny Schwarzblatt, with whom I attended nursery school (for one of my two years), elementary school, and high school. My primary partners-in-crime from Caltech are Kin Chan, Prista Charuworn, Jit Kee Chin, Vito Dai,

Mou Li, Brian Limketkai, Vincent Lin, Julius Su, Matt Sullivan, Steve Van Hooser, Louis Wang, and Ben Williamson. We had lots of good times there, have had some good times since, and will hopefully have additional ones in the future. Through phone calls, e-mails, and online chats, these punks continue to make my life better. Other noteworthy souls from Caltech (most of whom are from Lloyd but some of whom are not) include Jeremy Boulton, Larry Chen, Robert Chen, Daniel Chou, Brian D'Urso, Vicky D'Urso, Tim Elling, Nelson Escobar, Anatole Faykin, Greg Fricke, Steve Ginzburg, Travis Hime, Maria Huang, Bob Keeney, Melvin Leok, Jimmy Lin, Megan Linnehan, Tom Maccarone, Nishith Mahanty, Dan Marrone, Reza Mohsin, Aaron Oei, Michael Ontiveros, Alejandro Ortega, Mohammed Rizvi, Joe Schaeffer, Chuck Smith, Varun Tansuwan, and Gary Wu. Being part of Lloyd House at Caltech was mostly a good experience, so those Lloydies whom I have not already mentioned deserve to be acknowledged as well. I've also met some nice people with whom I did not overlap in Lloyd during my many visits as an alum. A few other friends from Hawthorne and/or Beverly High I'd like to acknowledge are Arash Ashourzadeh, Matt Brooks, Anat Caspi, Angela Chang, Belinda Chang, Amir Kashani, Arash Lalezary, Doug Rosen, Greg Stolerman, Julia Wang, and Amir Zarrinpar.

This dissertation was completed without assistance or inspiration from any deities, as no such beings exist.

TABLE OF CONTENTS

CHAPTER 1

INTRODUCTION

1.1 Statement of the Problem

Vibrating quantum billiards describe the wavefunctions associated with a quantum-mechanical particle (of mass m_0) confined in a time-dependent domain $D \subset X$, where (X, g) is a finite-dimensional Riemannian manifold with metric g.[159] This particle collides elastically against the boundary ∂D, which has mass $M \gg m_0$.

A vibrating quantum billiard is described mathematically using the Schrödinger equation,

$$i\hbar \frac{\partial \psi(\mathbf{x}, t)}{\partial t} = \hat{H}\psi(\mathbf{x}, t), \quad (\mathbf{x}, t) \in D \times \mathbb{R}, \tag{1.1}$$

with homogeneous Dirichlet boundary conditions on the boundary ∂D (so ψ vanishes when $\mathbf{x} \in \partial D$).[112, 158–160] The Hamiltonian operator $\hat{H}$ is given by

$$\hat{H} = \hat{K} + V(\mathbf{a}(t), t), \tag{1.2}$$

where V is an external potential, $\mathbf{a}(t) \in \mathbb{R}^s$ describes the (a priori unknown) time-dependence of ∂D and

$$\hat{K} = -\frac{\hbar^2}{2m_0}\nabla \tag{1.3}$$

is the kinetic energy of the confined particle.

This thesis is concerned with the special case in which

$$V(\mathbf{a}(t), t) = V(\mathbf{a}(t)), \tag{1.4}$$

so that V does not depend explicitly on time. As we shall discuss, this allows the mathematical problem of interest to be connected with important problems in atomic and molecular physics.[23, 137, 154, 156] This includes Jahn-Teller distortions[19, 20, 126, 189, 202] and the manifestation of such distortions in nanomechanical devices,[90, 98, 145, 185, 190] as well as the dynamics of atoms in a resonant cavity,[11] collective nuclear motion,[25] hadrons,[10] spin-particle interactions,[5] and solvated electrons.[179, 180] Of particular interest to us is the connection of vibrating quantum billiards to nonadiabatic dynamics in polyatomic molecules and its relation to Jahn-Teller theory.

In the literature concerning quantum systems with time-dependent potentials, it is more common to consider problems described by the special case

$$V(\mathbf{a}(t), t) = V(t), \tag{1.5}$$

for which different mathematical techniques are required.[4, 6, 23, 24, 27, 29, 70, 71, 114, 141, 160, 176] In particular, this latter situation is ordinarly studied in the semiclassical or high quantum-number regimes,[23, 70, 112, 159] but molecular data indicate that even low-lying states can behave chaotically.[189] The problem studied in this thesis addresses such situations.

1.2 Main Results

The primary results of this thesis are as follows:

a. The full vibrating quantum billiard problem described in the previous section has a Hamiltonian structure and is well-posed provided an initial wavefunction $\psi(\mathbf{x}(0), 0)$, an initial boundary $\mathbf{a}(0)$, and the initial momentum of the boundary $\mathbf{P}(0)$ are all specified.[160] Any d-dimensional Galërkin truncation of this problem (where d is finite) is likewise well-posed provided the same initial data is specified. Such truncations also have a Hamiltonian structure.

b. If $\mathbf{a} \in \mathbb{R}^s$, then a d-mode Galërkin expansion of $\psi(\mathbf{a}(\mathbf{t}), \mathbf{t})$ describes the wavefunction of a polyatomic molecule with s excited nuclear modes (yielding s classical degrees-of-freedom) and a d-fold electronic near-degeneracy (yielding $d-1$ quantum-mechanical degrees-of-freedom). The potential $V(\mathbf{a}(t))$ describes the stiffness of the spring used to model the intramolecular bonds. The physical problem of interest is related to Jahn-Teller distortions.[154, 160] For the case $s = 1$, the examples $d = 1$, $d = 2$, and $d = 3$ are extensively studied numerically.[112, 155, 158–160]

c. When $s = 1$, every equilibrium configuration corresponds to a *pure state*, in which a single eigenstate is present. (This is exactly what one would expect physically.) Each equilibrium is elliptic (and hence stable) provided $E \equiv V + K$ has exactly one minimum with respect to a at that point. Using this result, which is derived in Chapter 5 and illustrated in subsequent chapters, one may draw an analogy between molecular systems and quantum field-theoretic ones. The similarity between some systems in quantum field theory and molecular physics has been hinted by some authors but not explored in detail.[20]

d. When $s = 1$ and $d = 1$, saddle-center bifurcations can occur for potentials $V(a)$ with at least two local minima.[155] This is illustrated in particular for the "Landau transition" case in which $V(a)$ is a quartic, double-well potential. Such bifurcations cannot occur if $V(a)$ has a single minimum. (This result expands on the analogy discussed in (c).)

e. Suppose the Schrödinger equation (1.1) is globally separable in D and that D is convex and r-dimensional. Let $s = 1$. Consider the superposition of the eigenstate ψ_n with the vector of quantum numbers $n \equiv (n_1, \cdots, n_r)$ and

the eigenstate $\psi_{n'}$ with the vector of quantum numbers $n' \equiv (n'_1, \cdots, n'_r)$. Suppose without loss of generality that the rth quantum number is associated with the time-dependent portion of the boundary and that the others are associated with stationary portions of the boundary. Then ψ_n and $\psi_{n'}$ have a nonzero "interaction coefficient" $\mu_{nn'}$ (which measures how strongly they are coupled) if and only if $n_l = n'_l$ for all $l \in \{1, \cdots, r-1\}$.[159] This theorem, which is stated and proved in Chapter 6, may be termed the *Quantum Number Symmetry Theorem*. This result is conforms to our physical expectations.[137, 154, 159, 189]

f. The radially vibrating spherical quantum billiard is considered in detail as a particular example of the $s = 1$ case.[112, 158]

g. The vibrating rectangular quantum billiard is considered in detail as a particular example of the $s = 2$ case.[157]

h. Suppose that $s = 1$ and $d = 2$. Suppose also that the coupling coefficient $\mu_{nn'} = 0$, so that the configuration under consideration is integrable. Then, if one increases or decreases $\mu_{nn'}$, the quantum degrees-of-freedom become chaotic far sooner than do the classical degrees-of-freedom. This result follows from the Born-Oppenheimer approximation, so it is a general phenomenon in semiquantum systems.

h. Suppose $s = 1$. When $d = 2$, we apply a scalar Melnikov technique to verify the presence of homoclinic tangles when $V(a)$ is a quartic, double-well potential. For $d = 3$ and this same potential, we apply a vectorial Melnikov technique as a plausibility argument for a priori unstable Arnold diffusion.[74, 82, 114, 115]

1.3 Outline of the Thesis

Chapters 2-4 provide essential background information. Chapter 2, which is the most directly pertinent to this thesis, covers semiquantum physics. Chapter 3 connects the present work to the literature on quantum chaos, and Chapter 4 discusses quantum billiards.

Chapter 5 is concerned with vibrating quantum billiards and its connection with molecular systems. We define this class of infinite-dimensional Hamiltonian systems, examine the symmetries of such systems, and then consider finite-dimensional Galërkin truncations of vibrating quantum billiards and their physical interpretation.

In Chapter 6, we state and prove the Quantum Number Symmetry Theorem.

Chapters 7-9 respectively treat 1-mode, 2-mode, and 3-mode Galërkin expansions of vibrating quantum billiards with one nuclear degree-of-freedom. The radially vibrating spherical quantum billiard is discussed in Chapter 10, and the rectangular vibrating quantum billiard is discussed in Chapter 11. This latter billiard has two nuclear degrees-of-freedom.

In Chapter 12, we show that all finite dimensional Galërkin truncations of vibrating quantum billiards are Hamiltonian by using action-angle variables in an adiabatic basis and showing (with a momentum shift) that this formulation is equivalent to that derived in Chapter 5. We also apply scalar and vectorial Melnikov methods to consider, respectively, homoclinic tangles and a priori unstable Arnold diffusion.

In Chapter 13, we examine the relative facility of chaotic onset of a vibrating billiard's classical and quantum *dof* when perturbing from integrable configurations.

1.4 Significance of the Thesis

In this document, we connect the study of nonadiabatic phenomena (such as Jahn-Teller effects), which is of considerable interest to chemical physicists, to abstract mathematical models such as vibrating quantum billiards.[19, 20, 126, 154, 189, 202] We also examine chaos and Hamiltonian diffusion in such systems.

This study serves three purposes:

a. It connects the quantum chaos and theoretical chemical physics literatures. The problems that are studied in these two fields are very similar in spirit, but there is insufficient communication between these two communities.[41]

b. It applies a dynamical systems approach to problems in chemical physics and thereby helps fill an important gap in this literature. Notions such as separatrices (and approximate separatrices), the KAM transition from integrability to chaos, and Hamiltonian diffusion are of great interest in molecular systems.

c. It examines the incorporation of quantum effects in classical Hamiltonian systems, which is an essential step to study and understand the dynamics of single-molecule devices.[90, 145, 154, 185]

CHAPTER 2

SEMIQUANTUM DYNAMICS*

In this chapter, we discuss nonadiabatic behavior in semiquantum physics. When treated semiquantally, systems are studied using by a mixture of classical and quantum descriptions.[5, 137, 154, 156] Semiquantum descriptions arise naturally upon application of the Born-Oppenheimer approximation,[7, 19, 20, 126, 154, 189, 198] which provides a widely accepted procedure for dividing quantum-mechanical systems into slow and fast components. Among the systems that can be modeled semiquantally are Jahn-Teller molecules,[19, 20, 126, 189, 202] nanomechanical devices,[90, 98, 135, 145, 185, 190, 197] solvated electrons,[179, 180] atoms in a resonant cavity,[11] collective nuclear motion,[25] hadrons,[10] spin-particle interactions,[5] micromasers,[75] and superconducting quantum interference devices.[44, 156]

2.1 Introduction

Every physical regime approximates reality in some form or another. In continuum mechanics, one ignores the fact that a solid or fluid is composed of a finite number of discretely spaced particles, as it is not necessary to consider this at the scale under consideration. In classical mechanics, one does consider discrete objects, but quantities such as energy and light are permitted to vary continuously. In quantum physics, these quantities are treated as discrete–they have been *quantized*–and one expresses quantities such as position and momentum as operators rather

*This chapter is based on reference [154].

than simply vectors. This regime is an approximation of the even more finely grained domain of quantum field theory, which may, in turn, approximate even more fundamental regimes.

The picture painted above is far from complete, as there are several regimes we neglected to mention as well as others that lie at the borders between those discussed above. For example, semiclassical, quasiclassical, and semiquantum descriptions lie between classical and quantum physics. Despite their nomenclature, they are not the same.[5, 154]

2.2 A Semiquantum Approach to Nonadiabatic Phenomena

In this approach, one assumes that the classical nuclear motion of a molecular system is determined by its interaction with the electronic subsystem in a self-consistent manner.[137, 154, 189] Using the vibrational and rotational coupling terms in a molecular Hamiltonian, one obtains a time-dependent electronic Hamiltonian, which causes transitions in the molecule's electronic states because of its dependence on the nuclear *dof*. Time-dependence in these electronic states leads to a time-dependent nuclear potential, as the molecular Hamiltonian depends on the nuclear coordinates.[19, 20] This type of self-consistent coupling occurs in vibrating quantum billiards, which we discuss extensively in subsequent chapters.

To analyze a system semiquantally, one posits *a priori* that some of its *dof* are classical and others are quantum-mechanical. In contrast to semiclassical physics, one cannot simplify quantize a system fully and apply an appropriate asymptotic procedure to obtain such a description.[5, 154] Nevertheless, there are several situations for which semiquantum physics is appropriate. One may obtain a semiquantum description, for example, by directly coupling a classical system to a quantum-mechanical one. Additionally, semiquantum systems arise naturally when one ap-

plies the Born-Oppenheimer approximation to molecular systems.[7, 19, 20, 189]

The first step in a Born-Oppenheimer scheme is to quantize a system's fast ("electronic") components. If one obtains well-separated energy levels, then one may also quantize its slow ("nuclear") components. If, however, the eigenenergies of the fast components of a d-state system are close to each other, one ignores the rest of the spectrum and thereby obtains a system described by d electronic energy levels (each of which corresponds to the full contribution of a single eigenstate) that are coupled to a multitude of nuclear states. The semiquantum approximation consists of treating the nuclear *dof* classically. Because the electronic *dof* depend continuously on the nuclear subsystem, one obtains an effective classical Hamiltonian describing the system of interest. The quantum-mechanical information is incorporated into this Hamiltonian using the electronic eigenvalues.[154, 160, 189]

Although self-consistent coupling of classical and quantum dynamics has appeared often in the chemical physics literature, there remain conceptual difficulties and inconsistencies in the semiquantum approximation.[189] In this chapter, we discuss how one may study nonadiabaticity starting from the Born-Oppenheimer approximation. We discuss semiquantum chaos from a phenomenological perspective in Chapter 3.

2.3 Back-of-the-Envelope Calculations

Before we delve into the Born-Oppenheimer approximation, we perform some preliminary calculations.[7, 20, 154]

It is more difficult to find electron orbits in molecules than in atoms because the effective potential felt by the electrons is no longer well-approximated as spherically symmetric. One pictures the molecular nucleus as having classical equilibrium positions about which it slowly oscillates. The electrons travel rapidly around the

nucleus and are affected by the oscillations of the latter.

This perspective is effective because a nucleus (with mass M) is much more massive than electrons (each of which have mass m_0). The mass ratio m_0/M is typically about

$$\frac{m_0}{M} \approx 10^{-5} \text{ or } 10^{-4}, \tag{2.1}$$

so the magnitude of the zero-point motion of the nucleus is far smaller than that of the electrons. (*Zero-point motion* describes the minimal motion due to Heisenberg's Uncertainty Principle.[7, 105, 136, 174])

From the perspective of an electron, the nucleus is practically stationary. As long as the electronic energy levels are sufficiently far apart, the only effect of the slow nuclear vibrations is to adiabatically deform the electronic eigenstates. As a molecule with typical radius a has electrons with approximate momenta $\hbar/a$, the energetic spacing of these electrons is about $\hbar^2/m_0a^2$.

From the perspective of a nucleus, the electrons are a blurry cloud. The electronic wavefunctions distort as nuclei move, leading to small changes in the electronic energies. Nuclei, in turn, tend to move towards positions of minimum electronic energy and thus oscillate about energy minima.[7] (Two examples of vibrational motion in molecular systems are pulsing, which occurs in vibrating quantum billiards,[112, 157–160] and "bouncing" of the center-of-mass, which has been proposed as a mechanism for energy transfer in buckyballs.[90, 145, 154]).

One can estimate the frequency ω of nuclear oscillations by assuming that the nucleus resides in a harmonic potential $M\omega^2r^2/2$, where r is the displacement of the nucleus from equilibrium. If this displacement is given by the distance a, then the electronic energy experiences a change of about $\hbar^2/2m_0a^2$. Roughly,

$$\frac{M\omega^2a^2}{2} \approx \frac{\hbar^2}{2m_0a^2}, \tag{2.2}$$

so the nuclear frequency is given by[7]

$$\omega \approx \sqrt{\frac{m_0}{M}} \frac{\hbar}{m_0 a^2}. \tag{2.3}$$

The nuclear vibration energies $\hbar\omega$ are consequently a factor of $\sqrt{m_0/M}$ smaller than the electronic excitation energies and are on the order of tenths or hundredths the size of an electron volt.

The zero-point nuclear energy in a harmonic potential is

$$\frac{P^2}{2M} \approx \frac{\hbar\omega}{2}, \tag{2.4}$$

so its corresponding zero-point momentum is

$$P \approx \left(\frac{M}{m_0}\right)^{\frac{1}{4}} \frac{\hbar}{a}, \tag{2.5}$$

which is about ten times larger than the momentum of an electron. A typical nuclear velocity is thus

$$v_N = \frac{P}{M} \approx \left(\frac{m_0}{M}\right)^{\frac{3}{4}} \frac{\hbar}{ma}. \tag{2.6}$$

The nuclear deviation from equilibrium δ satisfies

$$\frac{M\omega^2\delta^2}{2} \approx \frac{\hbar\omega}{2}, \tag{2.7}$$

so

$$\left(\frac{\delta}{a}\right)^2 \approx \frac{\hbar\omega}{M\omega^2 a^2} \approx \frac{E_N}{E_e} \approx \sqrt{\frac{m_0}{M}}, \tag{2.8}$$

which implies that[7]

$$\left(\frac{\delta}{a}\right) \approx \left(\frac{m_0}{M}\right)^{\frac{1}{4}} \approx \frac{1}{10}. \tag{2.9}$$

In addition to undergoing vibrations as described above, a molecule can rotate about its center-of-mass. However, the energy due to such excitations is very small

since the molecule does not distort very much as a result of this motion.[7, 154] If the angular momentum of the rotational motion is $\hbar l$, then its accompanying energy is

$$E_{rot} \approx \frac{\hbar^2 l(l+1)}{2Ma^2} \approx \frac{m_0}{M} E_e. \tag{2.10}$$

In general, a molecular excited state can be decomposed into electronic, vibrational, and rotational excitations. Together, the vibrational and rotational excitations comprise the nuclear (or *rovibrational*) contribution to the energy of a molecule. The total molecular energy is given by the sum of the contributions from its three components:

$$E = E_e + E_N + E_{rot}. \tag{2.11}$$

2.4 The Born-Oppenheimer Approximation

Semiquantum descriptions of nonadiabatic phenomena are frequently obtained amidst the breakdown of the Born-Oppenheimer approximation.[5, 22, 23, 137, 154, 189] In particular, this is often associated with degenerate or nearly degenerate electronic states in polyatomic molecules. Such near-degeneracies (and sometimes exact degeneracies) among several states, which are often due to symmetries, is a common phenomenon in molecules–especially at higher energies.[189] The energy spectrum and intramolecular dynamics can both vary substantially from those observed during adiabatic behavior.[202] However, it is not easy to incorporate nonadiabatic behavior into simple models of molecular dynamics, in which the canonical portrait of nuclear motion is described on a single well-defined surface of potential energy near the electronic degeneracy. Consequently, it is important to develop a semiquantum description of such systems that incorporates essential features of the nonadiabatic coupling.

To apply the Born-Oppenheimer approximation to a molecular system, one first quantizes its fast components, which comprise the system's *electronic* degrees-of-freedom (*dof*). If one obtains well-separated energy levels, then one may also quantize the slow components, which constitute the system's *nuclear* degrees-of-freedom. If the electronic eigenenergies of a system with d electronic states are sufficiently close to each other, then one ignores the rest of the spectrum, thereby obtaining a system described by d electronic energy levels (each of which corresponds to the full contribution of a single eigenstate) that are coupled to a multitude of nuclear states. When using a semiquantum description, these nuclear states are treated classically. Recall that one does not fully quantize a molecular system and then pass to an appropriate asymptotic limit. Rather, one assumes *a priori* that a semiquantum description is appropriate.[154, 160, 189]

Nonadiabatic behavior occurs in simple molecules with symmetry-based degeneracy in their electronic eigenstates.[19, 20, 154] Without such degeneracy, one may approximate the molecular wavefunction using the Born-Oppenheimer approximation, in which the wavefunction is expressed as a product of electronic and nuclear wavefunctions. Near a d-fold degeneracy, on the other hand, one expands the molecular wavefunction in a d-dimensional electronic basis. Such degeneracies are common in the space spanned by nuclear coordinates.[189]

The stationary, spinless Schrödinger equation for a single molecule is[7, 19, 20, 189]

$$[K_N + H_e(q, Q)]\,\psi_d(q, Q) = E_d \psi_d(q, Q), \tag{2.12}$$

where K_N is the nuclear kinetic energy operator and

$$H_e(q, Q) \equiv K_e + U_{ee} + U_{eN} + U_{NN} + V \tag{2.13}$$

is the electronic Hamiltonian. The molecular Hamiltonian H is given by

$$H = K_N + H_e, \tag{2.14}$$

which represents the sum of the nuclear and electronic components. Because of vibronic coupling, H_e depends on the nuclear coordinates Q. Its components are the electronic kinetic energy K_e, the interelectron repulsion potential U_{ee}, the electron-nuclear attraction U_{eN}, the internuclear repulsion U_{NN}, and an external potential V. The nuclear kinetic energy K_N is proportional to $1/M$ and is thus a small term in the molecular Hamiltonian (2.14).

In Born-Oppenheimer schemes, one calculates the eigenenergies and eigenstates of (2.14) by treating K_N as a small perturbation with expansion parameter[7, 19, 20, 154]

$$\kappa \equiv (m_0/M)^{\frac{1}{4}}, \tag{2.15}$$

the ratio of nuclear vibrational displacement to the spacing between nuclei.

Some authors distinguish the adiabatic and Born-Oppenheimer approximations.[19, 20] The two approaches in question are linked by a unitary transformation of the electronic basis and are thus equivalent for exact solutions. However, their convergence rates differ, as the small parameter for the (proper) adiabatic approximation is

$$\kappa^3 = (m_0/M)^{\frac{3}{4}}. \tag{2.16}$$

There exist situations in which the adiabatic approximation is valid but the Born-Oppenheimer approximation is not.[19, 20]

Coupled vibrational equations can be derived using either *diabatic* or *adiabatic* formulations.[19, 20, 189] We discuss this below. Additional detail may be found in reference [20].

Using a *diabatic* basis, a molecular wavefunction is given by

$$\psi_d(q,Q) = \sum_k \varphi_k(q;Q_0)\chi_k(Q), \tag{2.17}$$

where the orthonormal electronic states φ_k are calculated by solving the electronic Schrödinger equation at a chosen reference configuration Q_0:

$$H_e(Q_0)\varphi_k(q) = E_k^0\varphi_k(q). \tag{2.18}$$

One then determines the vibrational wavefunctions χ_k using a set of coupled equations with Hamiltonian matrix elements given by

$$H_{kk'} = K_N\delta_{kk'} + \langle\varphi_k|H_e(Q)|\varphi_{k'}\rangle. \tag{2.19}$$

(Note that the nuclear kinetic energy K_N is diagonal in this basis.) One expands the matrix elements of the electronic Hamiltonian $H_e(Q)$ to obtain

$$H_{kk'} = (K_N + E_k^0 + \Delta U_{NN})\delta_{kk'} + \langle\varphi_k|\Delta U_{eN}|\varphi_{k'}\rangle, \tag{2.20}$$

so each diagonal element defines an effective vibrational Hamiltonian that consists of the sum of the nuclear kinetic energy operator K_N and the Hellman-Feynman potential for nuclear motion.[53, 189] This latter potential has one term due to internuclear repulsions U_{NN} and another due to the attraction to the electronic charge distribution $\varphi_k * \varphi_k$. Such a vibrational Hamiltonian neglects any response that the electronic state may have to the changing nuclear configuration. The off-diagonal coupling terms that have been neglected arise from the ΔU_{eN} component.

It is the change in the potential describing electronic-nuclear attraction as a function of the changing nuclear configuration that induces mixing in diabatic basis states. This yields both adiabatic and nonadiabatic correlations of electronic and nuclear motion.[189]

Alternatively, one may expand $\psi_d(q,Q)$ using a basis of *adiabatic* electronic states:

$$\psi_d(q,Q) = \sum_m \varphi_m(q;Q)\chi_m(Q), \tag{2.21}$$

where $\varphi_m(q;Q)$ is a solution of the electronic Schrödinger equation

$$H_e(Q)\psi_m(q;Q) = E_m(Q)\psi_m(q;Q). \tag{2.22}$$

Equation (2.21), the Born-Huang expansion, consists of the Born-Oppenheimer expansion plus the diagonal nuclear nonadiabatic coupling. The electronic eigenvalues, which depend on the nuclear configuration, determine the adiabatic potential surfaces. One derives equations of motion for the adiabatic vibrational amplitudes χ_m in which the coupling is now due to the off-diagonal matrix elements of the nuclear kinetic energy.

2.5 Jahn-Teller Distortions

The relevance of Jahn-Teller theory to the present work lies in the fact that the dynamical behavior that occurs in vibrating quantum billiards resembles the nonadiabaticty observed in Jahn-Teller distortions.[154]

Jahn-Teller distortions and related phenomena constitute an important class of nonadiabatic behavior that can occur in molecular systems.[19, 20, 126, 154] The *Jahn-Teller theorem* implies that if the adiabatic potential of a molecular system (which is a formal solution to the electronic part of the Schrödinger equation) has several crossing sheets, then at least one of these sheets has no extremum at the crossing point.[19, 20] Consequently, degenerate and nearly degenerate electronic energy levels cannot be analyzed directly using the Born-Oppenheimer approximation. (In the case of electronic near-degeneracies, the term *pseudo-Jahn-Teller*

effect is often employed.) The nuclear and electronic subsystems are nonadiabatically coupled. In the vicinity of electronic degeneracies and near-degeneracies, it is therefore appropriate to use a semiquantum description to study the dependence of the electronic eigenenergies on the system's nuclear *dof*.

Jahn-Teller deformations are relevant to the study of vibrations in crystals, numerous types of spectroscopy (NMR, Raman, *etc.*), multipole moments, the stereochemistry and instability of molecules, mechanisms of chemical reactions, and catalysis.[19, 20, 154] Effects analogous to Jahn-Teller distortions have also been observed in other physical systems–including the pion-nucleon interaction in quantum field theory, the α-cluster description of light nuclei, and the resonant interaction of light with matter.

Jahn-Teller distortions are classified according to their tensorial construction, which describes their (nuclear and electronic) symmetries and degeneracies. The canonical example of the Jahn-Teller effect involves an $E \times e$ molecule, in which one doubly degenerate vibrational mode e interacts with a (symmetry-induced) double electronic degeneracy E.[19, 20, 126, 189, 202] The simplest molecular systems in which this type of distortion occurs are triangular molecules X_3, tetrahedral molecules ML_4, and octahedral molecules ML_6.

Jahn-Teller deformations can be extremely complicated, and even the simplest such effects are dynamically interesting.[19, 20, 126, 154, 189, 202] Higher-order electronic degeneracies are often important, and multiple Jahn-Teller distortions can occur in the same molecule or crystal. Moreover, individual deformations in a given molecule need not possess the same symmetry. Multiple distortions can occur in crystals with point defects, as their energy spectra contain discrete, nearly-degenerate electronic eigenenergies well-separated from other energy levels.

Both theoretical and experimental analyses are vital to the study of nuclear-

electronic coupling in molecules. Treatments with few active modes–that is, low-mode Galërkin projections–have been particularly useful, as they ease the analytical difficulty of theoretical studies. One may then consider a fully quantum variational treatment of the nuclear part of the Hamiltonian, so that model parameters can be fit to experimental data. As one increases the order of the Galërkin approximation, however, this procedure becomes increasingly difficult both analytically and computationally. Hence, using a fully quantum description to study nonadiabaticity in molecular systems quickly becomes untenable. In order to analyze molecular systems, it is thus important to develop semiclassical and semiquantum techniques even for few-term superposition states.[154, 189]

2.5.1 Nanomechanical devices

A particular class of systems for which semiquantum modeling is relevant are nanomechanical devices,[90, 98, 145, 154, 185, 190] as their electronic and nuclear subsystems interact nonadiabatically.

Electronic-nuclear coupling heavily influences molecular motion, even though electrons are much less massive than entire molecules.[145] The mechanical control of nanoscale structures ("NEMs") will allow smaller, faster, and more efficient versions of existing micro-electro-mechanical devices (MEMs).[90, 145] For example, a single-electron current can both detect and excite mechanical oscillations in a buckyball. It has been shown experimentally that an electron with surplus energy precisely equal to the vibrational energy of the buckyball can cause the buckyball to begin bouncing due to spontaneous emission of this energy.[145] The electron then continues to hop on and off the buckyball, thereby yielding an "electron turnstile" that allow electrons to pass one at a time. Jahn-Teller theory comes into play because the buckyball experiences internal distortions while it bounces.[154, 156]

CHAPTER 3

QUANTUM CHAOS*

One of the goals in the field of quantum chaos is to marry the scientific paradigms of nonlinear dynamics and quantum mechanics into one theory to describe situations in which both subjects are relevant. Loosely speaking, quantum chaos is the study of chaotic structure in the quantum regime. Though still in its infancy, this field has seen much activity during the past quarter century. The notion of quantum chaos is not yet fully developed–there remains substantial disagreement among physicists, mathematicians, and chemists about what types of behavior constitute quantum chaos. The purpose of the present chapter is to clarify what is meant by the term "quantum chaos." To do this, we must first clarify what we mean by "(classical) chaos."

3.1 Definition of Chaotic Behavior

A (classical) trajectory is said to be *chaotic* if it satisfies the following three properties:[41, 43, 70]

a. *Boundedness*: There exists a ball of sufficiently large radius that contains the trajectory.

b. *Poincaré Recurrence*: Consider an arbitrarily small neighborhood about the initial point of a trajectory. The trajectory returns to the neighborhood infinitely many times.

*This chapter is based on portions of references [160], [158], and "An Introduction to Quantum Chaos," which won a SIAM Student Paper Prize in 2001.

c. *Sensitive Dependence on Initial Conditions*: Two trajectories that emanate arbitrarily close together diverge from each other at an exponential rate. (More precisely, they are characterized by positive Lyapunov exponents.[67, 114, 194])

Chaos can be defined in numerous other manners.[42, 67, 194] Additionally, it is often appropriate to relax some of the requirements in its various definitions as well as to extend the notion of chaotic dynamics to other regimes (such as quantum mechanics and spatially extended systems) that necessitate other modifications to the definition. The essential purpose of chaos is to provide a notion of unpredictability in deterministic systems.

3.2 Quantum Chaos

There are three types of quantum chaos.[23, 158] *Quantized chaos* (or *quantum chaology*) refers to the study of the quantum signatures of classical chaos in the semiclassical or high quantum-number regimes. *Semiquantum chaos*, which is the primary concern of this thesis, refers to rigorously chaotic dynamics in semiquantum systems. *Genuine quantum chaos*, whose existence is an open question, refers to rigorously chaotic behavior in fully quantum systems. In the next two subsections, we briefly discuss quantum chaology and semiquantum chaos in a phenomenological manner.

3.2.1 Quantum Chaology

Quantum chaology is the most commonly studied type of quantum chaos. In this subject, one quantizes classically chaotic systems, just as one would a classically integrable system. When studying quantum systems semiclassically, one observes that those whose classical counterparts are chaotic exhibit far different behavior

than those whose classical counterparts are integrable. The systems that exhibit so-called quantized chaos are not rigorously chaotic, however, as the concept of Lyapunov exponents breaks down in the quantum regime.[70, 71] Nevertheless, configurations obtained via quantization of classically chaotic systems retain many of the features of their classical counterparts. Their behavior is quite irregular, and they still satisfy the properties of boundedness and infinite recurrence that are present in the definition of classical chaos.[41, 70] Techniques used to study quantum chaology include random matrix theory, level dynamics, and periodic orbit expansions.[23, 71]

3.2.2 Semiquantum Chaos

Semiquantum chaos refers to chaos in systems with both classical and quantum components.[23] Although typically studied in the context of conservative systems (so that one is considering Hamiltonian chaos in the semiquantum regime), semiquantum chaos can occur in dissipative systems as well.[44, 154, 156]

Semiquantum descriptions typically arise from the dynamic Born-Oppenheimer approximation, which we discussed in Chapter 2. Part of the value of semiquantum physics is that one may study chaos even in low-energy systems, such as nuclei that have been coupled to two-level electronic systems consisting of the ground state and the first excited state of appropriate symmetry.[112, 154, 158] Quantum chaology, on the other hand, typically focuses on highly energetic states.[23, 70, 71] Thus, the notion of semiquantum chaos is important for capturing the chaotic dynamics of low-energy states of molecular systems. As behavior that is best described as "chaotic" has been observed experimentally in such systems,[189] semiquantum chaos is an important type of quantum chaos.

Both the classical and quantum components of semiquantum systems can behave chaotically. Chaos in the quantum subsystem manifests in the quantum

probabilities. Even the chaotic dynamics of the classical subsystem has quantum consequences, however, as the quantum normal modes (i.e., eigenstates) and eigenenergies of a semiquantum system depend on its classical *dof*. Hence, the wavefunctions of semiquantum chaotic systems exhibit quantum-mechanical *wave chaos*.[22, 23, 158] Additionally, as the lengthscales of the wavefunctions are determined by the classical degrees-of-freedoms, semiquantum chaos leads to a chaotic superposition of chaotic normal modes.[160] The signature of semiquantum chaos in real space is the sequence of intersections with a fixed displacement that the wavefunction's nodal surfaces make at any instant subsequent to a number of transversal times.[112, 160]

In the language of Blümel and Reinhardt[23] as well as that in our previous work,[112, 157–160] vibrating quantum billiards can exhibit semiquantum chaos, as they consist of a classical system (the walls of the billiard) coupled to a quantum-mechanical one (the particle confined within the billiard). When a vibrating billiard's classical and quantum components interact, both subsystems can behave chaotically even in cases in which the individual components are integrable. Note finally that quantizing the motion of the billiard walls leads to a higher-dimensional, fully-quantized system that exhibits so-called quantized chaos.[23]

CHAPTER 4

QUANTUM BILLIARDS*

Quantum billiards describe the wavefunctions of particles confined in a domain $D \subset X$ (where X is a finite-dimensional Riemannian manifold) and colliding perfectly elastically against the domain's boundary ∂D.[70, 105] Their behavior is determined by solutions to the Schrödinger equation (1.1) with homogenous Dirichlet boundary conditions on the given domain. In the present chapter, it assumed that the billiard boundaries are time-independent.

Two-dimensional, closed quantum billiards may be used to model ballistic microstructures such as quantum dots.[118, 125] However, the theory of quantum billiards pertains to any situation that is describable by the Helmholtz equation with Dirichlet boundary conditions.[27, 107] Such systems occur in optics, acoustics, electromagnetics, and numerous other disciplines.[71, 93]

Just like their classical counterparts, quantum billiards can be integrable, pseudointegrable, pseudochaotic, and chaotic.[65, 70, 71, 80, 119, 120, 167, 193] Their dynamical behavior, which we do not discuss here, is determined by the geometry of D. We instead introduce the notion of *globally separability*, as it is needed in subsequent chapters.

*This chapter is based, in part, on portions of "The Transition From Integrability to Chaos in Classical and Quantum Billiards," which has been submitted for publication.

4.1 Global Separability

A quantum billiard is said to be *globally separable* (or simply *separable*) when solutions $\psi(\mathbf{x}, t)$ to the Schrödinger equation (1.1) are expressible in all parts of the domain D as sums of eigenfunctions that may be written in a product form:

$$\psi(\mathbf{x}, t) = \sum_j \exp\left(-\frac{iE_j t}{\hbar}\right) A_j f_1^j(x_1) \cdots f_n^j(x_n), \tag{4.1}$$

where $\mathbf{x} \in \mathbb{R}^n$ and A_j is a constant complex amplitude. The time-dependent phase factor $\exp(-iE_j t/\hbar)$ may always be separated with

$$\psi_j = \exp\left(-\frac{iE_j t}{\hbar}\right) \varphi(\mathbf{x}), \tag{4.2}$$

where $\varphi(\mathbf{x})$ satisfies the Helmholtz ("Stationary Schrödinger") equation

$$\nabla^2 \varphi + \Lambda^2 \varphi = 0 \tag{4.3}$$

for some constant Λ. Hence, a quantum billiard is separable on D when its associated Helmholtz equation is separable on D. The adjective 'global' is applied to signify that for each j, the set of functions $\{f_1^j, \cdots, f_n^j\}$ is the same throughout the entire domain D.

The main result of this chapter is the following:

Theorem 4.1 A globally separable quantum billiard with time-independent boundaries is not chaotic in the sense that it does not experience quantum signatures of classical chaos.

Proof: Separate the eigenfunctions ψ_j of (1.1) as in equation (4.1). In (1.1),

$$\hat{H} \equiv -\frac{\hbar^2}{2m_0}\nabla^2 + V(x), \tag{4.4}$$

where m_0 is the mass of the particle confined within the billiard and

$$V(x) = \begin{cases} 0, & \mathbf{x} \in D, \\ \infty, & \mathbf{x} \notin D. \end{cases} \tag{4.5}$$

Additionally,

$$\nabla^2 = \frac{1}{\sqrt{g}} \sum_{j=1}^{n} \frac{\partial}{\partial u_j} \left(\frac{\sqrt{g}}{g_{jj}} \frac{\partial}{\partial u_j} \right) \tag{4.6}$$

is the Laplace-Beltrami operator on (X, g).[159, 205]

Each component function $f_k^j(x_k)$ in (4.1), where $k \in \{1, \cdots, n\}$ is an eigenfunction of a Sturm-Liouville ordinary differential equation.[178] The form of these Sturm-Liouville problems is determined by using a Stäckel determinant, an analysis of which determines the geometries on which the Helmholtz operator is separable.[9, 142, 159, 205] As Sturm-Liouville equations are second order, the dynamics of the individual component functions are not chaotic. Consequently, neither their product ψ_j nor any linear combinations thereof are chaotic. Hence, the wavefunctions associated with the quantum billiard are not chaotic. *QED*

Theorem 4.1 essentially says that global separability produces a decoupling in the dynamics of the eigenstates of vibrating quantum billiards. Note, morever, that globally separable quantum billiards can be integrable, pseudointegrable, or pseudochaotic.[65, 70, 71, 80, 119, 120, 167, 193] In this thesis, we consider vibrating quantum billiards whose associated stationary configurations are completely integrable. Examples of such configurations include spherical, cylindrical, and rectangular quantum billiards.[142, 159, 205]

Another way to prove Theorem 4.1 is to consider quantum billiards semiclassically (by using the WKB approximation).[8, 39, 81, 105, 136, 174] In so doing, one obtains Hamilton-Jacobi equations corresponding to a classical billiard with the same geometry.[70, 71, 114] For a given domain D, the Hamilton-Jacobi equation is separable if and only if the Schrödinger equation is also separable. Separability of these equations guarantees that no classical chaos occurs. Together, these results indicate that the concept of global separability provides a deep characterization

of the complexity of the dynamics of classical and quantum billiards of a given geometry.[71]

Finally, as inseparable systems can be fully integrable (e.g., Toda lattices),[70, 114], the inverse of Theorem 4.1 is not true.

CHAPTER 5

VIBRATING QUANTUM BILLIARDS*

5.1 Hamiltonian Structure

Theorem 5.1 Vibrating quantum billiards have a Hamiltonian structure given by the union of an infinite-dimensional component describing its quantum subsystem and a finite-dimensional component describing its classical subsystem. Vibrating quantum billiards are also well-posed provided initial data is given for both subsystems.

Proof: Recall that vibrating quantum billiards are described by the Schrödinger equation,

$$i\hbar\frac{\partial\psi(\mathbf{x},t)}{\partial t} = \hat{H}\psi(\mathbf{x},t), \quad (\mathbf{x},t) \in D \times \mathbb{R}, \tag{5.1}$$

with homogeneous Dirichlet boundary conditions on the boundary ∂D.[112, 158–160] The Hamiltonian operator $\hat{H}$ is given by

$$\hat{H} = \hat{K} + V(\mathbf{a}(t)), \tag{5.2}$$

where V is an external potential, $\mathbf{a}(t) \in \mathbb{R}^s$ describes the (*a priori* unknown) time-dependence of ∂D, and

$$\hat{K} = -\frac{\hbar^2}{2m_0}\nabla^2 \tag{5.3}$$

*This chapter is based in part on portions of reference [160].

is the kinetic energy of the confined particle (i.e., the "electronic" kinetic energy). Additionally, $D \subset X$, which is an r-dimensional Riemannian manifold (where r is finite).

The Lagrangian density $\mathcal{L}$ corresponding to Schrödinger's equation (5.1) for $\mathbf{a}(t) \equiv \mathbf{a} = \text{constant}$ is[128, 184]

$$\begin{aligned}\mathcal{L} &= \frac{i\hbar}{2}\left(\psi^*\psi_t - \psi\psi_t^*\right) - \frac{\hbar^2}{4m_0}\left\{\nabla\psi, \nabla\psi^*\right\} \\ &= \frac{i\hbar}{2}\left(\psi^*\psi_t - \psi\psi_t^*\right) - \frac{\hbar^2}{4m_0}\left(\nabla\psi\cdot\nabla\psi^* + \nabla\psi^*\cdot\nabla\psi\right) \\ &= \frac{i\hbar}{2}\left(\psi^*\psi_t - \psi\psi_t^*\right) - \frac{\hbar^2}{2m_0}\|\nabla\psi\|^2, \end{aligned} \tag{5.4}$$

where ψ_t denotes the derivative of ψ with respect to time and $\{X, Y\}$ is the anti-commutator of X and Y.[136, 150, 174] In (5.4), the wavefunction ψ and its complex conjugate ψ^* are treated as independent variables.

As $\mathbf{a}(t)$ is time-dependent, one obtains the Lagrangian

$$L = \int_D \mathcal{L} d\mathbf{x} - K_N(\dot{\mathbf{a}}) - V(\mathbf{a}) \equiv T - V, \tag{5.5}$$

where T is the sum of the vibrating quantum billiard's nuclear and electronic kinetic energies, the external potential V is its potential energy, and the nuclear kinetic energy K_N is given by

$$\sum_{j=1}^{s} \frac{M_j}{2}\dot{a}_j^2, \tag{5.6}$$

where a_j is the jth time-dependent *constituent* of the boundary and M_j is its mass. A single distance dimension of the boundary of a billiard constitutes one of its "constituents". For example, a planar rectangular billiard has two constituents: its length and its width. The radius of a spherical billiard is its only constituent. A three-dimensional cylindrical billiard has both radial and longitudinal constituents. An annular spherical billiard has two constituents: its inner and outer radii.

This yields the action

$$S[\psi,\psi^*] = \int_{t_0}^{t_1} \left[\int_D \mathcal{L} d\mathbf{x} - K_N(\dot{\mathbf{a}}) - V(\mathbf{a}) \right] dt, \tag{5.7}$$

which is a functional on all admissible functions ψ satisfying the prescribed conditions $\psi(\mathbf{x},t_0)=\psi_0$ and $\psi(\mathbf{x},t_1)=\psi_1$. Admissible wavefunctions ψ are elements of the Hilbert space

$$H_\psi = L^2_\psi(D, d\mathbf{x}) \tag{5.8}$$

of square-integrable waves ψ with Lebesgue measure dx.[160, 172] In (5.8), we use ψ as a subscript to differentiate the notation for Hilbert spaces and square-integrability from that for Hamiltonians and Lagrangians.

One computes the variation of (5.7) to be

$$\begin{aligned} \delta S = \int_{t_0}^{t_1} \left[\int_D \left[\frac{\partial \mathcal{L}}{\partial \psi} - \nabla \cdot \left(\frac{\partial \mathcal{L}}{\partial(\nabla\psi)} \right) - \frac{\partial}{\partial t} \left(\frac{\partial \mathcal{L}}{\partial \psi_t} \right) \right] d\mathbf{x} - K_N(\dot{\mathbf{a}}) - V(\mathbf{a}) \right] \delta\psi dt \\ + \left[\frac{\partial \mathcal{L}}{\partial \psi_t} \delta\psi \right]_{t_0}^{t_1} + \text{c.c.}, \end{aligned} \tag{5.9}$$

where c.c. denotes the complex conjugate of all the preceeding terms in (5.9 and

$$\frac{\partial \mathcal{L}}{\partial(\nabla\psi)} \equiv \left(\frac{\partial \mathcal{L}}{\partial(\partial_1\psi)}, \cdots, \frac{\partial \mathcal{L}}{\partial(\partial_r\psi)} \right), \tag{5.10}$$

where $\partial_j\psi \equiv \partial\psi/\partial x_j$.

The wavefunction $\psi(\mathbf{x},t)$ is an extremum of (5.7) provided the Euler-Lagrange equations are satisfied.[1, 128, 150, 184] Computing these equations with the Lagrangian (5.5) reproduces Schrödinger's equation (5.1). Consequently, vibrating quantum billiards possess a Hamiltonian structure with Hamiltonian given by[184]

$$\begin{aligned} H &= \frac{i\hbar}{2} \int_D (\psi^*\psi_t - \psi\psi_t^*) - L \\ &= \int_D \mathcal{H} d\mathbf{x} + K_N(\mathbf{P}) + V(\mathbf{a}), \end{aligned} \tag{5.11}$$

where $P_j \equiv M_j \dot{a}_j$ ($j \in \{1, \cdots, s\}$) is the momentum of the jth constituent of the billiard boundary and

$$\mathcal{H} = \frac{i\hbar}{2}(\psi^* \psi_t - \psi \psi_t^*) - \mathcal{L} = \frac{\hbar^2}{2m_0} \|\nabla \psi\|^2 \tag{5.12}$$

is the Hamiltonian density. The Hamiltonian H has an infinite-dimensional component (encoded by the Hamiltonian density $\mathcal{H}$) as well as a finite-dimensional component (due to the time-dependent boundary $\mathbf{a}(t)$). (Associated with the Hamiltonian is a symplectic structure.[128])

Applying Hamilton's equations yields a partial differential equation describing the infinite-dimensional component,

$$i\hbar \psi_t = \frac{\delta H}{\delta \psi^*} = \frac{\delta \mathcal{H}}{\delta \psi^*} = \hat{K}\psi, \tag{5.13}$$

which we recognize as Schrödinger's equation (5.1), and coupled ordinary differential equations describing the finite-dimensional component

$$\begin{aligned} \dot{a}_j &= \frac{P_j}{M_j}, \\ \dot{P}_j &= -\frac{\hbar^2}{4m_0} \int_{\partial D} \{\nabla \psi, \nabla \psi^*\} d\sigma(x) - \frac{\partial V}{\partial a_j} = -\frac{\hbar^2}{2m_0} \int_{\partial D} \|\nabla \psi\|^2 d\sigma(x) - \frac{\partial V}{\partial a_j}, \end{aligned} \tag{5.14}$$

where $d\sigma(x)$ is a Lebesgue measure on the boundary of the billiard. The potential $V(\mathbf{a})$ need not be included in Schrödinger's equation (5.13), as it shifts all eigenvalues of $\hat{K}$ by the same value.[159, 160] It is included, however, in the finite-dimensional component (5.14) of Hamilton's equations describing the motion of the billiard boundary.

Quantum billiards with time-independent boundaries are well-posed provided an initial wavefunction $\psi(\mathbf{x}(0), 0)$ is specified.[128] Quantum billiards with time-dependent boundaries are also well-posed as long as the initial size $\mathbf{a}(0)$ and momentum $\mathbf{P}(0)$ of the boundary are also given. (The finite-dimensional Hamiltonian

structure of the classical subsystem provides a unique way to determine $\mathbf{a}(\Delta t)$ and $\mathbf{P}(\Delta t)$ for a time-step Δt.) *QED*

An alternate perspective on the results discussed in this section is examined in reference [160].

5.2 Symmetries

To further study the structure of vibrating quantum billiards, we consider the symmetries of the full system and its d-mode truncations.[160]

Expand the solution ψ to (5.1) as a d-mode Galërkin projection of eigenstates:

$$\psi = \sum_{j=1}^{d} A_j(t)\psi_j. \tag{5.15}$$

Equation (5.15) is often called a *superposition state* in the context of quantum mechanics. In (5.15), d may be either finite or infinite. If d is infinite, it is assumed that the expansion (5.15) contains every possible eigenstate rather than a subset of these states. The amplitude $A_j(t) \in \mathbb{C}$ is time-dependent because the boundary $\mathbf{a}(t)$ is time-dependent. (We will discuss this in more detail later in the present chapter.)

One may define ψ as an element of its invariant Lie group, as on the normalized Hilbert space $\mathcal{H}$, it is completely determined by the coefficients A_j in its eigenfunction expansion (5.15) once a basis set $\{\psi_j\}$ has been chosen.[160] The initial wavefunction is then determined by its initial complex amplitudes $A_j(0)$. If d is finite, the initial wavefunction is determined by finitely many such amplitudes. (The others all vanish.) As the ensuing finite-dimensional system retains a Hamiltonian structure (see Chapter 12), it follows that given $\mathbf{a}(0)$, $\mathbf{P}(0)$, and $\mathbf{A}(0)$ for all $j \in \{1, \cdots, d\}$, a d-mode Galërkin expansion of a vibrating quantum billiard is well-posed.[160]

Consider a wavefunction (5.15), where d might be infinite and each of the coefficients $A_j(t) \in \mathbb{C}$. Because of their scale-invariance–two wavefunctions are equivalent if one is a constant multiple of the other–wavefunctions may be treated as elements of the complex projective space $\mathbb{CP}^{d-1}$, which is the set of lines in $\mathbb{C}^d$, or equivalently the set $\mathbb{C}^d/\{\text{change of scales}\}$.[1, 160]

If $d = \infty$, then one must consider the group $\mathbb{C}^\infty$ and hence $\mathbb{CP}^\infty$. The infinite-dimensional projective space $\mathbb{CP}^\infty$ is given by the union

$$\mathbb{CP}^\infty = \bigcup_{j \geq 0} \mathbb{CP}^j. \tag{5.16}$$

It is well-defined because of the embedding $\mathbb{CP}^j \hookrightarrow \mathbb{CP}^{j+1}$, which is defined by appending a 0 to the last coordinate of $\zeta^j \in \mathbb{CP}^j$.

Wavefunctions are normalized and expressed as eigenfunction expansions of orthonormal bases, so $\langle \psi_j | \psi_k \rangle = \delta_{jk}$ for any pair of eigenfunctions ψ_j and ψ_k in the expansion. Hence, $\psi \in U(\mathbb{C}^d)$, the unitary group on $\mathbb{C}^d$. By invariance under global phase shifts, ψ and $\exp(i\vartheta)\psi$ describe equivalent physical systems for any $\vartheta \in \mathbb{R}$, so wavefunctions ψ may be further restricted by being treated as elements of the group $U(\mathbb{C}^d)/\{e^{i\vartheta} I\}$, where $\{e^{i\vartheta} I\}$, the set of all global phase shifts, is the center of the group $U(\mathbb{C}^d)$.

Note that for a given basis $\{\psi_j\}$, a wavefunction is determined by its amplitude tuple $\mathbf{A}(t) \equiv \{A_1(t), \cdots, A_j(t), \cdots\}$. Conservation of probability,

$$\sum_{j=1}^{d} |A_j|^2 = 1, \tag{5.17}$$

follows from the fact that $\psi \in U(\mathbb{C}^d)/\{e^{i\vartheta} I\} \subset U(\mathbb{C}^d)$. This entails restrictions on the density matrix $\rho_{kj} = A_k A_j^*$, which may be written as a projection operator

$$\rho \equiv P_\varphi, \tag{5.18}$$

where $P_\varphi \psi = \langle \psi, \varphi \rangle \varphi$ for the $\{\varphi\}$-basis.

If d is finite, then $\psi \in U(d)/\{e^{i\vartheta}I\}$. It then follows from the invariance of wavefunctions under scaling that there is a natural action of the group $U(d)/\{e^{i\vartheta}I\}$: $\mathbb{C}^d \longrightarrow \mathbb{C}^d$ that induces an action from $\mathbb{CP}^{d-1}$ to $\mathbb{CP}^{d-1}$. The set $U(d)/\{e^{i\vartheta}I\}$ is the invariance group of the action described above. When $d = \infty$, there is similarly an action

$$U(\mathbb{C}^d)/\{e^{i\vartheta}I\} : \mathbb{CP}^\infty \longrightarrow \mathbb{CP}^\infty \tag{5.19}$$

under the invariance group $U(\mathbb{C}^d)/\{e^{i\vartheta}I\}$.

When $d = \infty$, the action of $U(\mathbb{C}^d)/\{e^{i\vartheta}I\}$ is generally an $\infty : 1$ map. By restricting one's attention to the finite-dimensional subgroup $U(n)/\{e^{i\vartheta}I\}$, however, one instead obtains a $n : 1$ map. This procedure is equivalent to taking an n-term Galërkin projection. In general, for $d \geq n$ (including $d = \infty$), one obtains an $n : 1$ map by restricting the wavefunction ψ to be an element of $U(n)/\{e^{i\vartheta}I\}$.) This, in turn, is accomplished by restricting the coefficient tuple $\mathbf{A}$ to be an element of $\mathbb{C}^n$ (and retaining the invariance properties of the coefficients that are consequences of the invariance properties of ψ).

Note that the Lie algebra $\mathfrak{u}(\mathfrak{d})/\{\mathfrak{e}^{\mathrm{i}\vartheta}\mathfrak{I}\}$ (of the Lie group $U(d)/\{e^{i\vartheta}I\}$) is isomorphic to the Lie algebra $\mathfrak{su}(\mathfrak{d})$. However, the associated Lie groups are not themselves isomorphic. When d is odd, for example, $U(d)/\{e^{i\vartheta}I\}$ has a trivial center, whereas $-I$ is in the center of $SU(d)$. When $d = 2$, $U(d)/\{e^{i\vartheta}I\}$ is isomorphic to the rotation group $SO(3)$, which differs from $SU(2)$ because the latter is simply connected whereas the former is not.[188] Nevertheless, because their Lie algebras are isomorphic, $U(d)/\{e^{i\vartheta}I\}$ and $SU(d)$ are "locally isomorphic."[38, 160]

5.3 Galërkin Expansions

To consider a d-term Galërkin expansion, insert the wavefunction

$$\psi(\mathbf{x}, t; \mathbf{a}) \equiv \sum_{j=1}^{d} A_{n_j}(t)\psi_{n_j}(x, t; \mathbf{a}), \tag{5.20}$$

which is a superposition of n_1st through n_dth eigenstates, into the Schrödinger equation (5.1).

Taking the expectation of both sides of (5.1) for the state (5.20) when $\mathbf{a} \in \mathbb{R}^s$ yields[160]

$$\begin{aligned} \left\langle \psi \left| -\frac{\hbar^2}{2m_0}\nabla^2\psi \right. \right\rangle &= K\left(|A_{n_1}|^2, \cdots, |A_{n_d}|^2; \mathbf{a}\right), \\ i\hbar \left\langle \psi \left| \frac{\partial\psi}{\partial t} \right. \right\rangle &= i\hbar \left[\sum_{k,j=1, k\neq j}^{d} \dot{A}_{n_k} A^*_{n_j} \right. \\ &\quad \left. + \sum_{k=1}^{d} \nu_{n_k n_k} |A_{n_k}|^2 + \sum_{k,j=1, k\neq j}^{d} \nu_{n_k n_j} A_{n_k} A^*_{n_j} \right]. \end{aligned} \tag{5.21}$$

Denoting $A_j \equiv A_{n_j}$, equating coefficients in the quadratic form (5.21) leads to the amplitude equations

$$i\dot{A}_k = \sum_{j=1}^{d} D_{kj} A_j, \tag{5.22}$$

which describe the electronic *dof* of vibrating quantum billiards.[154, 160, 189]

When $s = 1$, one defines the *coupling parameter* $\mu_{n_k n_j}$ with the relation

$$\nu_{n_k n_j} \equiv \frac{\dot{a}}{a}\mu_{n_k n_j}. \tag{5.23}$$

(When $s \geq 2$, the factor $\dot{a}/a$ is replaced by a sum of factors representing each of the boundary constituents. This is illustrated for $s = 2$ in Chapter 11 using the vibrating rectangular quantum billiard.) In (5.22), the diagonal terms of the Hermitian matrix $D \equiv (D_{kj})$ are

$$D_{kk} = \frac{\epsilon_{n_k}}{\hbar a^2} \tag{5.24}$$

and the off-diagonal terms are given by

$$D_{kj} = -i\mu_{n_k n_j}\frac{\dot{a}}{a}. \tag{5.25}$$

The parameter $\mu_{kj} \equiv \mu_{n_k n_j} = -\mu_{n_k n_j} \neq 0$ is the coupling coefficient for the cross term $A_{n_k}A^*_{n_j}$. If a coupling coefficient vanishes, the present situation reduces to a lower-dimensional case. The *Quantum Number Symmetry Theorem*, which is stated and proved in Chapter 6, gives the conditions under which coupling coefficients vanish when $s = 1$.

The equations of motion describing the nuclear *dof* are given by Hamilton's equations applied to the boundary:

$$\begin{aligned} \dot{a} &= \frac{\partial H}{\partial P}, \\ \dot{P} &= -\frac{\partial H}{\partial a}. \end{aligned} \tag{5.26}$$

Using a diabatic basis, the Hamiltonian H is given by

$$H = \frac{P^2}{2M} + \left(|A_1|^2, \cdots, |A_d|^2; a\right) + V(a). \tag{5.27}$$

We postpone writing equations (5.26) explicitly the complex amplitudes A_j have been transformed to real variables. This may be done using either Bloch coordinates (described below) or action-angle coordinates (described in Chapter 12).

5.4 Bloch Variables

Tranforming to Bloch variables using equations (A.1) and simplifying using equations (A.4) yields a coupled system of $d^2 + 1$ nonlinear ordinary differential equations to describe a d-mode Galërkin expansion of a vibrating quantum billiard, which is a d *dof* Hamiltonian system when written canonically.[160] There are $(d-1)d/2$ equations of motion for the x-Bloch variables, $(d-1)d/2$ equations of

motion for the y-Bloch variables, $(d-1)$ equations for the z-Bloch variables, and Hamilton's equations for $\dot{a}$ and $\dot{P}$.

The equation for $\dot{x}_{kl}$ takes the form

$$\dot{x}_{kl} = -\frac{\omega_{kl} y_{kl}}{a^2} - \frac{2\mu_{kl} P z_{kl}}{Ma} + \frac{P}{Ma} \sum_{j=1,\ k\notin\{k,l\}}^{d} \pm\mu_{kj} x_{jl}, 256 \tag{5.28}$$

where the *coupling frequency* $\omega_{kl} \equiv (\epsilon_l - \epsilon_k)/\hbar$ and the terms in the sum in the equation for $\dot{x}_{12}$ all have negative signs. The signs of the terms in the other x-Bloch variable equations are then determined from the constraints derived in the Appendix. One differentiates equation (A.2) to obtain

$$\sum_{k,l=1,\ k<l}^{d} \left[d\left(x_{kl}\dot{x}_{kl} + y_{kl}\dot{y}_{kl} \right) + 2 z_{kl}\dot{z}_{kl} \right] = 0. \tag{5.29}$$

In order to satisfy (5.29), the signs of the terms in the sum in equation (5.28) must cancel each other out appropriately. One thereby determines all the appropriate signs in the equations of motion for the x-Bloch variables from the known signs in the equation for $\dot{x}_{12}$, as the terms in question (that are of the form $x_{ij}x_{kl}$) all come from dynamical equations for other x-Bloch variables.

The equations of motion for the y-Bloch variables take the form

$$\dot{y}_{kl} = \frac{\omega_{kl} x_{kl}}{a^2} + \frac{P}{Ma} \sum_{j=1,\ j\notin\{k,l\}}^{d} \pm\left(\mu_{kj} x_{jl} - \mu_{lj} y_{kj} \right), \tag{5.30}$$

where all the terms are positive in the dynamical equation for $\dot{y}_{12}$ and the signs of the terms in the other equations are determined using equations (5.29,5.30).

The equations of motion for $\dot{z}_{k,k+1}$ take the form

$$\dot{z}_{k,k+1} = 2\frac{\mu_{k,k+1} P x_{k,k+1}}{Ma} + \frac{P}{Ma} \sum_{j=1,\ j\notin\{k,k+1\}}^{d} \left[\mu_{kj} x_{kj} + \mu_{j,k+1} x_{j,k+1} \right], \tag{5.31}$$

as all terms with k as the left subscript or $(k+1)$ as the right subscript are positive. To obtain equation (5.31), one then uses the fact that $\mu_{n_j n_k} = -\mu_{n_k n_j}$.

Hamilton's equations,

$$\dot{a} = \frac{P}{M} \equiv \frac{\partial H}{\partial P},$$
$$\dot{P} = -\frac{\partial V}{\partial a} - \frac{\partial K}{\partial a} \equiv -\frac{\partial H}{\partial a}, \tag{5.32}$$

are derived using the kinetic and potential energies and the dynamical equations for the z-Bloch variables (5.31).[160]

The kinetic energy is expressed as

$$K = \frac{2}{da^2}\left[\sum_{k<l} z_{kl}\epsilon_{kl}^{-} + \epsilon^{+}\right], \tag{5.33}$$

where

$$\epsilon_{kl}^{-} \equiv \frac{\epsilon_l - \epsilon_k}{2},$$
$$\epsilon^{+} \equiv \frac{1}{2}\sum_{j=1}^{d} \epsilon_j. \tag{5.34}$$

Hence,

$$\frac{\partial K}{\partial a} = -\frac{4}{da^3}\left[\sum_{k,l=1,\ k<l}^{d} z_{kl}\epsilon_{kl}^{-} + \epsilon^{+}\right]$$
$$+ \frac{2}{da^3}\left[\epsilon_{kl}^{-}\left(2\mu_{kl}x_{kl} + \sum_{j=1,\ j\notin\{k,l\}}^{d}\left[\mu_{kj}x_{kj} + \mu_{jl}x_{jl}\right]\right)\right]. \tag{5.35}$$

5.5 Equilibria

The equilibria of the present (d^2+1)-dimensional dynamical system (5.28, 5.30, 5.31, 5.32) satisfy $P = 0$, $x_{kl} = y_{kl} = 0$,

$$\sum_{k,l=1,k<l}^{d} z_{kl}^2 = d - 1, \tag{5.36}$$

and

$$\frac{\partial V}{\partial a} = \frac{4}{da^3}\left[\epsilon^{+} + \sum_{k,l=1,k<l}^{d} z_{kl}\epsilon_{kl}^{-}\right]. \tag{5.37}$$

Using $z_{lk} = \rho_{ll} - \rho_{kk}$, the definition of density matrices, equation (5.36), and constraints analogous to those given by equations (A.5)-(A.7) for the case $d = 4$ shows (after an extraordinarily tedious calculation that is most easily done after one has specified the parameter d) that for each equilibrium, the jth complex amplitude $|A_j|$ (where $j \in \{1, \cdots, d\}$) is unity and all the others vanish.[160] That is, the jth equilibrium corresponds to the jth *pure state* (in which only the jth eigenfunction is present). This is exactly what we expected physically.

The jth equilibrium eigenstate has energy

$$E_j = \frac{2\epsilon_j}{a_*^2}, \tag{5.38}$$

where a_* is the value of the displacement at equilibrium. Hence, the equilibrium condition (5.37) may also be expressed as

$$\frac{\partial V}{\partial a}(a_*) = \frac{2\epsilon_j}{a_*^3}, \quad j \in \{1, \cdots, d\}. \tag{5.39}$$

The fact that each equilibrium of a vibrating quantum billiard must be a pure state corresponds to our physical expectations of the simple molecular systems they model. (This physical interpretation is discussed in more detail below.)

The equilibrium radii of pure states are determined by equation (5.39). If the energy

$$E \equiv V(a) + K(z_{ij}, a) \tag{5.40}$$

has exactly one minimum with respect to a, then the time-derivative of the momentum $\dot{P}$ vanishes precisely once if one varies a and holds the quantum variables constant. In this situation, each equilibrium pure state has a single corresponding equilibrium radius. Hence, these equilibria must be stable elliptic.[160] (An equilibrium is said to be *elliptic* if the real parts of its eigenvalues all vanish.[23, 70, 114])

As the kinetic energy $K(a) > 0$, the only way for E to have multiple minima is to adjust the external potential $V(a)$, which we interpret physically in section

5.6.[160] If $V(a)$ is has a single minimum (i.e., if $V(a)$ is a "single-well potential" in quantum-mechanical terminology), as is case with the harmonic potential,

$$V(a) = V_0(a - a_0)^2, \tag{5.41}$$

then E necessarily has a single minimum.

The occurrence of multiple minima is reminiscent of the "symmetry breaking" that occurs in quantum field theory and condensed matter physics.[40, 150] The present model shows that this can occur in molecular physics as well, so vibrating quantum billiards provide a further hint at the relationship between molecular systems and quantum field-theoretic systems at which some authors have hinted.[20] In particular, if one uses a quartic, double-well potential (as is discussed in Chapter 7), one recovers the same Landau transition.[155]

5.6 Physical Interpretation

A d-mode Galërkin expansion of a vibrating quantum billiard with s time-dependent boundary constituents models d-fold electronic near-degeneracies in a polyatomic molecule with s excited nuclear modes. The potential $V(\mathbf{a})$ *describes the mechanical motion of the molecule's interatomic bonds.*[154] The resulting vibronic interaction between the nuclear and electronic *dof* of vibrating quantum billiards is reminiscent of Jahn-Teller distortions.[19, 20, 126, 189, 202]

In the context of quantum-mechanical systems, d-mode Galërkin projections correspond to d-term superposition states.[154, 160] We wish to consider when such a state occurs in physical systems relevant to vibrating quantum billiards in light of the discussion of semiquantum physics in Chapter 2.

In a d-mode Galërkin expansion, the eigenstates that have been ignored are assumed to contribute negligibly to the system's dynamics. As vibrating quantum billiards are Hamiltonian, this is not true mathematically in the systems of inter-

est. Hence, a different choice of d yields a different physical system. In Jahn-Teller theory, it is permissible to consider only d eigenstates when they are energetically close and are energetically isolated from the states being ignored. As the problem of interest is a type of Jahn-Teller distortion, this physical justification carries over to vibrating quantum billiards.[154, 160] Hence, a d-fold electronic near-degeneracy in a molecular system requires at least a d-mode Galërkin projection of the Schrödinger equation (5.1) to be described from the perspective of this work. A common cause of such near-degeneracy is symmetry,[18, 189] which we will discuss in more detail in Chapter 6 when we state and prove the Quantum Number Symmetry Theorem.[154, 157, 159]

The semiquantum regime aptly describes the dynamics of molecules when they undergo nonadiabatic transitions.[154, 189, 202] In this regime, the nuclear degrees-of-freedom are treated classically, whereas the electronic degrees-of-freedom are treated quantum-mechanically.[36, 189] One uses a d-term Galërkin projection when the (electronic) eigenenergy corresponding to the $(d+1)$st term is sufficiently larger than that corresponding to the 1st through dth states that it may be ignored. As the first d electronic energy levels are either degenerate or nearly so, the use of d-mode Galërkin expansions allows one to explore the nonadiabatic transitions involving their associated eigenstates.[20, 154]

From equation (5.33), observe that when $s = 1$, near-degeneracies occur as a becomes large. (This is also true for $s \geq 2$.) An exact degeneracy occurs at $a = \infty$, although the displacement variable a is always finite for real molecular systems. Such near-degeneracies have been observed in the lowest ionic and covalent states of alkali halides such as NaCl.[79] In terms of the present model, the resulting nonadiabatic transitions in diatomic molecules are described by the case $s = 1$, $d = 2$. It is noteworthy that the prediction of near-degeneracies at large radii was

obtained before we were aware that this fact was known experimentally. Moreover, analogous situations are known to occur in more complicated polyatomic molecules.

Molecular systems frequently exhibit degeneracies or near-degeneracies involving only a few eigenstates.[19, 20, 189] This, along with the results discussed in the above paragraph, provides a rationale for the analysis of few-mode Galërkin expansions and the resulting low-dimensional systems of ordinary differential equations.

The time-dependent constituents of the boundary of the vibrating quantum billiard are treated classically, so they yield the billiard's nuclear *dof*. Hence, the s *dof* describing the motion of its boundary represent s excited nuclear modes in a polyatomic molecule such as benzene.[154, 160]

Finally, the external potential $V(\mathbf{a})$ represents the stiffness of the spring used to model the interatomic bonds of the molecule of interest. When V is harmonic, the spring under consideration is a linear one.[155] In light of prior discussions, the stability of equilibrium pure states is a consequence of the stiffness of the interatomic bonds.[155, 157] We consider the dynamical consequences of this stiffness in Chapters 7 and 8.

CHAPTER 6

QUANTUM NUMBER SYMMETRY*

Theorem 6.1 **Quantum Number Symmetry Theorem** Suppose Schrödinger's equation (5.1) is globally separable in D and that D is convex and r-dimensional. Consider a quantum billiard on D with $s = 1$ nuclear *dof*. Consider the superposition of the eigenstate ψ_n with the vector of quantum numbers $n \equiv (n_1, \cdots, n_r)$ and the eigenstate $\psi_{n'}$ with the vector of quantum numbers $n' \equiv (n'_1, \cdots, n'_r)$. Suppose without loss of generality that the rth quantum number is associated with the time-dependent portion of the boundary and that the others are associated with stationary portions of the boundary. Then ψ_n and $\psi_{n'}$ have a nonzero "interaction coefficient" $\mu_{nn'}$ if and only if $n_l = n'_l$ for all $l \in \{1, \cdots, r-1\}$.[159]

In words, the Quantum Number Symmetry Theorem implies that two eigenstates $\{\psi_n, \psi_{n'}\}$ in a Galërkin expansion of a globally separable quantum billiard with one nuclear *dof* whose domain D is r-dimensional must have $(r-1)$ equal quantum numbers (corresponding to the stationary dimensions of the billiard's boundary ∂D) to yield a nonzero interaction coefficient $\mu_{nn'}$.[159] If D is a sphere, for example, this symmetry condition means that these eigenstates must have the same angular-momentum quantum numbers.[112, 158] (This special case is discussed in detail in Chapter 10.) Additionally, Theorem 6.1 yields a necessary condition for a Galërkin expansion with $d = 2$ modes to behave chaotically.

*This chapter is based on portions of reference [159].

Proof of Theorem 6.1: The wavefunction ψ of a quantum billiard is given by the Galërkin expansion

$$\psi(\mathbf{x},t) = \beta(a(t)) \sum_n \exp\left(-\frac{iE_n t}{\hbar}\right) A_n(t)\varphi_n(\mathbf{x};\mathbf{a}(\mathbf{t})), \tag{6.1}$$

where $\mathbf{x} \in D$ and the time-dependent phase $\exp(-iE_n t/\hbar)$ of the nth eigenstate may always be separated as in equation (6.1). As in Chapter 5, $A_n(t)$ is a complex, time-dependent amplitude. Additionally, $\beta(a(t))$ is a normalization factor associated with the billiard domain D. It is the same for all eigenstates.

As $s = 1$, the vibrating quantum billiard of interest is said to have one movable-boundary (mb) quantum number and $(r-1)$ fixed-boundary (fb) quantum numbers. The components of the vector $\mathbf{x}$ associated with fb and mb quantum numbers are given the same adjective. Without loss of generality, suppose that the rth component n_r of the vector of quantum numbers $(n_1, \cdots, n_r)$ corresponds to the time-dependent boundary.

Absorbing the time-dependent phases into the complex amplitudes yields

$$\psi(\mathbf{x},t) = \beta(a(t)) \sum_n A_n(t)\varphi_n(\mathbf{x};\mathbf{a}(\mathbf{t})), \tag{6.2}$$

Because of global separability, one may write

$$\varphi_n(\mathbf{x};a(t)) = \prod_{j=1}^{r} f_j^{n_j}(x_j), \tag{6.3}$$

where the component functions $f_j^{n_j}$ are the same throughout D.

Substitute the two-term superposition state

$$\psi = A_n(t)\psi_n + A_{n'}(t)\psi_{n'}, \tag{6.4}$$

into the Schrödinger equation (5.1) to yield the quadratic form (5.21) with $d = 2$. To prove the Quantum Number Symmetry Theorem, we need to show that the interaction coefficient $\mu_{nn'}$, which is defined in equation (5.23), vanishes unless $(n_1, \cdots, n_{r-1}) = (n'_1, \cdots, n'_{r-1})$.

Separate the eigenfunctions ψ_n and $\psi_{n'}$ as in (6.3). Each of the r component functions of ψ_n and $\psi_{n'}$ is the solution of a Sturm-Liouville boundary value problem.[27, 159, 178] Consequently, each of these component functions satisfies the following orthogonality property:

$$\left\langle f_j^{n_j} \middle| f_j^{n_j'} \right\rangle = \delta_{n_j n_j'}. \tag{6.5}$$

To calculate the inner products in equations (5.21), one integrates with respect to all r spatial variables. The set of terms relevant to this argument are those in the second equation with the prefactor $\nu_{nn'}$, as–by definition–this quantity vanishes exactly when $\mu_{nn'}$ does. These terms arise from $\langle\psi|\partial\psi/\partial t\rangle$ via the product rule as follows.

Differentiating the wavefunction ψ with respect to time yields

$$\frac{\partial\psi}{\partial t} = \dot{A}_n\psi_n + \dot{A}_{n'}\psi_{n'} + A_n\frac{\partial\psi_n}{\partial t} + A_{n'}\frac{\partial\psi_{n'}}{\partial t}, \tag{6.6}$$

where

$$\begin{aligned}\frac{\partial\psi_k}{\partial t} &= \frac{\partial}{\partial t}\left[\beta(a(t))\psi_k(\mathbf{x}, a(t))\right] \\ &= \beta'(a(t))\dot{a}\psi_k + \beta(a(t))\frac{\partial\psi_k}{\partial a}\dot{a} \\ &= \dot{a}\left[\beta'(a)\psi_k + \beta(a)\frac{\partial\psi_k}{\partial a}(a)\right].\end{aligned} \tag{6.7}$$

Consequently,

$$\begin{aligned}\left\langle \psi_j \middle| \frac{\partial\psi_k}{\partial t} \right\rangle &= \left\langle \beta(a)\psi_j(a) \middle| \dot{a}\beta'(a)\psi_k(a) + \beta(a)\frac{\partial\psi_k}{\partial a}(a) \right\rangle \\ &= \langle\beta(a)\psi_j(a)\,|\dot{a}\beta'(a)\psi_k(a)\,\rangle + \left\langle \beta(a)\psi_j(a) \middle| \dot{a}\beta(a)\frac{\partial\psi_k}{\partial a}(a) \right\rangle \\ &= \dot{a}\left[\beta(a)\right]^2\left\langle \psi_j(a) \middle| \frac{\partial\psi_k}{\partial a}(a) \right\rangle\end{aligned} \tag{6.8}$$

where $\langle\psi_j|\psi_k\rangle = 0$ when $j \neq k$ by orthogonality. (The fact that $j \neq k$ was not used in any other place in (6.8).)

The dependence of ψ_j on a arises only in the mb coordinates, so–with global separability–this implies that

$$\begin{aligned}\dot{a}\left[\beta(a)\right]^2\left\langle\psi_j(a)\,|\psi'_k(a)\right\rangle &= \dot{a}\left[\beta(a)\right]^2\prod_{l=1}^{r}\left\langle f_l^{j_l}\,\middle|\,f_l^{k_l}\right\rangle\cdot\left\langle f_r^{j_r}(x_r;a(t))\,\middle|\,\frac{\partial f_r^{k_r}}{\partial a}(x_r;a(t))\right\rangle \\ &\equiv \mu_{jk}\left\langle f_r^{j_r}(x_r;a(t))\,\middle|\,\frac{\partial f_r^{k_r}}{\partial a}(x_r;a(t))\right\rangle \\ &= \mu_{nn'}\left\langle f_r^{n_r}(x_r;a(t))\,\middle|\,\frac{\partial f_r^{n'_r}}{\partial a}(x_r;a(t))\right\rangle \qquad (6.9)\end{aligned}$$

for $j = n$ and $n = n'$. Applying the orthogonality condition (6.5) to each of the *fb* components in (6.9) then shows that $\mu_{nn'} = 0$ unless $f_l^{n_l} = f_l^{n'_l}$ for all $l \in \{1,\cdots,r-1\}$. This, in turn, holds exactly when $n_l = n'_l$ for all $l \in \{1,\cdots,r-1\}$. This completes the proof of Theorem 6.1. *QED*

CHAPTER 7

ONE-MODE GALËRKIN EXPANSIONS*

Applying a one-mode Galërkin expansion, in which one considers a single eigenstate in the Schrödinger equation (5.1), yields the case of so-called *Ehrenfest dynamics.*[160] Equivalently, this situation describes the nuclear (classical) degrees-of-freedom of molecular systems after one has averaged over their electronic (quantum-mechanical) degrees-of-freedom.[154, 189] When the number of nuclear *dof* is $s = 1$, a billiard's Ehrenfest dynamics are described by a one *dof* Hamiltonian system.

7.1 Equations of Motion

Let $d = 1$ in equation (5.20), so that one is considering a single eigenstate

$$\psi(\mathbf{x}, t) = \psi_n(\mathbf{x}, t; a(t)). \tag{7.1}$$

The quantum probability $|A_n|^2 = 1$, so one obtains a classical system with Hamiltonian[155, 160]

$$H(a, P) = \frac{P^2}{2M} + K(a) + V(a), \tag{7.2}$$

where the quantum-mechanical information (consisting of the nth electronic eigenvalue of the Schrödinger equation) is encoded in the electronic kinetic energy K. The resulting equations of motion are

$$\begin{aligned} \dot{a} &= \frac{P}{M} \equiv \frac{\partial H}{\partial P}, \\ \dot{P} &= -\frac{\partial V}{\partial a} + \frac{2\epsilon_n}{a^3} \equiv -\frac{\partial H}{\partial a}, \end{aligned} \tag{7.3}$$

*This chapter is based on portions of references [155, 159, 160].

where ϵ_n is the energy parameter corresponding to the nth eigenstate of (5.1).[159] The influence of the quantum subsystem on the classical one is encompassed entirely by the parameter ϵ_n.

An equivalent way of obtaining equations (7.3) is to consider multiple eigenstates in (5.20) that fail to couple together. (See Chapter 6.) In this situation, $2\epsilon_n$ is replaced by a *reduced energy parameter*

$$\lambda \equiv 2\left(\sum_{j=1}^{d} \epsilon_j |C_j|^2\right), \tag{7.4}$$

where C_j is the jth complex amplitude, and

$$\sum_{j=1}^{d} |C_j|^2 = 1 \tag{7.5}$$

by conservation of probability. The parameter λ is positive because $\epsilon_j > 0$ and the $|C_j|^2 \geq 0$ correspond to quantum probabilities.

For the remainder of this chapter, we consider the resulting equations of motion:

$$\begin{aligned} \dot{a} &= \frac{P}{M} \equiv \frac{\partial H}{\partial P}, \\ \dot{P} &= -\frac{\partial V}{\partial a} + \frac{\lambda}{a^3} \equiv -\frac{\partial H}{\partial a}. \end{aligned} \tag{7.6}$$

7.2 Saddle-Center Bifurcation

For some potentials $V(a)$, bifurcations can occur in (7.6) as λ is varied. Equilibria of (7.6) are of the form $(a_*, 0)$, where

$$\frac{\partial V}{\partial a}(a_*) = \frac{\lambda}{a_*^3}. \tag{7.7}$$

The corresponding eigenvalues are

$$\sigma = \pm\sqrt{-\frac{1}{M}\left(\frac{\partial^2 V}{\partial a^2}(a_*) + \frac{3\lambda}{a_*^4}\right)}, \tag{7.8}$$

which are either real with opposite sign or are pure-imaginary, complex-conjugate pairs. Hence, each equilibrium is either a center or a saddle point.[155]

Every equilibrium is a center when

$$A \equiv \frac{\partial^2 V}{\partial a^2}(a_*) + \frac{3\lambda}{a_*^4} > 0. \tag{7.9}$$

This is the case, in particular, when $V(a)$ has a single minimum, such as for the harmonic potential $V = V_2(a - a_0)^2$.[155] Another interesting situation is the quartic potential $V = V_4(a - a_0)^4$, in which the interatomic bonds of the molecule of interest are stiffer.

Assuming $V_2 = V_4$ and considering the same initial conditions for both potentials, the phase-plane trajectory for the quartic potential has a larger radius of curvature. For a given initial condition, the trajectory associated with the quadratic potential tends to attain larger maximum a. For initial conditions with sufficiently small $a(0)$, the quadratic potential induces trajectories with smaller maximum $|P|$, but the quartic potential eventually yields a larger maximum $|P|$ as $a(0)$ is increased.

An equilibrium for which $A < 0$ is a saddle point. The dynamical system (7.6) is invariant under reflection about the a-axis ($P \mapsto -P$) because it is Hamiltonian and hence reversible.[67, 114, 155, 194] Hence, the local stable and unstable manifolds of an equilibrium are mapped to each other under this reflection. By symmetry, the dynamical system (7.6) has saddle connections whenever it has at least one saddle point.

As λ is increased, the quantity A also increases. Equilibria at which $A = 0$ correspond to *saddle-center bifurcations*. Such equilibria have two vanishing eigenvalues with corresponding Jacobian matrix[67, 155, 194]

$$\begin{pmatrix} 0 & 1 \\ 0 & 0 \end{pmatrix}. \tag{7.10}$$

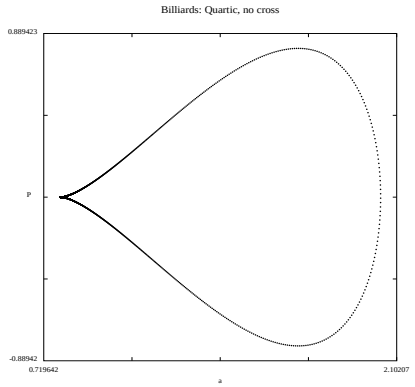

Figure 7.1: Approximate cuspidal homoclinic orbit. The initial point used was $(0.7886751, 0.001)$, which is just above the equilibrium.

Hence, saddle-center bifurcations have codimension two. Moreover, these local bifurcations are accompanied by a global bifurcation corresponding to the breaking of the separatrix.[67, 72] At saddle-center bifurcations, the Hamiltonian (7.2) has a double zero, so

$$H(a_*, 0) = \frac{\partial H}{\partial a}(a_*, 0) = 0. \tag{7.11}$$

Hence, a saddle-center bifurcation occurs when

$$\lambda_* = a_*^3 \frac{\partial V}{\partial a}(a_*, 0) \tag{7.12}$$

at the point $(a_*, 0)$ satisfying

$$\frac{\partial V}{\partial a}(a_*, 0) = -\frac{a_*}{3}\frac{\partial^2 V}{\partial a^2}(a_*, 0)\,. \tag{7.13}$$

Any solution to (7.13) with $\lambda < 0$ is discarded as nonphysical.

At the saddle-center bifurcation, the stable and unstable eigenvectors of the equilibrium coincide along the a-axis, so the stable and unstable manifolds overlap near this stationary point. The resulting cusp causes difficulties in numerical continuation attempts. The two homoclinic orbits that exist when $A < 0$ have

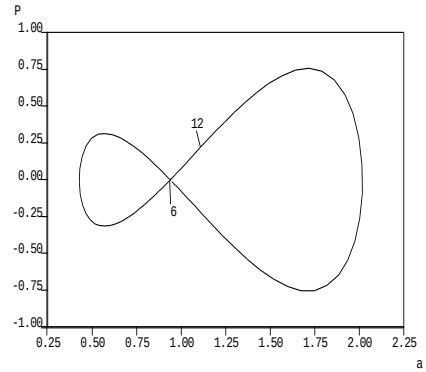

Figure 7.2: Homoclinic orbits emanating from $(0.8916637, 0)$ for $\lambda = 0.15$. The label 12 refers to the right homoclinic orbit, and the label 6 refers to the left one.

coalesced into one. As A increases, the homoclinic orbit on the left shrinks, becoming a single point at the saddle-center. Trajectories have infinite derivative with respect to arclength at the saddle-center point.

As a specific example of this phenomenon, consider the quartic potential

$$V(a) = V_4(a - a_0)^4 + V_3(a - a_0)^3 + V_2(a - a_0)^2 + V_1(a - a_0), \tag{7.14}$$

which yields a *Landau transition* analogous to those that occur in quantum field theory and condensed matter systems.[40, 150] Quartic potentials have either one or two local minima. In the latter case, a single saddle-center bifurcation occurs. Without loss of generality, suppose $V_3 = V_1 = 0$. For our numerical simulations purposes, we utilized the parameter values $a_0 = 1, V_2 = -1$, and $V_4 = 1$. (When $V_4 = -V_2$, the potential $V(a)$ is sometimes called a *Duffing potential.*) There is a saddle-center bifurcation at $\lambda_* = \frac{1}{972}\left[3 + \sqrt{3}\right]^3 \sqrt{3} \approx 0.1888176$. The corresponding stationary point is $\left(\frac{1}{2} + \frac{\sqrt{3}}{6}, 0\right) \approx (0.7886751, 0)$. Using DsTool[68], we plotted an approximation of the homoclinic orbit emanating from this equilibrium (Figure 7.1).

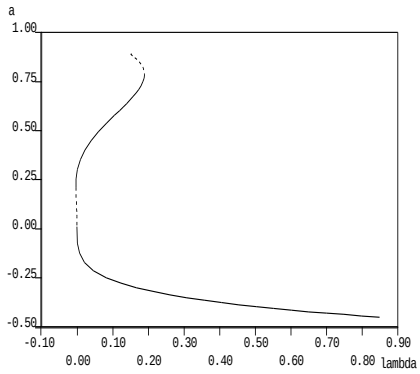

Figure 7.3: Continuation of the detuned system in the parameter λ.

7.2.1 Continuation Past the Bifurcation

Suppose the initial value of the reduced energy parameter is $\lambda < \lambda_*$ and one wishes to continue past the saddle-center point. Using AUTO,[47, 48] we follow the two homoclinic orbits for $\lambda = 0.15$ (Fig. 7.2). The codimension of the saddle connection in the present system is greater than one, as both regularity and nondegeneracy conditions are violated.[32, 33] *Degeneracy* is violated because for all $\lambda < \lambda_*$, there are two homoclinic orbits emanating from the saddle point. *Regularity* is violated because the saddle point's two eigenvalues are negatives of each other.

As the dynamical system (7.6) is degenerate and irregular, one cannot continue in λ past the saddle-center directly, as described in the AUTO manual.[47] There are several ways to resolve this problem.[32, 33, 155] In this work, we "detune" the system by adding a dissipation term to destroy the genericity of homoclinic orbits.

Hamiltonian systems are described by

$$\dot{x} = J\nabla H(x, \lambda), \quad x \in \mathbb{R}^{2n}, \tag{7.15}$$

where

$$J \equiv \begin{pmatrix} 0 & I \\ -I & 0 \end{pmatrix} \tag{7.16}$$

is the canonical $2n \times 2n$ symplectic matrix[128]. One can detune the system by using a small perturbation parameter ϵ as follows.[32] The perturbed dynamical

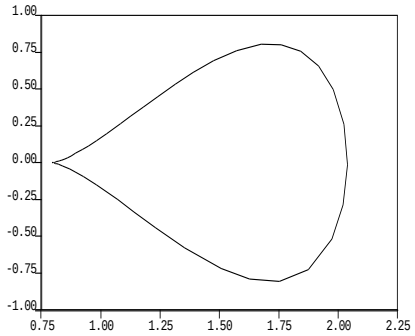

Figure 7.4: Right homoclinic orbit for $\lambda = 0.1887$.

system,

$$\dot{x} = J\nabla H(x,\lambda) + \epsilon\nabla H(x,\lambda), \tag{7.17}$$

is no longer Hamiltonian, but–by construction–the location of all equilibrium points is preserved. With this detuning, the saddle-center bifurcation becomes a saddle-node bifurcation, as the eigenvalues of the stationary point are now of the form $a \pm \sqrt{b'}$ $(a \neq 0)$ rather than of the form $\pm\sqrt{b}$. One can then continue λ past this point using AUTO.

With this technique, one can compute the value of λ at which the saddle-center bifurcation occurs as well as the cusp point of the homoclinic orbit corresponding to that value. Once one has successfully continued past the cusp, one lets $\epsilon \longrightarrow 0$ and recovers the system of interest in the regime $\lambda > \lambda_*$. In our work, we used $\epsilon < 0$, since the equilibria that are centers for $\epsilon = 0$ become stable spirals for $\epsilon < 0$. The continuation curve (in λ) is shown in Figure 7.3.

In general, AUTO has difficulties near cusps. As with DSTool, one can approximate the cuspidal homoclinic orbit using AUTO. To do so, one provides initial values for the continuation parameters (corresponding to the initial point in the (a, P)-plane) to the right of the saddle point $(a^*, 0)$. This allows AUTO to continue along the homoclinic orbit for values of λ closer to λ_* than if one had started as close to the saddle point as machine precision would allow. For the present exam-

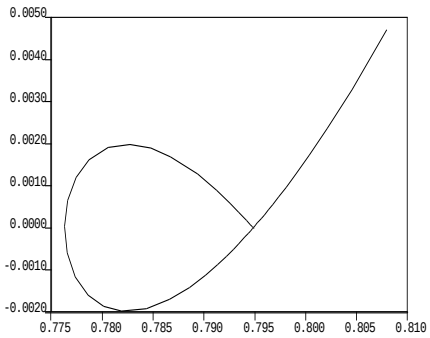

Figure 7.5: Left homoclinic orbit for $\lambda = 0.1887$.

ple, the closest plot we obtained corresponds to $\lambda = 0.1887$. The right homoclinic orbit is shown in Figure 7.4, and the left one is shown in Figure 7.5. Observe that the one on the right *looks* like it has a cusp at the saddle point because the left homoclinic orbit is very small. As the saddle-center is approached, the left homoclinic orbit shrinks to a single point and the right one becomes more cusplike.

7.3 Dynamics Near $a = \infty$

To examine the Ehrenfest dynamics of quantum billiards with one nuclear *dof* near $a = \infty$, one makes the transformation

$$\begin{aligned} v &\equiv \frac{P}{a}, \\ w &\equiv \frac{1}{a}. \end{aligned} \tag{7.18}$$

From (7.18), one obtains

$$\frac{\partial V}{\partial a} = -\frac{1}{a^2}\frac{\partial V}{\partial w} = -w^2\frac{\partial V}{\partial w}. \tag{7.19}$$

This yields the follow equations of motion:

$$\begin{aligned} \dot{v} &= -\frac{v^2}{M} + w^3\frac{\partial V}{\partial w} + \lambda w^4, \\ \dot{w} &= -\frac{vw}{M}. \end{aligned} \tag{7.20}$$

Equilibria of (7.20) satisfy either $v = 0$ or $w = 0$. Applying (7.18), we note that $a = P$ when $v = 0$ and $a = \infty$ when $w = 0^+$. We are concerned with positive values of the variable w because the displacement a must be positive. When $v = 0$, the relation

$$\frac{\partial V}{\partial w} + \lambda w = 0 \tag{7.21}$$

must also hold. When $w = 0$, one instead obtains

$$v^2 = M w^3 \frac{\partial V}{\partial w}, \tag{7.22}$$

which forces the condition $v = 0$ for some choices of the potential V. The Jacobian matrix is

$$J = \begin{pmatrix} -\frac{2v}{M} & 3w^2 \frac{\partial V}{\partial w} + w^3 \frac{\partial^2 V}{\partial w^2} + 4\lambda w^3 \\ -\frac{w}{M} & -\frac{v}{M} \end{pmatrix}. \tag{7.23}$$

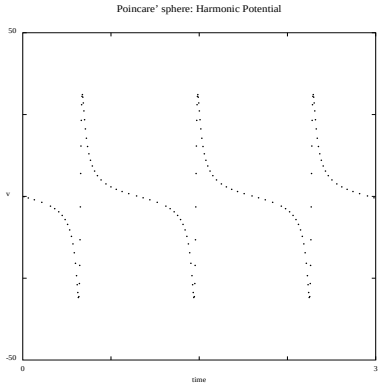

Figure 7.6: Time series in $v(t)$ for the Ehrenfest dynamics at infinity in a harmonic potential. The initial conditions are $v(0) = 0$, $w(0) = 0.2$, $\epsilon_1 = \pi^2/2 \approx 4.9348022$, $\epsilon_2 = 2\pi^2 \approx 19.7392088$, $c_1^2 = 0.75$, $c_2^2 = 0.25$, $V_2 = 5$, and $V_1 = 1$.

Suppose $V = V_2(a - a_0)^2 + V_1(a - a_0)$ and let $a_0 = 0$ without loss of generality. The equations of motion (7.20) become

$$\begin{aligned} \dot{v} &= -\frac{v^2}{M} - 2V_2 - V_1 w + \lambda w^4, \\ \dot{w} &= -\frac{vw}{M}. \end{aligned} \tag{7.24}$$

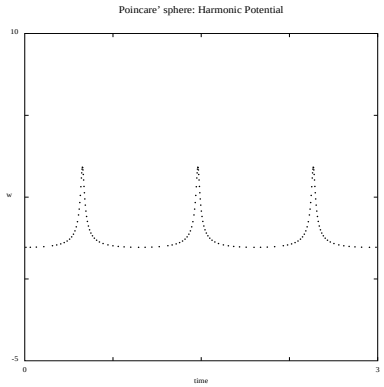

Figure 7.7: Time series in $w(t)$ corresponding to the same equations of motion, initial conditions, and parameter values as in Figure 7.6.

The condition $w = 0$ then implies that $v^2 = -2MV_2$, which cannot occur since $V_2 > 0$. Hence, all equilibria satsify $v = 0$ and

$$-2V_2 - V_1 w + \lambda w^4 = 0. \tag{7.25}$$

The Jacobian (7.23) becomes

$$J = \begin{pmatrix} -\frac{2v}{M} & -V_1 + 4\lambda w^3 \\ -\frac{w}{M} & -\frac{v}{M} \end{pmatrix}. \tag{7.26}$$

The eigenvalues of this system's equilibria consequently satisfy

$$\sigma = -\frac{3v}{2M} \pm \frac{1}{2}\sqrt{\frac{v^2}{M^2} + \frac{4V_1}{M}w - \frac{16\lambda}{M}w^4}. \tag{7.27}$$

One obtains saddles when $2v^2/M - V_1 w + 4\lambda w^4 < 0$, stable nodes when the reverse inequality holds, and a saddle-node bifurcation if there is equality. Analogous to the saddle-center in equation (7.6), this bifurcation occurs as one increases the energy parameter λ. The equilibria undergo a transition from a saddle to a sink by decreasing V_1 since $w = 1/a > 0$. Note additionally that V_1 must be positive for a saddle to occur. Moreover, the special case with $\lambda = 0$ (zero energy) and $V_1 = 0$ (symmetric harmonic potential) yields the eigenvalues $\sigma = -v/M, -2v/M$.

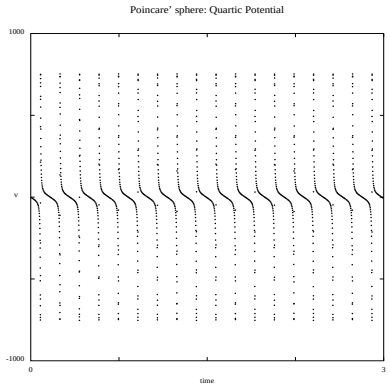

Figure 7.8: Time series in $v(t)$ for the Ehrenfest dynamics at infinity in a quartic potential. The initial conditions are $v(0) = 0$, $w(0) = 0.2$, $\epsilon_1 = \pi^2/2 \approx 4.9348022$, $\epsilon_2 = 2\pi^2 \approx 19.7392088$, $c_1^2 = 0.75$, $c_2^2 = 0.25$, $V_4 = 5$, $V_3 = V_2 = 0$, and $V_1 = 1$.

If $w(0) = 0$, then $w = 0$ for all time. This yields an invariant manifold that solutions cannot cross. The flow on this manifold is given by solutions to

$$\dot{v} = -\frac{v^2}{M} - 2V_2 < 0. \tag{7.28}$$

As $w = 1/a$, we are interested in the case $w > 0$. To approach $a = \infty$ (i.e., $w = 0^+$), we examine solutions asymptotically as they approach the line $w = 0$ from above.

From equation (7.24), one obtains

$$\frac{dw}{w} = -\frac{v}{M}dt \tag{7.29}$$

with separation of variables. Hence,

$$w = w^0 \exp\left[-\frac{1}{M}\int_{-\infty}^{t} v ds\right], \tag{7.30}$$

where $w^0 \equiv w(0)$. One then inserts (7.30) into (7.24) to obtain

$$\dot{v} = -\frac{v^2}{M} - 2V_2 - V_1 w^0 \exp\left[-\frac{1}{M}\int_{-\infty}^{t} v ds\right] + \lambda (w^0)^4 \exp\left[-\frac{4}{M}\int_{-\infty}^{t} v ds\right]. \tag{7.31}$$

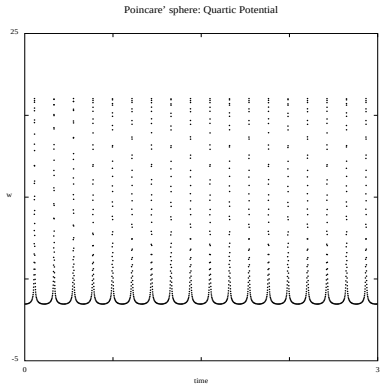

Figure 7.9: Time series in $w(t)$ corresponding to the same equations of motion, initial conditions, and parameter values as in Figure 7.8.

Near $a = \infty$, $w^0 = 1/a(0) \approx 0$, so the last two terms in equation (7.31) become increasingly negligible as the interatomic distance a becomes large. Consequently,

$$\dot{v} \sim -\frac{v^2}{M} - 2V_2 \tag{7.32}$$

as $w^0 \longrightarrow 0$. Therefore,

$$v \sim \sqrt{2MV_2}\tan\left[-\sqrt{\frac{2V_2}{M}}t + c_0\right] \tag{7.33}$$

as $a(0) \longrightarrow \infty$. The parameter c_0 is a constant of integration reflecting the initial condition $v(0) = P(0)/a(0)$. The units of the variable v are mass/time, so its initial value represents a frequency during the transition $a \longrightarrow \infty$. Figure 7.6 illustrates the tangent-like time-dependence in the variable v. Figure 7.7 shows the corresponding bursting behavior in the inverse displacement w. (The mass M was normalized to unity in both plots.)

Now consider the case $V = V_4a^4 + V_3a^3 + V_2a^2 + V_1a$, for which the equations of motion (7.20) become

$$\begin{aligned}\dot{v} &= -\frac{v^2}{2M} - \frac{4V4}{w^2} - \frac{3V_3}{w} - 2V_2 - V_1w + \lambda w^4, \\ \dot{w} &= -\frac{vw}{M}.\end{aligned} \tag{7.34}$$

As $w = 0$ is now singular, all equilibria satisfy $v = 0$ and

$$-4V_4 - 3V_3 w - 2V_2 w^2 - V_1 w^3 + \lambda w^6 = 0. \tag{7.35}$$

The presence of powers of w in denominators in equation (7.34) prevents the use of the simple asymptotic procedure we applied above. The time-dependence obtained numerically in this case with $V_4 = 0$, $V_2 = 0$, and all other parameter values and initial conditions the same as in Figures 7.6 and 7.7 is of a similar form as that for harmonic potentials. However, the range of v is considerably larger and the periodicity of both v and w is smaller. (The range of w is larger as well, but the magnitude of its increase is much smaller than that of v.) Figures 7.8 and 7.9 respectively depict time series in v and w. (The mass M was normalized to unity for these numerical calculations as well.)

CHAPTER 8

TWO-MODE GALËRKIN EXPANSIONS*

Applying a two-mode Galërkin expansion, in which one considers two eigenstates in the Schrödinger equation (5.1), allows one to examine nonadiabatic dynamics in polyatomic molecules with double electronic near-degeneracies. When $s = 1$, a two-mode Galërkin expansion yields a two *dof* Hamiltonian system.[154, 159, 160]

8.1 Equations of Motion

Let $d = 2$ in equation (5.20), so that one is considering the superposition of two eigenstates[160]

$$\psi_{nn'}(\mathbf{x}, t) \equiv A_n(t)\psi_n(\mathbf{x}, t) + A_{n'}(t)\psi_{n'}(\mathbf{x}, t), \tag{8.1}$$

which is inserted into the Schrödinger equation (5.1).

Taking the expectation of both sides of (5.1) for the state (8.1) yields

$$\begin{aligned} \left\langle \psi_{nn'} \left| -\frac{\hbar^2}{2m_0}\nabla^2\psi_{nn'} \right\rangle \right. &= K\left(|A_n|^2, |A_{n'}|^2; a_1, \cdots, a_s\right) \\ i\hbar \left\langle \psi_{nn'} \left| \frac{\partial\psi_{nn'}}{\partial t} \right\rangle \right. &= i\hbar\left[\dot{A}_n A^*_{n'} + \dot{A}_{n'}A^*_n \right. \\ &\quad \left. + \nu_{nn}|A_n|^2 + \nu_{n'n'}|A_{n'}|^2 + \nu_{nn'}A_nA^*_q + \nu_{n'n}A_{n'}A^*_n\right]. \end{aligned} \tag{8.2}$$

When $s = 1$, the electronic kinetic energy is given by

$$K = K\left(|A_n|^2, |A_{n'}|^2; a\right). \tag{8.3}$$

*This chapter is based on portions of references [155, 159, 160].

Defining $A_1 \equiv A_n$ and $A_2 \equiv A_{n'}$, the quadratic form (8.2) yields

$$i\dot{A}_k = \sum_{j=1}^{2} D_{kj} A_j, \tag{8.4}$$

where

$$(D_{kj}) = \begin{pmatrix} \frac{\epsilon_1}{\hbar a^2} & -i\mu_{12}\frac{\dot{a}}{a} \\ i\mu_{12}\frac{\dot{a}}{a} & \frac{\epsilon_2}{\hbar a^2} \end{pmatrix}, \tag{8.5}$$

the parameter ϵ_j is the jth energy coefficient, and $\mu_{12} \equiv \mu_{nn'} = -\mu_{21} \neq 0$ is a coupling coefficient for the cross term $A_n A_{n'}^*$.

The parameter $\mu_{nn'}$, which describes the strength of the interaction between ψ_n and $\psi_{n'}$, is defined by the relation

$$\nu_{nn'} \equiv \frac{\dot{a}}{a}\mu_{nn'}. \tag{8.6}$$

If $\mu_{nn'} = 0$, ψ_n and $\psi_{n'}$ do not couple with each other, so one obtains the one *dof* Hamiltonian system (7.6) studied in Chapter 7.[159, 160] The Quantum Number Symmetry Theorem, which we stated and proved in Chapter 6, gives the conditions under which $\mu_{nn'}$ vanishes for a given pair of eigenstates $\{\psi_n, \psi_{n'}\}$. For the remainder of this chapter, it is assumed that $\mu_{12} \neq 0$.

Using Bloch variables,[160] the kinetic energy K is given by

$$K(z, a) = \frac{1}{a^2}(\epsilon_+ + z\epsilon_-), \tag{8.7}$$

where

$$\epsilon_\pm \equiv \frac{1}{2}(\epsilon_2 \pm \epsilon_1). \tag{8.8}$$

Two-mode Galërkin expansions of vibrating quantum billiards with $s = 1$ nu-

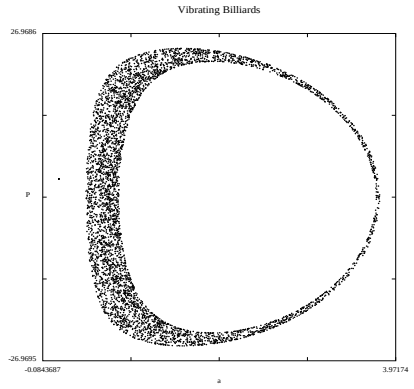

Figure 8.1: Poincaré section for the cut $x = 0$ showing both hard chaos and global chaos.

clear *dof* are thus described by the following equations of motion:

$$\begin{aligned}
\dot{x} &= -\frac{\omega_0 y}{a^2} - \frac{2\mu_{12} P z}{Ma}, \\
\dot{y} &= \frac{\omega_0 x}{a^2}, \\
\dot{z} &= \frac{2\mu_{12} P x}{Ma}, \\
\dot{a} &= \frac{P}{M}, \\
\dot{P} &= -\frac{\partial V}{\partial a} + \frac{2[\epsilon_+ + \epsilon_-(z - \mu_{12} x)]}{a^3},
\end{aligned} \tag{8.9}$$

where

$$\omega_0 \equiv \frac{\epsilon_2 - \epsilon_1}{\hbar}. \tag{8.10}$$

The equilibria for the dynamical system (8.9) satisfy $x = y = 0$, $z = \pm 1$, $a = a_*$, and $P = 0$, where the equilibrium radii $\{a_*\}$ are solutions of the equation

$$\frac{\partial V}{\partial a}(a_*) = \frac{2}{a_*^3}(\epsilon_+ \pm \epsilon_-). \tag{8.11}$$

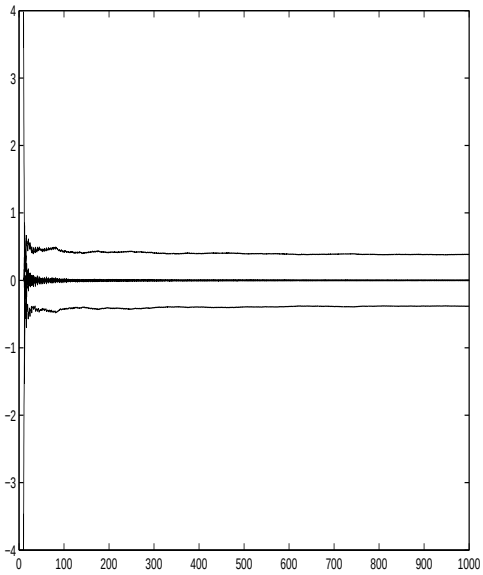

Figure 8.2: Liapunov exponents computed over 1000 time steps for the trajectory depicted in Figure 8.1. Observe the convergence of the largest Liapunov exponent, indicating that the configuration under consideration exhibits (exponentially) sensitive dependence on initial conditions.

Consequently,

$$\frac{\partial V}{\partial a}(a_*) = \frac{2\epsilon_j}{a_*^3}, \quad j \quad \in \{1, 2\}. \tag{8.12}$$

For the harmonic potential (5.41), the equilibrium radii $a_* = a_\pm$ satisfy

$$a - a_0 = \frac{\epsilon_k}{V_0 a^3}, \quad k \in \{1, 2\}, \tag{8.13}$$

where the subscript $\pm$ corresponds to $z = \pm 1$. When $z = +1$, the system is entirely in the 2nd state, whereas when $z = -1$, the system is entirely in the 1st state. Each equilibrium has one identically zero eigenvalue that corresponds to the row in the Jacobian matrix arising from the derivatives of $\dot{z}(a, P, x, y, z) \equiv f_3(a, P, x, y, z)$. Additionally, each equilibrium is elliptic provided $V(a) + K(a)$ has a single minimum with respect to a. For elliptic equilibria, the other four eigenvalues constitute two pure imaginary complex conjugate pairs.

Generalizations of saddle-center bifurcations occur when this ellipticity condition is not satisfied.[155] In this event, some equilibrium pure states admit multiple

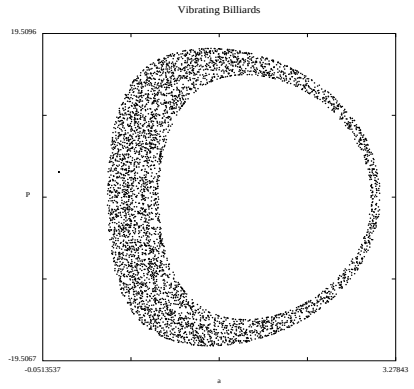

Figure 8.3: Poincaré section for the cut $x = 0$ showing global chaos. Note, however, there are some islands of integrability.

corresponding radii, as for non-elliptic equilibria, equation (8.12) is satisfied for multiple values of a_* for the given eigenstate. We examined an example of such a symmetry-breaking for the case $d = 1$ in Chapter 7.

8.2 Numerical Simulations

We investigate the dynamics of equation (8.9) numerically when the potential V is harmonic (5.41). In this situation (as discussed in Chapter 5), all equilibria are elliptic.

One may examine the transitions from local to global chaos and from soft to hard chaos in equations (8.9).[70] In accord with KAM theory,[67, 74, 114, 159, 194] the number of nonresonant tori that have been broken up depends on the initial condition of a given trajectory. Figure 8.1 and Figures 8.3–8.7 illustrate several types of behavior. Each of these plots displays a $x = 0$ Poincaré section projected into the (a, P) plane. The parameter values in each figure are $\hbar = 1$, $M = 10$, $\epsilon_1 = \pi^2/2 \approx 4.9348022$, $\epsilon_2 = 2\pi^2 \approx 19.7392088$, $\mu = 4/3$, $V_0 = 5$, and $a_0 = 1.25$.

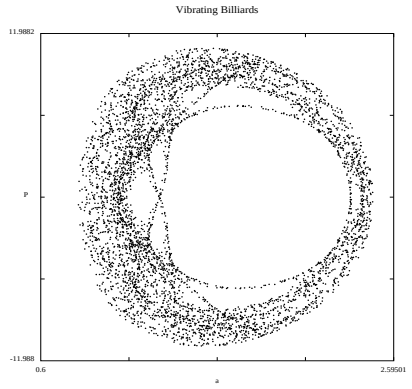

Figure 8.4: Poincaré section for the cut $x = 0$ showing global but soft chaos.

The initial values of the Bloch variables are $x(0) \approx 0.15643446504$, $y(0) = 0$, and $z(0) \approx -0.987688340595$.

Figure 8.1 exhibits both global and hard chaos, as no KAM tori have been preserved. The initial radius in this plot is $a(0) \approx 0.421559382$, and the initial momentum is $P(0) \approx 4.108129046$. Figure 8.2 shows a plot of the Liapunov exponents (up to 1000 time steps) of the corresponding trajectory. (The algorithm used to produce this data was formulated by Alan Wolf and co-workers[51, 195] and was implemented in Matlab by Steve Wai Kam Siu.) For each of the Liapunov exponents calculated for (8.9), the initial conditions and parameter values discussed above were truncated to five significant digits after the decimal point.

The computed Liapunov exponents (after 1000 time steps) in Figure 8.2 are 0.38405, 0.0013189, 0.0012954, -0.0030214, and -0.38365. In exact arithmetic, the central three eigenvalues must always vanish, so they yield an estimate of the level of precision of this calculation. The five-dimensional dynamical system (8.9) can be represented canonically as a four-dimensional (two *dof*) Hamiltonian system (see Chapter 12), so the middle eigenvalue must vanish. (Recall the related fact

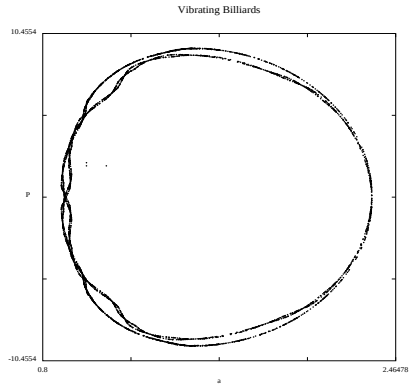

Figure 8.5: Poincaré section for the cut $x = 0$ showing local and soft chaos. Unlike in Figure 8.4, the trajectory whose Poincaré cut is depicted in this plot has not experienced large excursions outside the trapping region.

that each equilibrium point of (8.9) has an eigenvalue that always vanishes.) As the present system is Hamiltonian, the other two central eigenvalues must also vanish in exact arithmetic.[114] Moreover, the largest and smallest eigenvalues are negatives of each other. Hence, we need only consider the largest Liapunov exponent. The other exponents yield information about the precision of the calculation rather than about the dynamical system itself.

The largest Liapunov exponent after 1000 time steps is $\sigma_1 \approx 0.38405 > 0$. Figure 8.2 indicates a nice convergence to this value (and a gradual decrease in value of the other exponents), so one may confidently assert that Figure 8.1 demonstrates exponential divergence and hence chaotic dynamics.

Figure 8.3 was produced with $(a(0), P(0)) \approx (0.56446338, 1.4483064979)$. It exhibits global chaos, but some islands of integrability are present. The largest Liapunov exponent for the corresponding trajectory is $\sigma_1 \approx 0.28152$. Figure 8.4 has initial conditions $(a(0), P(0)) \approx (0.834426762, 2.741617601)$, whereas Figure

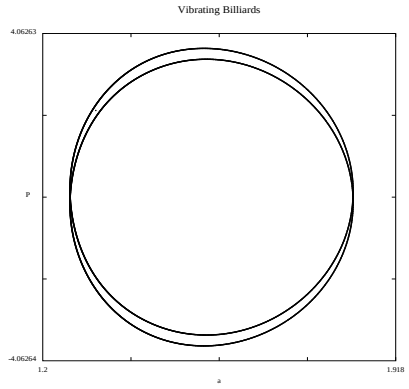

Figure 8.6: Poincaré section for the cut $x = 0$ showing integrability (or at least near-integrability).

8.5 has initial values $(a(0), P(0)) = (0.9, 2)$. Examining these two plots together provides a good picture of the transition from local to global chaos, which occurs before the transition from soft to hard chaos. The largest Liapunov exponent for the trajectory in Figure 8.4 is $\sigma_1 \approx 0.084145$, whereas that for the trajectory in Figure 8.5 is $\sigma_1 \approx 0.01564$. Although their Liapunov exponents and consequently their degrees of instability are of the same order of magnitude, their associated Poincaré sections reveal contrasting behavior. Figure 8.4 depicts global soft chaos, whereas Figure 8.5 shows local soft chaos. The configuration in the former figure exhibits a *trapping region*, near which the trajectory spends a significant amount of time. (Such trapping regions are related to structures known as *cantori*, which refer to recently broken KAM tori.[70, 114])

The global nature of the chaotic dynamics in Figure 8.4 indicates that the trajectory of interest exhibits large excursions from the trapping region. By contrast, the trajectory in Figure 8.5 has not experienced such an excursion in the time-frame under examination. Additionally, the manifestation of islands in a globally

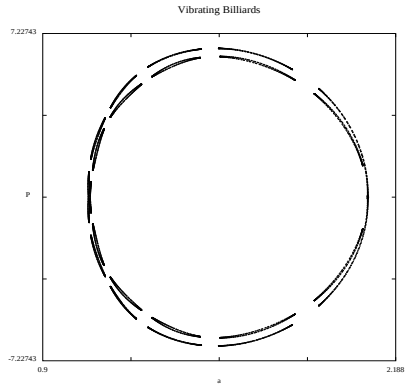

Figure 8.7: Poincaré section for the cut $x = 0$ also showing near-integrability. This trajectory is near a periodic orbit of higher period than is the one in Figure 8.6.

chaotic trajectory like that in Figure 8.4 signifies the presence of long-time correlations. Such correlations are absent in ergodic configurations (such as that depicted in Figure 8.1), so the transition from soft to hard chaos can be characterized by the destruction of long-time correlations.[114]

Figures 8.6 and 8.7 show Poincaré maps of trajectories that appear integrable when plotted numerically. By KAM theory, however, some invariant tori have been broken up (even though the numerical calculations do not reveal this).[67, 114, 194] The initial conditions for Figure 8.6 are $(a(0), P(0)) \approx (1.30794702, 2.15231788)$, and the largest Liapunov exponent is $\sigma_1 \approx 0.0052902$. This is about twice as large as the magnitude of the largest exponent ($\sigma_4 \approx -0.0025784$) that is guaranteed to vanish in exact arithmetic. This trajectory is near-integrable, but one requires better computations of Liapunov exponents to rely further on their values in this instance. Figure 8.7, whose initial conditions are $(a(0), P(0)) \approx (2.088567103, 0.000829468)$ and largest Liapunov exponent is computed to be $\sigma_1 \approx 0.0039474$ (which is not much larger than the second largest exponent), shows a

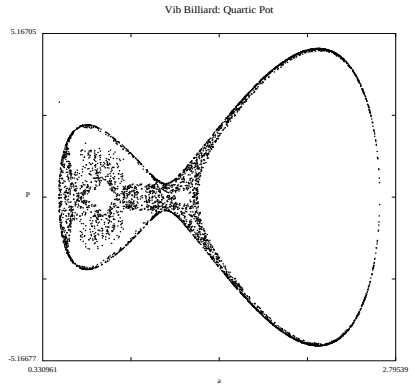

Figure 8.8: Poincaré section projected into the (a, P)-plane showing the remnants of a homoclinic orbit.

near-integrable configuration near a periodic orbit of higher period. The closed trajectories in these two surfaces of section indicate the presence of periodic and quasiperiodic behavior in the regions they enclose.[67, 114, 159, 194] One does not observe the "fuzziness" that manifests in the locally, softly chaotic situation depicted in Figure 8.5.

8.2.1 Evidence of Bifurcations

As discussed above, equilibria of (8.9) satisfy $x = P = y = 0$, $z = \pm 1$, and equation (8.11). The eigenvalues corresponding to these equilibria are of the form

$$\sigma = 0, \quad \pm \frac{\sqrt{-2M(\eta \pm \sqrt{\zeta})}}{2Ma^2}, \tag{8.14}$$

where both η and ζ have terms whose signs depend on whether z is 1 or -1. The quantities $\eta_\pm$ and $\zeta_\pm$ are given by

$$\begin{aligned}
\eta_+ &= a^4 \frac{\partial^2 V}{\partial a^2} + \omega_0^2 M - 4\mu^2 \epsilon_- + 6(\epsilon_+ + \epsilon_-), \\
\eta_- &= a^4 \frac{\partial^2 V}{\partial a^2} + \omega_0^2 M + 4\mu^2 \epsilon_- + 6(\epsilon_+ - \epsilon_-), \\
\zeta_+ &= I_1 + I_2^+ + I_3^+ + I_4^+,
\end{aligned} \tag{8.15}$$

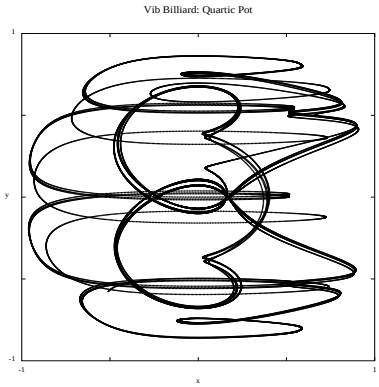

Figure 8.9: A homoclinic tangle projected onto the (x, y)-plane of the Bloch sphere.

where

$$
\begin{aligned}
I_1 &\equiv a^8 \left(\frac{\partial^2 V}{\partial a^2} \right)^2 , \\
I_2^+ &\equiv \frac{\partial^2 V}{\partial a^2} \left(12a^4\epsilon_+ - 2\omega_0^2 M a^4 + 12a^4\epsilon_- - 8\mu^2 a^4 \epsilon_- \right) , \\
I_3^+ &\equiv 16\mu^4\epsilon_-^2 - 8\omega_0^2 M\mu^2 - 48\mu^2\epsilon_-^2 - 12\omega_0^2 M\epsilon_+ + 72\epsilon_+\epsilon_- - 12\omega_0^2 M\epsilon_-, \\
I_4^+ &\equiv -48\mu^2\epsilon_+\epsilon_- + \omega_0^4 M^2 + 36(\epsilon_+^2 + \epsilon_-^2),
\end{aligned} \tag{8.16}
$$

and

$$
\zeta_- = I_1 + I_2^- + I_3^- + I_4^- , \tag{8.17}
$$

where I_1 is as before and

$$
\begin{aligned}
I_2^- &\equiv \frac{\partial^2 V}{\partial a^2} \left(12a^4\epsilon_+ - 2\omega_0^2 M a^4 - 12a^4\epsilon_- + 8\mu^2 a^4 \epsilon_- \right) , \\
I_3^- &\equiv 16\mu^4\epsilon_-^2 + 8\omega_0^2 M\mu^2 - 48\mu^2\epsilon_-^2 - 12\omega_0^2 M\epsilon_+ - 72\epsilon_+\epsilon_- + 12\omega_0^2 M\epsilon_-, \\
I_4^- &\equiv 48\mu^2\epsilon_+\epsilon_- + \omega_0^4 M^2 + 36(\epsilon_+^2 + \epsilon_-^2).
\end{aligned} \tag{8.18}
$$

Analogous to the $s = 1$ situation discussed in Chapter 7, only saddle-center bifurcations and generalizations thereof can occur[155]. As the energy is increased, bifurcations correspond to an increase in the dimension of the center manifold by

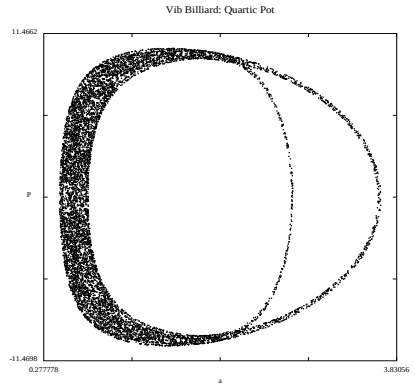

Figure 8.10: Chaotic Poincaré maps in the (a, P)-plane for billiards in both a quartic and a quadratic potential. The plot with the quartic potential is the one with a smaller maximum value for the distance a. Notice that the trajectory corresponding to the quartic potential generally has a larger radius of curvature. Additionally, these Poincaré maps approximately overlap for small a.

two (or four) as a pair (or two pairs) of real eigenvalues of opposite signs become a pair (or two pairs) of pure imaginary eigenvalues. As before, one can compute the location of this bifurcation by finding the equilibria for which $H(a, P)$ has a double root. One again finds that the equilibrium point $(0, 0, \pm 1, a_*, 0)$ at the bifurcation satisfies

$$\frac{\partial V}{\partial a}(a_*) = -\frac{a_*}{3}\frac{\partial^2 V}{\partial a^2}(a_*). \tag{8.19}$$

From a theoretical perspective, one can adjust the probabilities (i.e., complex amplitudes) corresponding to different eigenstates just as we did when $s = 1$.[155] One can also vary the form and coefficients of the potential $V(a)$ to examine bifurcations corresponding to different bond stiffnesses in polyatomic molecules. Numerical observations indicate that bifurcations occurs at low energies (corresponding to superpositions of states with low quantum numbers), so that for a given billiard, most superposition states have only elliptic equilibria. Saddle-center bifurcations (and generalizations thereof) then occur as one considers superpositions

of increasingly excited states.

Figure 8.8 suggests that homoclinic orbits exist for (8.9) when $V(a)$ is a quartic, double-well potential. Approximate homoclinic orbits certainly exist.[67, 194] For the degenerate case of zero interaction coefficient $\mu_{12} = 0$, we rigorously demonstrated the existence of homoclinic orbits in Chapter 7. Slight perturbations away from homoclinic orbits, such as those represented by nonzero values of the coupling coefficient μ_{12}, lead to homoclinic tangles, which are depicted in Figure 8.9. We explore the presence of homoclinic tangles in vibrating quantum billiards analytically using Melnikov techniques in Chapter 12. In preparation, we also (in the same chapter) reformulate vibrating quantum billiards in terms of action-angle coordinates.

Interest in homoclinic and heteroclinic orbits in chemical physics arises from their nature as separatrices. In two *dof* systems, they divide phase space into regions with qualitatively different nuclear dynamics exactly for integrable systems and approximately for nonintegrable ones. Trajectories within the separatrix experience a smaller range of lengthscales than those outside it, analogous to the division between librations and rotations in pendula.[64] Additionally, homoclinic orbits define dividing surfaces in phase space, the flux across which provides an optimal estimate of the rate of unimolecular disassociation processes.

CHAPTER 9

THREE-MODE GALËRKIN EXPANSIONS*

As discussed in Chapter 5, three-mode Galërkin expansions may be used to study molecular systems with triple electronic near-degeneracies.[160] As in Chapters 7 and 8, we consider the case $s = 1$ in which a single nuclear *dof* has been excited.

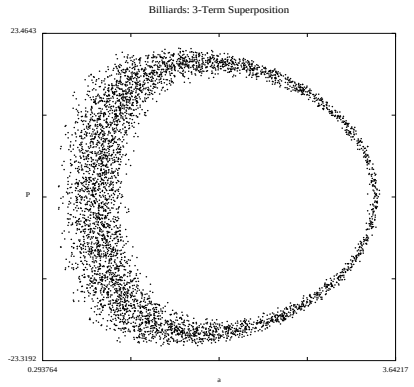

Figure 9.1: Poincaré section for the cut $x_{12} = 0$ in the (a, P)-plane for a three-term superposition state. This plot shows fully chaotic regions similar to those observed in two-term superpositions.

9.1 Equations of Motion

Insert the wavefunction

$$\psi(\mathbf{x}, t) \equiv A_{n_1}(t)\psi_{n_1}(\mathbf{x}, t) + A_{n_2}(t)\psi_{n_2}(\mathbf{x}, t) + A_{n_3}(t)\psi_{n_3}(\mathbf{x}, t), \qquad (9.1)$$

*This chapter is based on portions of reference [160].

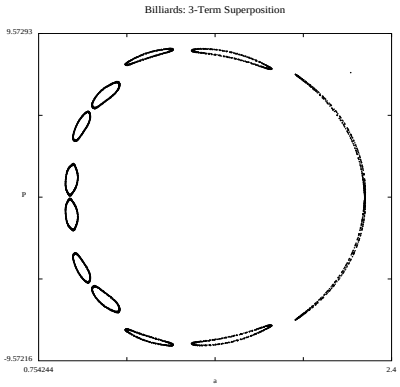

Figure 9.2: Poincaré section for the cut $x_{12} = 0$ in the (a, P)-plane for a three-term superposition state.

which is a superposition of n_1st, n_2nd, and n_3rd eigenstates, into the Schrödinger equation (5.1). Equivalently, let $d = 3$ in equation (5.20).

Taking the expectation of both sides of (5.1) for the state (9.1) yields

$$\begin{aligned}
\left\langle \psi \left| -\frac{\hbar^2}{2m_0}\nabla^2\psi \right. \right\rangle &= K\left(|A_{n_1}|^2, |A_{n_2}|^2, |A_{n_3}|^2; a\right), \\
i\hbar \left\langle \psi \left| \frac{\partial\psi}{\partial t} \right. \right\rangle &= i\hbar \Big[\dot{A}_{n_1}A^*_{n_2} + \dot{A}_{n_1}A^*_{n_3} + \dot{A}_{n_2}A^*_{n_1}\dot{A}_{n_2}A^*_{n_3} + \dot{A}_{n_3}A^*_{n_1} + \dot{A}_{n_3}A^*_{n_2} \\
&\qquad + \nu_{n_1n_1}|A_{n_1}|^2 + \nu_{n_2n_2}|A_{n_2}|^2 + \nu_{n_3n_3}|A_{n_3}|^2 \\
&\qquad + \nu_{n_1n_2}A_{n_1}A^*_{n_2} + \nu_{n_1n_3}A_{n_1}A^*_{n_3} + \nu_{n_2n_1}A_{n_2}A^*_{n_1} \\
&\qquad + \nu_{n_2n_3}A_{n_2}A^*_{n_3} + \nu_{n_3n_1}A_{n_3}A^*_{n_1} + \nu_{n_3n_2}A_{n_3}A^*_{n_2} \Big] \\
&= i\hbar \left[\sum_{k,j=1,k\neq j}^{3} \dot{A}_{n_k}A^*_{n_j} + \sum_{k=1}^{3} \nu_{n_kn_k}|A_{n_k}|^2 + \sum_{k,j=1,k\neq j}^{3} \nu_{n_kn_j}A_{n_k}A^*_{n_j} \right], \qquad (9.2)
\end{aligned}$$

which corresponds to equation (5.21) with $d = 3$.

Defining $A_j \equiv A_{n_j}$, the quadratic form (9.2) gives

$$i\dot{A}_k = \sum_{j=1}^{3} D_{kj}A_j, \qquad (9.3)$$

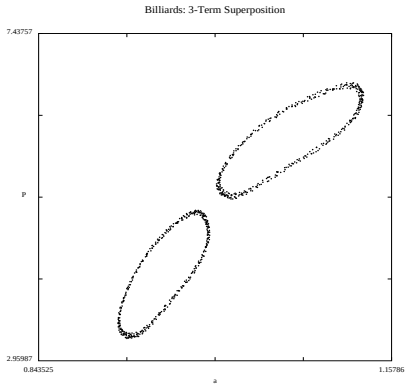

Figure 9.3: A closer look at a portion of the Poincaré section for the cut $x_{12} = 0$ in the (a, P)-plane for a three-term superposition state.

where

$$(D_{kj}) = \begin{pmatrix} \frac{\epsilon_1}{\hbar a^2} & -i\mu_{12}\dot{a}/a & -i\mu_{13}\dot{a}/a \\ i\mu_{12}\dot{a}/a & \frac{\epsilon_2}{\hbar a^2} & -i\mu_{23}\dot{a}/a \\ i\mu_{13}\dot{a}/a & i\mu_{23}\dot{a}/a & \frac{\epsilon_3}{\hbar a^2} \end{pmatrix}, \tag{9.4}$$

the parameter $\epsilon_j \equiv \epsilon_{n_j}$ is the jth energy coefficient, and $\mu_{kj} \equiv \mu_{n_k n_j} = -\mu_{n_j n_k} \neq 0$ is a coupling coefficient for the cross term $A_{n_k} A^*_{n_j}$.

Recall from Chapter 6 that $\mu_{kj} \neq 0$ when the fb quantum numbers of the n_kth and n_jth states are the same. When one or more of the interaction coefficients vanish, the associated amplitudes decouple in equation (9.3). In this event, the matrix (D_{kj}) is diagonal if all μ_{kj} vanish or block-diagonal (with one 1×1 block and one 2×2 block) if only some of them do. In the first case, one obtains dynamics like that studied in Chapter 7. In the second case, the dynamics corresponds to that examined in Chapter 8. Hence, without loss of generality, we assume that $\mu_{kj} \neq 0$ for the remainder of this chapter.

Using generalized Bloch variables,[160] the kinetic energy K is given by

$$\begin{aligned} K &= \frac{2}{3a^2}\left(\left[z_{12}\epsilon_{12}^{-} + z_{13}\epsilon_{13}^{-} + z_{23}\epsilon_{23}^{-}\right] + \epsilon_{+}\right) \\ &= \frac{2}{3a^2}\left(\left[z_{12}\epsilon_{12}^{-} + (z_{12}+z_{23})\epsilon_{13}^{-} + z_{23}\epsilon_{23}^{-}\right] + \epsilon_{+}\right), \end{aligned} \tag{9.5}$$

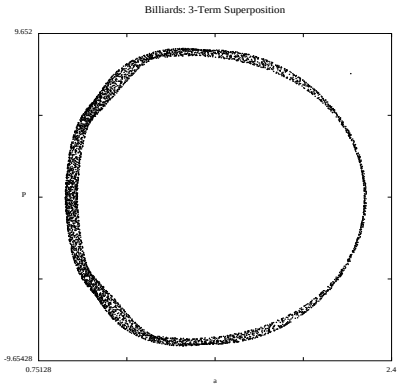

Figure 9.4: Poincaré section for the cut $x_{23} = 0$ in the (a, P)-plane for a three-term superposition state. The initial conditions are the same as those for Figure 9.2.

where

$$\begin{aligned} \epsilon_{kl}^{-} &\equiv \frac{\epsilon_l - \epsilon_k}{2}, \\ \epsilon^{+} &\equiv \frac{\epsilon_k + \epsilon_l + \epsilon_m}{2}. \end{aligned} \tag{9.6}$$

With Bloch variables, one obtains the following equations of motion to describe three-mode Galërkin expansions of vibrating quantum billiards with $s = 1$ nuclear *dof*:[160]

$$\begin{aligned} \dot{x}_{12} &= -\frac{\omega_{12}}{a^2} y_{12} - \frac{2\mu_{12} P z_{12}}{Ma} - \frac{P}{Ma}\left[\mu_{23} x_{13} + \mu_{13} x_{23}\right], \\ \dot{x}_{13} &= -\frac{\omega_{13}}{a^2} y_{13} - \frac{2\mu_{13} P (z_{12} + z_{23})}{Ma} + \frac{P}{Ma}\left[\mu_{23} x_{12} - \mu_{12} x_{23}\right], \\ \dot{x}_{23} &= -\frac{\omega_{23}}{a^2} y_{23} - \frac{2\mu_{23} P z_{23}}{Ma} + \frac{P}{Ma}\left[\mu_{13} x_{12} + \mu_{12} x_{13}\right], \end{aligned}$$

$$\begin{aligned} \dot{y}_{12} &= \frac{\omega_{12} x_{12}}{a^2} + \frac{P}{Ma}\left[\mu_{13} y_{23} - \mu_{23} y_{13}\right] \\ \dot{y}_{13} &= \frac{\omega_{13} x_{13}}{a^2} + \frac{P}{Ma}\left[\mu_{23} y_{12} - \mu_{12} y_{23}\right] \\ \dot{y}_{23} &= \frac{\omega_{23} x_{23}}{a^2} + \frac{P}{Ma}\left[\mu_{12} y_{13} - \mu_{13} y_{12}\right], \end{aligned}$$

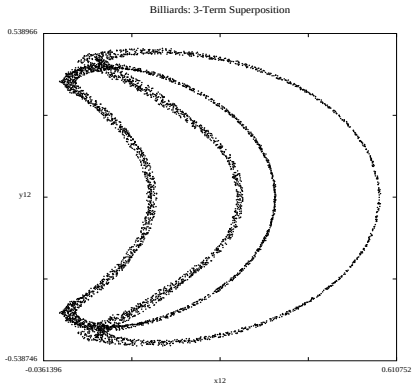

Figure 9.5: Poincaré section for the cut $P = 0$ in the (x_{12}, y_{12})-plane for a three-term superposition state. The initial conditions are the same as those for Figure 9.2.

$$\dot{z}_{12} = \frac{2\mu_{12}Px_{12}}{Ma} + \frac{P}{Ma}\left[\mu_{13}x_{13} - \mu_{23}x_{23}\right],$$
$$\dot{z}_{23} = \frac{2\mu_{23}Px_{23}}{Ma} + \frac{P}{Ma}\left[\mu_{13}x_{13} - \mu_{12}x_{12}\right],$$

$$\dot{a} = \frac{P}{M} \equiv \frac{\partial H}{\partial P},$$
$$\dot{P} = -\frac{\partial V}{\partial a} - \frac{\partial K}{\partial a} \equiv -\frac{\partial H}{\partial a}, \tag{9.7}$$

where

$$\begin{aligned}\frac{\partial K}{\partial a} = &-\frac{4\epsilon^+}{3a^3} - \frac{4}{3a^3}\left[z_{12}\epsilon_{12}^- + (z_{12}+z_{23})\epsilon_{13}^- + z_{23}\epsilon_{23}^-\right] \\ &+ \frac{2}{3a^3}\epsilon_{12}^-(2\mu_{12}x_{12} + \mu_{13}x_{13} - \mu_{23}x_{23}) + \frac{2}{3a^3}\epsilon_{13}^-\left(\mu_{12}x_{12} + 2\mu_{13}x_{13} + \mu_{23}x_{23}\right) \\ &+ \frac{2}{3a^3}\epsilon_{23}^-(-\mu_{12}x_{12} + \mu_{13}x_{13} + 2\mu_{23}x_{23}).\end{aligned} \tag{9.8}$$

Equation (9.8) is obtained using

$$\frac{\partial z_{12}}{\partial a} = \frac{\partial z_{12}}{\partial t}\frac{\partial t}{\partial a} \equiv \frac{\dot{z}_{12}}{\dot{a}} = \frac{2\mu_{12}x_{12}}{a} + \frac{1}{a}\left[\mu_{13}x_{13} - \mu_{23}x_{23}\right],$$
$$\frac{\partial z_{23}}{\partial a} = \frac{\partial z_{23}}{\partial t}\frac{\partial t}{\partial a} \equiv \frac{\dot{z}_{23}}{\dot{a}} = \frac{2\mu_{23}x_{23}}{a} + \frac{1}{a}\left[\mu_{13}x_{13} - \mu_{12}x_{12}\right]. \tag{9.9}$$

Additionally, recall from Chapter 5 that

$$\omega_{kl} \equiv \frac{\epsilon_l - \epsilon_k}{\hbar}. \tag{9.10}$$

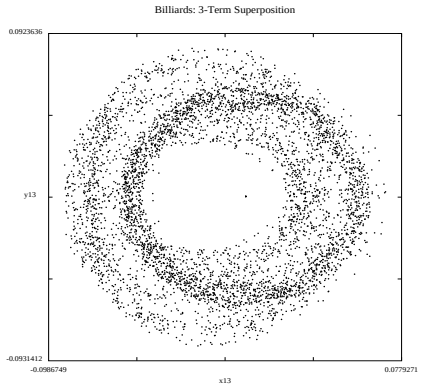

Figure 9.6: Poincaré section for the cut $P = 0$ in the (x_{13}, y_{13})-plane for a three-term superposition state. The initial conditions are the same as those for Figure 9.2.

Finally, note that one may also obtain (9.7) by inserting $d = 3$ into equations (5.28,5.30,5.31,5.32).

The equilibria of the 10-dimensional dynamical system (9.7) satisfy $P = 0$, $x_{kj} = y_{kj} = 0$, $z_{12}^2 + z_{12}z_{23} + z_{23}^2 = 1$, and

$$\frac{\partial V}{\partial a} = \frac{4}{3a^3}\left[\epsilon^+ + z_{12}\epsilon_{12}^- + (z_{12} + z_{23})\epsilon_{13}^- + z_{23}\epsilon_{23}^-\right]. \tag{9.11}$$

Applying the constraints (5.29) with $x_{kj} = y_{kj} = 0$ yields three possible sets of values for the z-Bloch variables:

$$(z_{12}, z_{13} \equiv z_{12} + z_{23}, z_{23}) = (0, 1, 1), \quad (1, 0, -1), \quad (-1, -1, 0). \tag{9.12}$$

Each equilibrium of (9.7) is a pure state, as argued in Chapter 5. If $z_{12} = 0$, then $|A_1|^2 = |A_2|^2 = 0$ and $|A_3|^2 = 1$, so only the third eigenstate is present. If $z_{13} = 0$, then only the state with complex ampltude A_2 gives a nonvanishing contribution. Finally, for $z_{23} = 0$, only the first pure state is present. Recall that when only the jth state is present at equilibrium, its kinetic energy is

$$E_j = \frac{\epsilon_j}{a_*^2}, \tag{9.13}$$

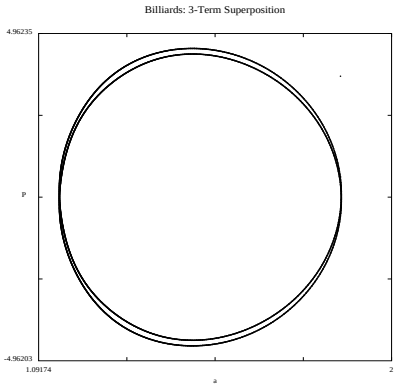

Figure 9.7: Poincaré section for the cut $x_{12} = 0$ in the (a, P)-plane for a three-term superposition state. The behavior in the plot appears quasiperiodic.

where a_* is an associated equilibrium radius. Additionally,

$$\frac{\partial V}{\partial a}(a_*) = \frac{2\epsilon_j}{a^3}, \quad j \in \{1, 2, 3\}. \tag{9.14}$$

As before, the form of the external potential $V(a)$ determines the number of radii associated with each pure-state equilibrium,[160] every one of which is elliptic provided

$$E(a) \equiv V(a) + K(a) \tag{9.15}$$

has a single minimum with respect to the displacement a. When this happens, $\dot{P}$ vanishes exactly once if one varies a quasistatically by holding the z-Bloch variables (and hence the probability amplitudes A_j) constant. There is then exactly one nuclear configuration corresponding to each pure-state equilibrium. At any non-elliptic equilibrium, $\dot{P}$ vanishes at multiple displacements a_*.

9.2 Numerical Simulations

We investigate the dynamics of equation (9.7) numerically when the potential V is harmonic (5.41). In this situation (as discussed in Chapter 5), all equilibria

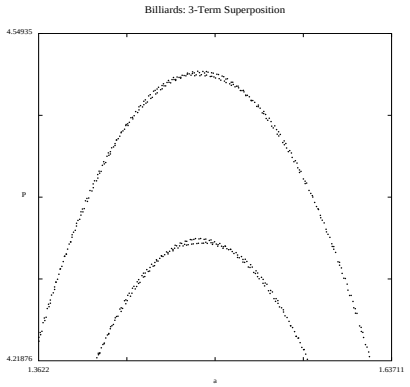

Figure 9.8: A magnification of Figure 9.7. This zoomed view reveals a small region that suggests the presence of some chaotic behavior.

are elliptic. As expected, the dynamics determined by equations (9.7) are more intricate than those determined by equations (7.3). For some choices of parameters and initial conditions, however, one obtains plots whose dynamics are very similar to those for two-term superpositions.

Figures 9.1–9.13 illustrate the dynamics of a three-term superposition consisting of the ground state and the first two excited null angular-momentum ($l = 0, m = 0$) states of the radially vibrating spherical quantum billiard.[160] (In Chapter 10, we discuss this billiard in more detail.) The values of the parameters are $\hbar = 1$, $M = 10$, $m = 1$, $\epsilon_1 = \pi^2/2m \approx 4.9348022$, $\epsilon_2 = 4\pi^2/2m \approx 19.7392088$, $\epsilon_3 = 9\pi^2/2m \approx 44.4132198$, $V_0 = 5$, and $a_0 = 1.25$. The coupling coefficients are $\mu_{12} = 4/3$, $\mu_{13} = 3/4$, and $\mu_{23} = 12/5$.

Figure 9.1 shows a Poincaré map (of the cut $x_{12} = 0$) projected into the (a, P)-plane. The initial conditions for this plot are $x_{12}(0) = \sin(0.95\pi) \approx 0.156434$, $x_{13}(0) = x_{23}(0) = 0$, $y_{12}(0) = y_{13}(0) = y_{23}(0) = 0$, $z_{12}(0) = \cos(0.95\pi) \approx -0.987688$, $z_{23}(0) = 0$, $a(0) \approx 3.3774834$, and $P(0) \approx 7.2847682$. In subsequent figures, we alter only the initial radius and conjugate momentum.

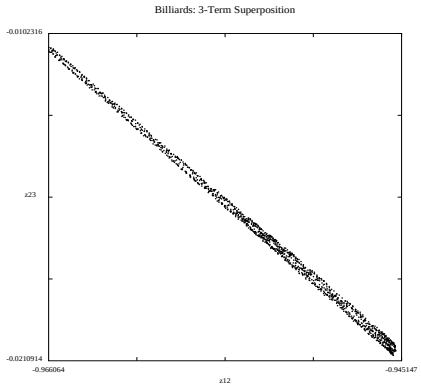

Figure 9.9: Poincaré section for the cut $x_{12} = 0$ in the (z_{12}, z_{23})-plane for a three-term superposition state. The behavior depicted in the plot is chaotic.

Figure 9.2 shows a $x_{12} = 0$ Poincaré map projected into the (a, P)-plane. The initial radius is $a(0) \approx 2.2095438$, and the initial momentum is $P(0) \approx 3.6672913$. The dynamics in this figure are almost integrable, but a closer look reveals chaotic characteristics (see Figure 9.3). It appears that this trajectory may be near a periodic orbit (of period 6), although an additional plot reveals that another of its degrees-of-freedom has departed quite a bit from a periodic or even quasiperiodic configuration. Figure 9.4 shows the $x_{23} = 0$ Poincaré cut for the same initial conditions. The chaotic behavior in this plot has less structure, which demonstrates a different level of "excitation" corresponding to different coupling coefficients. Poincaré maps obtained using $y_{ij} = 0$ reveal similar behavior as that in corresponding $x_{ij} = 0$ cuts.

Figure 9.5 shows a $P = 0$ Poincaré map projected into the (x_{12}, y_{12})-plane. Figure 9.6 reveals the same configuration projected into the (x_{13}, y_{13})-plane. This latter figure appears to be have departed further from integrability than the former one. As discussed above, different quantum-mechanical components of the system can exhibit different degrees of "excitation" or departure from integrability. In the

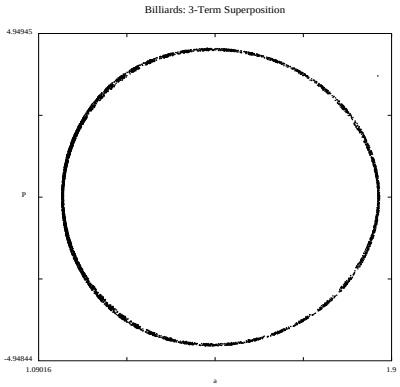

Figure 9.10: Poincaré section for the cut $x_{23} = 0$ in the (a, P)-plane for a three-term superposition state. The behavior depicted in the plot is chaotic.

present context, each "component" of the quantum-mechanical subsystem represents the interaction of one pure eigenstate with a second one. When $d = 3$, there are three such interaction pairs corresponding to the three coupling coefficients μ_{kj}. When $d = 2$, there is only one such interaction. In a physical context, we conclude that as electronic near-degeneracies encompass more eigenstates, they yield additional interactions that take the form of additional behavioral "modes" from a dynamical systems perspective.[160] In particular, the transition from $d = 2$ to $d = 3$ permits some modes to be excited while others are not. One observes fewer KAM islands as more modes become excited. This phenomenon may be interpreted as some sort of "commensurability" effect in coupled (quantum-mechanical) oscillators.

Figure 9.7 shows a $x_{12} = 0$ Poincaré cut in the (a, P)-plane corresponding to the initial conditons $a(0) \approx 1.8685499$ and $P(0) \approx 0.6140458$. It appears to depict quasiperiodic motion, but a portion of the same plot suggests that it is not quite integrable (see Figure 9.8). KAM theory also implies that this is the case, as any nonzero perturbation from an integrable configuration will cause some chaos

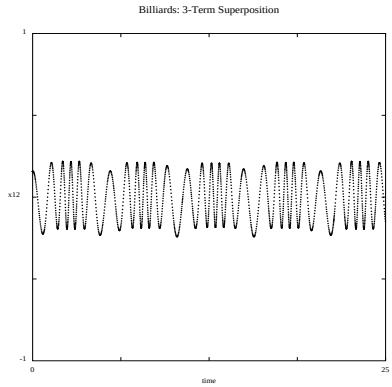

Figure 9.11: Time series in $x_{12}(t)$ from $t = 0$ to $t = 25$ revealing near-integrable behavior.

(although it may be so small as to be impossible to resolve numerically).[67, 194] Moreover, a magnification of the same plot in the (z_{12}, z_{23})-plane (Figure 9.9) reveals chaotic behavior in the Bloch variables. Unlike the classical variables, the z-Bloch variables appear to have departed quite a bit from integrability. Thus, it is possible for the classical variables to behave in a nearly integrable fashion while the quantum variables behave quite chaotically. We discuss this in detail in Chapter 13. In particular, we show that when perturbing from integrable configurations, the onset of chaos occurs far sooner in a vibrating quantum billiard's classical *dof* than in its quantum *dof*. This follows from the Born-Oppenheimer approximation, so it is a general phenomenon in molecular systems.

Further plots suggest that the present configuration is almost integrable with respect to the interaction between the ground state and first excited state but chaotic with respect to other interactions. This is supported by the chaotic characteristics in the Poincaré section in the (a, P)-plane corresponding to the cut $x_{23} = 0$ (which is depicted in Figure 9.10). Time series (displayed in Figures 9.11, 9.12, and 9.13) suggest the same phenomenon. Time series for the corresponding y-Bloch variables reveal similar features, whereas time series for the radius and

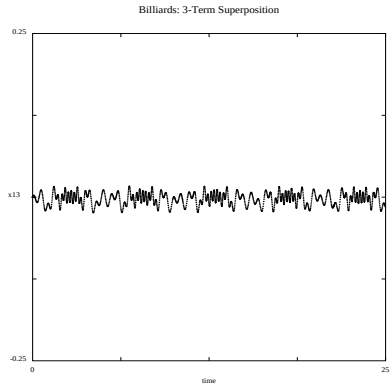

Figure 9.12: Time series in $x_{13}(t)$ from $t = 0$ to $t = 25$ revealing chaotic behavior.

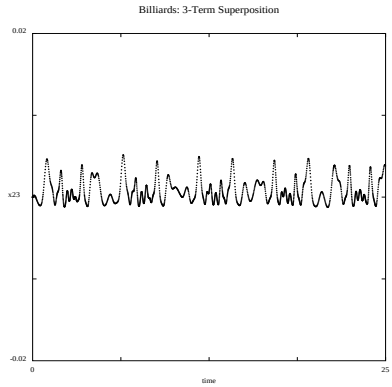

Figure 9.13: Time series in $x_{23}(t)$ from $t = 0$ to $t = 25$ revealing chaotic behavior.

momentum reveal motion that is almost regular. Based on the observed behavior of the classical and quantum mechanical *dof*, this configuration seems to be one for which the irregularities of the dynamics of the radius and the momentum are extremely difficult to observe numerically. The corresponding eigenfunctions are thus also very regular. Nevertheless, there is some chaotic structure due to the coupling between the first and second excited electronic states. The presence of a triple electronic near-degeneracy has given rise to a situation in which interactions of the ground state yield almost integrable dynamics but the interaction between

the two excited states is highly irregular.

To phrase the above discussion more rigorously, recall from Chapter 5 that a two-term superposition state approximates an infinite *dof* Hamiltonian system (which describes the full dynamics of the vibrating billiard) with a two *dof* Hamiltonian system. One is ignoring infinitely many quantum *dof*. As discussed in Chapter 5, these *dof* contribute non-negligibly to the dynamics of the vibrating quantum billiard from a mathematical perspective, but they are justifiably ignored on physical grounds.[160] Likewise, three-term superposition states yield a three *dof* Hamiltonian system to describe nonadiabatic dynamics in molecular systems near triple electronic near-degeneracies.[154] One observes more intricate behavior as a result.

CHAPTER 10

EXAMPLE: THE RADIALLY VIBRATING SPHERICAL QUANTUM BILLIARD*

10.1 Introduction

The radially vibrating spherical quantum billiard addresses the quantum dynamics of a particle of mass m_0 confined to the interior of a spherical cavity of mass $M \gg m_0$ with smooth walls of radius a. The radius vibrates in an a priori unspecified manner, so that $a \equiv a(t)$.

A two-term superposition state (Galërkin projection) of this quantum billiard is given using Dirac notation by[112, 158–160]

$$|\psi(r,\theta,\phi,t;a(t))\rangle = A_1(t)|nlm,t\rangle + A_2(t)|n'l'm',t\rangle, \tag{10.1}$$

where $A_1(t)$ and $A_2(t)$ are complex amplitudes. The numbers $\{n,l,m\}$ are, respectively, the principal, orbital, and azimuthal quantum numbers. The eigenstates in (10.1) are products of spherical Bessel functions and spherical harmonics.[105, 112, 158] In coordinate representation,

$$\langle\vec{r}|nlm,t\rangle = \psi_{nlm}(r,\theta,\phi,t;a(t)) = \sqrt{\frac{2}{a(t)^3}}\left(\frac{1}{j_{l+1}(x_{ln})}\right) j_l\left(\frac{rx_{ln}}{a(t)}\right) Y_{lm}(\theta,\phi), \tag{10.2}$$

where x_{ln} is the nth zero of j_l, the spherical Bessel function of order l. The explicit radial time-dependence occurs both in the arguments of the spherical Bessel functions and in the normalization factors of the eigenstates. The spherical harmonics are unaffected by the radial vibrations of the billiard.

*This chapter is based on reference [158].

Later in this chapter, we show directly that the two eigenstates in (10.1) must have common rotational symmetry ($l = l', m = m'$) for their superposition to behave chaotically. This is a special case of the Quantum Number Symmetry Theorem derived in Chapter 6. First, we present an example to motivate this result. We then demonstrate its validity for arbitrary superpositions of finitely many states. We subsequently discuss chaotic superpositions.

10.2 Formulation

The Schrödinger equation describing the radially vibrating spherical quantum billiard is given by

$$i\hbar\frac{\partial\psi}{\partial t} = K\psi, \quad r \leq a(t), \tag{10.3}$$

where

$$K = -\frac{\hbar^2}{2m_0}\nabla^2 \tag{10.4}$$

is the kinetic energy of the confined particle. The radial component of the Laplacian ∇^2 is given in spherical coordinates by[27, 105]

$$\nabla^2 = \frac{1}{r}\left(\frac{\partial^2}{\partial r^2}r\right) = -\frac{p_r^2}{2\hbar^2}, \tag{10.5}$$

where p_r is the *radial momentum operator.*[111]

The molecular Hamiltonian is

$$H = \frac{P^2}{2M} + V + K, \tag{10.6}$$

where P is the momentum of the billiard boundary and V is an external potential. The potential energy V and kinetic energy $P^2/(2M)$ of the billiard walls are classical quantities, so the present system has both classical and quantum-mechanical components. (The billiard boundary is classical, whereas the confined

particle is quantum-mechanical.) We hence utilize the Born-Oppenheimer approximation,[22, 154] so that only the electronic Hamiltonian $K + V$ is inserted into the Schrödinger equation (10.3). As the potential V shifts every electronic eigenvalue by the same constant value (which depends parametrically on the nuclear displacement a), one actually only inserts K into (10.3). In this approximation, we are ignoring the effects of Berry phase.[15, 154, 203]

Taking expectations of (10.3) using the superposition state (10.1) yields

$$\begin{aligned} \left\langle \psi \left| -\frac{\hbar^2}{2m_0}\nabla^2\psi \right\rangle \right. &= \frac{1}{a^2}\left[\epsilon_1|A_1|^2 + \epsilon_2|A_2|^2\right] \equiv K(A_1, A_2; a) \\ i\hbar \left\langle \psi \left| \frac{\partial\psi}{\partial t} \right\rangle \right. &= i\hbar\left[\dot{A}_1 A_1^* + \dot{A}_2 A_2^* + \nu_{11}|A_1|^2 \right. \\ &\quad \left. + \nu_{12}A_1 A_2^* + \nu_{21}A_2 A_1^* + \nu_{22}|A_2|^2\right], \end{aligned} \tag{10.7}$$

where the energy parameters in (10.7) are given by

$$\begin{aligned} \epsilon_1 &\equiv \frac{\hbar^2 x_{ln}^2}{2m_0}, \\ \epsilon_2 &\equiv \frac{\hbar^2 x_{l'n'}^2}{2m_0}. \end{aligned} \tag{10.8}$$

The diagonality of the quadratic form obtained in the expectation of the Laplacian operator follows from the orthogonality relations of spherical Bessel functions.[27, 105] This orthogonality does not carry over to the second quadratic form, as the act of differentiating with respect to time causes r-dependent terms to appear in the integrand when taking expectations. These terms come from application of the chain rule to the arguments of the spherical Bessel functions, which depend on $a(t)$.[112, 158]

10.3 Integrable Configuration

The diagonal coefficients ν_{11} and ν_{22} vanish no matter which eigenstates one considers in (10.1). Examination of the superposition of $|100\rangle$ and $|110\rangle$ using (10.7)

and orthogonality of spherical harmonics shows that the cross-term coefficients

$$\nu_{12} = \nu_{21} = 0. \tag{10.9}$$

Equating the inner products (10.7) in both sides of the Schrödinger equation (10.3) yields amplitude equations:

$$\begin{aligned} i\dot{A}_1 &= \frac{1}{\hbar a^2}\epsilon_1 A_1, \\ i\dot{A}_2 &= \frac{1}{\hbar a^2}\epsilon_2 A_2, \end{aligned} \tag{10.10}$$

which are integrated to obtain

$$\begin{aligned} A_1(t) &= C_1 \exp\left[-\frac{i\epsilon_1}{\hbar}\int a^{-2}(t)dt\right], \\ A_2(t) &= C_2 \exp\left[-\frac{i\epsilon_2}{\hbar}\int a^{-2}(t)dt\right]. \end{aligned} \tag{10.11}$$

From (10.11), one obtains a (one *dof*) Hamiltonian in the radius a and conjugate momentum P:

$$H = \frac{P^2}{2M} + K(A_1, A_2, a) + V(a) = \frac{P^2}{2M} + \frac{1}{a^2}\left[\epsilon_1\alpha + \epsilon_2\beta\right] + V(a), \tag{10.12}$$

where the parameter α_j is given by

$$\alpha_j \equiv |A_j|^2 = |C_j|^2, \quad , j \in \{1, 2\}. \tag{10.13}$$

A Hamiltonian system with no explicit time-dependence and one *dof* corresponds to a two-dimensional autonomous system of ordinary differential equations and is therefore not chaotic.[67, 183, 194]

The prefactor ν_{jk} $(j \neq k)$ represents the strength of the interaction between the jth and kth eigenstates in the superposition (10.1). When there is no electronic-nuclear coupling, which occurs when $\nu_{jk} = 0$ for all pairs (j, k), the *dof* of the resulting Hamiltonian are purely classical, as they correspond to the billiards nuclear *dof.*[154, 158] When a two-term superposition has a non-vanishing coupling

coefficient, the number of *dof* of the resulting Hamiltonian system is one plus the number of nuclear *dof*. Consequently, a superposition state of a quantum billiard with more than one nuclear *dof* is expected to behave chaotically even if every one of its coupling coefficients vanishes. The vibrating rectangular quantum billiard, which we study in Chapter 11, provides a specific example of this situation.[157]

Hamilton's equations corresponding to (10.12) are

$$\begin{aligned} \dot{a} &= \frac{P}{M} \equiv \frac{\partial H}{\partial P}, \\ \dot{P} &= -\frac{\partial V}{\partial a} + \frac{\lambda}{a^3} \equiv -\frac{\partial H}{\partial a}, \end{aligned} \tag{10.14}$$

where

$$\lambda \equiv 2\left(\epsilon_1 |C_1|^2 + \epsilon_2 |C_2|^2\right) > 0. \tag{10.15}$$

The energy parameter λ is positive because $\epsilon_j > 0$ and the $|C_j|^2$ correspond to probabilities (so $|C_1|^2 + |C_2|^2 = 1$). The bifurcation structure of (10.14) was discussed in Chapter 7.[155]

10.4 Necessary Conditions for Chaos in d Coupled States

Consider a d-state superposition

$$\psi = A_1 \psi_{q_1} + A_2 \psi_{q_2} + \cdots + A_d \psi_{q_d}, \tag{10.16}$$

where $q_j \equiv (n_j, l_j, m_j)$ is a vector of quantum numbers. If there does not exist a pair of eigenstates in (10.16) with common angular-momentum quantum numbers (i.e., if there is no pair $\{j, j'\}$ such that $l_j = l_{j'}$ and $m_j = m_{j'}$), then inserting (10.16) into the Schrödinger equation (10.3) returns a diagonal quadratic form

$$\dot{A}_1 A_1^* + \cdots + \dot{A}_d A_d^* = \nu_{11} |A_1|^2 + \cdots + \nu_{dd} |A_d|^2, \tag{10.17}$$

as the prefactprs ν_{jk} of the interaction terms vanish because spherical harmonics corresponding to different angular momenta are orthogonal.[27, 105] The diagonal terms in (10.17) stem from the Laplacian.[112, 158]

This yields the Hamiltonian

$$H(a,P) = \frac{P^2}{2M} + \frac{1}{a^2}\sum_{j=1}^{k} \epsilon_j \alpha_j + V(a), \tag{10.18}$$

where $\alpha_j \equiv |A_j|^2 = |C_j|^2$, $\sum_{j=1}^{k} |C_j|^2 = 1$, and the C_j are constants. The superposition (10.16) is not chaotic, as the Hamiltonian (10.18) is autonomous with one degree-of-freedom.

Consequently, a necessary condition for chaos to occur in any finite-term superposition state of the radially vibrating spherical quantum billiard is that at least one pair of eigenstates in the superposition (10.1) have common angular-momentum quantum numbers. (This is a special case of the Quantum Number Symmetry Theorem, which was stated and proved in Chapter 6.) For example, the two states

$$\begin{aligned} &j_l\left(\frac{r x_{ln}}{a(t)}\right) Y_{lm}(\theta,\phi), \\ &j_l\left(\frac{r x_{ln'}}{a(t)}\right) Y_{lm}(\theta,\phi) \end{aligned} \tag{10.19}$$

interact with each other, so a superposition of these two states behaves chaotically for some initial conditions and parameter values.

10.5 Chaotic Configuration

As an example of a chaotic configuration of the radially vibrating spherical quantum billiard, consider the azimuthally symmetric superposition state

$$|\psi(n,l,m)\rangle = A_1|110\rangle + A_2|210\rangle. \tag{10.20}$$

This superposition has an interaction coefficient $\mu \equiv \mu_{12} \approx 0.4395263$.[112, 158] (The parameter μ may be expressed exactly in terms of spherical Bessel functions.)

Equating coefficients in the quadratic form (10.7) yields

$$i\dot{A}_n = \sum_{k=1}^{2} D_{nk} A_k, \tag{10.21}$$

where $D \equiv (D_{ij})$ is the Hermitian matrix

$$D = \begin{pmatrix} \frac{\epsilon_1}{\hbar a^2} & -i\mu\frac{\dot{a}}{a} \\ i\mu\frac{\dot{a}}{a} & \frac{\epsilon_2}{\hbar a^2} \end{pmatrix}. \tag{10.22}$$

Additionally,

$$\begin{aligned} \epsilon_1 &\equiv \frac{\hbar^2 x_{11}^2}{2m_0}, \\ \epsilon_2 &\equiv \frac{\hbar^2 x_{12}^2}{2m_0} > \epsilon_1. \end{aligned} \tag{10.23}$$

Defining the density matrix[105] by $\rho_{qn} = A_q A_n^*$, introducing (dimensionless) Bloch variables)[2] $x = \rho_{12} + \rho_{21}$, $y = i(\rho_{21} - \rho_{12})$, and $z = \rho_{22} - \rho_{11}$, and using (10.21), we obtain the following equations of motion for the quantum-mechanical *dof*:

$$\begin{aligned} \dot{x} &= -\frac{\omega_0 y}{a^2} - \frac{2\mu P z}{Ma}, \\ \dot{y} &= \frac{\omega_0 x}{a^2}, \\ \dot{z} &= \frac{2\mu P x}{Ma}. \end{aligned} \tag{10.24}$$

In (10.24),

$$\omega_0 \equiv \frac{\epsilon_2 - \epsilon_1}{\hbar}. \tag{10.25}$$

Rewriting the kinetic energy $K(A_1, A_2; a)$ in terms of the Bloch variable z gives

$$K(z, a) = \frac{1}{a^2}(\epsilon_+ + z\epsilon_-), \tag{10.26}$$

where

$$\epsilon_{\pm} \equiv \frac{1}{2}(\epsilon_2 \pm \epsilon_1). \tag{10.27}$$

Inserting $K(z;a)$ into the Hamiltonian (10.6) yields Hamilton's equations:

$$\begin{aligned} \dot{a} &= \frac{P}{M}, \\ \dot{P} &= -\frac{\partial V}{\partial a} + \frac{2}{a^3}\left[\epsilon_+ + \epsilon_-(z - \mu x)\right]. \end{aligned} \tag{10.28}$$

Equations (10.24) and (10.28) constitute a set of five coupled nonlinear ordinary differential equations. One can show that this system is equivalent to a two *dof* Hamiltonian system.[160] We discussed this from a geometric perspective in Chapter 5 and show this directly using action-angle variables in Chapter 12.

The constants of motion of the dynamical system (10.24,10.28) are the radius of the Bloch sphere

$$x^2 + y^2 + z^2 \equiv |A_1|^2 + |A_2|^2 = 1 \tag{10.29}$$

and the energy (molecular Hamiltonian)

$$H = \frac{P^2}{2M} + V(a) + K(z;a). \tag{10.30}$$

Equilibria satisfy $x = y = 0$, $z = \pm 1$, $P = 0$, and $a = a_{\pm}$, where $a_{\pm}$ are solutions to the equation $\dot{P} = 0$ for $x = P = 0$ and $z = \pm 1$. That is, $a_{\pm}$ satisfies

$$\frac{\partial V}{\partial a} = \frac{2}{a^3}(\epsilon_+ \pm \epsilon_-), \tag{10.31}$$

where the subscript of $a_{\pm}$ corresponds to the sign of z. Assuming that $V(a) + K(z;a)$ has a single minimum with respect to a, these equilibria are elliptic.[112, 155, 158] These equilibria have one zero eigenvalue and two conjugate pairs of pure imaginary eigenvalues.

The oscillations of the radius $a(t)$ lie in a bounded radial interval when $V(a)$ harmonic (5.41). In this situation, the electronic Hamiltonian is given by

$$V(a) + K(a) = V_0(a - a_0)^2 + \frac{\epsilon_+ + z\epsilon_-}{a^2}. \tag{10.32}$$

Furthermore, equation (10.31) becomes

$$a - a_0 = \frac{\epsilon_\pm}{V_0 a^3}. \tag{10.33}$$

Equation (10.33) has two solutions–one corresponding to ϵ_+ and one corresponding to ϵ_-. Additionally,

$$a_+ \geq a_- \geq a_0, \tag{10.34}$$

so the resistance of the confined particle against localization increases the equilibrium radius relative to the reference value a_0. Moreover, as $a_+ > a_-$, the more energetic equilibrium state has a larger radius than the less energetic one.[158, 160] Finally, as $a_- \leq a(0) \leq a_+$, the displacement $a(t)$ remains bounded in the interval $[a_-, a_+]$.[22, 23, 112, 158]

10.6 Special Case: Null Angular-Momentum Eigenstates

In this special case, the eigenfunctions of ψ are given by spherical Bessel functions of order 0. That is,

$$\psi(r,t) = \sum_{n=1}^{\infty} A_n(t)\alpha_n(t)\psi_n(r,t), \tag{10.35}$$

where

$$\psi_n(r,t) = j_0\left(\frac{n\pi r}{a(t)}\right),$$
$$j_0(x) = \frac{sin(x)}{x}. \tag{10.36}$$

The triple summation of eigenstates (10.2) of the vibrating spherical billiard with any $\{n, l, m\}$ has reduced to a single sum, as we consider only states for which $l = m = 0$. In this special case, the normalization coefficient α_n is given by

$$\alpha_n = \frac{\sqrt{2}}{a^{\frac{3}{2}} j_1(n\pi)}, \tag{10.37}$$

where $x_{0n} \equiv n\pi$ is the nth zero of $j_0(x)$. The electronic kinetic energy K is still given by equation (10.4). Additionally, the energy coefficient ϵ_j is

$$\epsilon_j \equiv \frac{(j\pi\hbar)^2}{2m_0}, \tag{10.38}$$

and the interaction coefficient μ_{nq} of two states ψ_n and ψ_q $(n \neq q)$ is

$$\mu_{nq} = \frac{2qn}{(n+q)(q-n)}. \tag{10.39}$$

10.6.1 d-State Superposition

Consider the superposition of the first d states of the radially vibrating spherical quantum billiard with null angular-momentum eigenstates,

$$\psi(r) = \sum_{n=1}^{d} A_n(t)\alpha_n\psi_n(r,t). \tag{10.40}$$

To analyze (10.40), one examines the superposition of ψ_n and ψ_q, and then superposes the couplings one obtains as n and q $(n \neq q)$ run from 1 to d.

The two-term superposition of interest is

$$\psi_{nq} = A_n(t)\alpha_n\psi_n(r,t) + A_q(t)\alpha_q\psi_q(r,t). \tag{10.41}$$

The dynamical equations for A_j are described by a $d \times d$ matrix and are a straightforward generalization of (10.21,10.22). Note additionally the necessary conditions for a superposition state to evolve chaotically are satisfied automatically when one considers only null angular-momentum eigenstates. (The symmetry condition is satisfied because the quantum numbers m and l vanish for each state.)

10.6.2 Numerical simulations

Consider a superposition of the ground state and first excited state, for which

$$\begin{aligned} \mu_{12} &= \frac{4}{3}, \\ \epsilon_1 &= \frac{\pi^2\hbar^2}{2m_0}, \\ \epsilon_2 &= \frac{2\pi^2\hbar^2}{m_0}. \end{aligned} \tag{10.42}$$

Additionally, note that we utilized a harmonic potential (5.41) in our simulations.

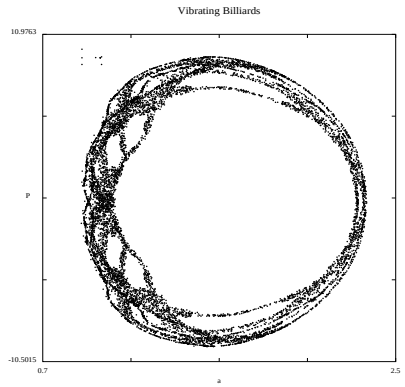

Figure 10.1: Poincaré section ($x = 0$) in the (a, P)-plane illustrating that not all invariant tori are destroyed in the present configruation.

Figure 10.1 shows a Poincaré map in the (a, P)-plane corresponding to $x = 0$, and Figure 10.2 shows a Poincaré section projected onto the (x, y)-plane for $P = 0$. For each of these two plots, we used the parameter values $\hbar = 1$, $M = 10$, $\epsilon_1 = \pi^2/2 \approx 4.9348022$, $\epsilon_2 = 2\pi^2 \approx 19.7392088$, $V_0 = 5$, and $a_0 = 1.25$. The initial conditions for the two figures are $x(0) = \sin(0.95\pi) \approx 0.156434$, $y(0) = 0$, $z(0) = \cos(0.95\pi) \approx -0.987688$, $a(0) \approx 1.6$, and $P(0) \approx 9.45$.

The chaotic behavior of this configuration is evident in both plots, although there remains a lot of structure, as we discussed in Chapter 8.[112, 158, 159] In the language of KAM theory, some of the nonresonant tori persist for the present

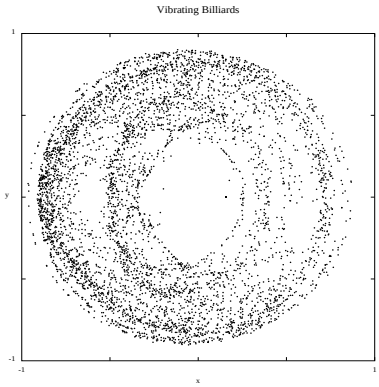

Figure 10.2: Poincaré section ($P = 0$) of the Bloch sphere projected onto the (x, y)-plane. The structure in this diagram likewise illustrates the survival of some invariant tori.

choice of initial conditions.[67, 88, 194] One may also choose initial conditions corresponding to a different level of persistence of the nonresonant tori. For example, Figure 10.3 shows an $x = 0$ Poincaré map in the (a, P)-plane with the same initial conditions and parameter values as above, except $a(0) = 3$ and $P(0) = 10$. Figure 10.4 shows a $P = 0$ Poincaré map in the (x, y)-plane for the same conditions. There are fewer invariant tori in these two figures than there are in Figures 10.1–10.2.

The chaotic behavior in null angular-momentum eigenstates is not restricted to the superposition of the ground state and the first excited state, as one expects to find chaotic behavior for *any* null angular-momentum two-state superposition of the radially vibrating spherical quantum billiard.[158] Additionally, recall that wavefunctions that are superpositions of eigenstates with both zero and finite angular momenta need not be chaotic in general. It is necessary that at least two of these eigenstates exhibit common rotational symmetry (i.e., have equal angular-momentum quantum numbers). For zero angular-momentum eigenstates, this condition is satisfied automatically, so every d-term superposition ($d \geq 2$) in the null angular-momentum case behaves chaotically for some choice of initial conditions

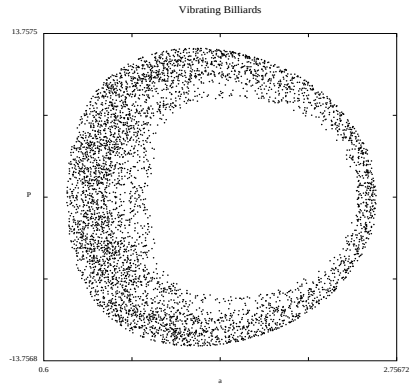

Figure 10.3: Poincaré section ($x = 0$) in the (a, P)-plane for slightly different initial conditions in which fewer invariant tori persist, in accord with KAM theory.

and parameter values.[112, 158]

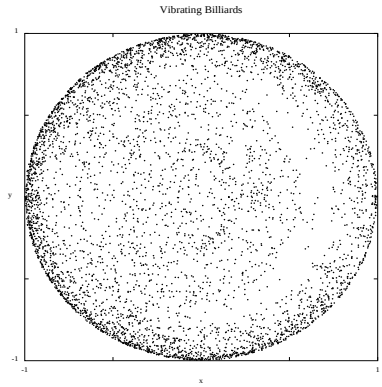

Figure 10.4: Poincaré section ($P = 0$) of the Bloch sphere projected onto the (x, y)-plane. The initial conditions in this plot correspond to those in Figure 10.3.

10.7 Phenomenology

As semiquantum chaos has been established for the present system, it is natural to ask about the nature of the corresponding chaotic behavior in real space. Due to

conservation of angular momentum, one finds that for the stationary spherical classical billiard, the enclosed particle sweeps out an annular domain of constant inner radius. Vibration of the wall of the sphere destroys this constant, and chaotic motion is expected to develop. (The 'moment arm' of the reflected trajectory increases during, say, the expansion phase of the sphere.) In the present quantum-mechanical situation, we note that null angular-momentum wavefunctions are composed only of spherical waves. The nodal surfaces of these wavefunctions are likewise spherical.

The chaotic signature in real space of superpositions of null-angular momentum eigenstates of the radially vibrating spherical quantum billiard is the sequence of intersections with a fixed radius that nodal surfaces make at any instant subsequent to a number of transversal times.[112, 158] At $t = t_1$, the eigenstates $\psi_1(r, t; a(t))$, $\psi_2(r, t; a(t))$ each vanish for a countably infinite set of values of r (which are determined by $a(t_1)$). At $t = t_2 > t_1$, the eigenstates vanish for two other countably infinite sets of values of r, *etc.* The number of transversal times in the sequence $\{t_1, \cdots, t_k\}$ simply refers to the number k, which describes how many times we strobe the system (i.e., the number of dots in a Poincaré section). Finally, note that the behavior just described is consistent with the standard long-time behavior of chaotic dynamical systems.[70]

CHAPTER 11

EXAMPLE: THE VIBRATING RECTANGULAR QUANTUM BILLIARD*

In this thesis, we have focused primarily on the case $s = 1$ describing vibrating quantum billiards with one nuclear *dof*. However, as multiple nuclear modes of molecular systems can be excited simultaneously, we briefly exanmine in this chapter the vibrating rectangular quantum billiard, for which $s = 2$. With $d = 2$, one obtains a three *dof* Hamiltonian system that behaves quite differently from the three *dof* systems studied in Chapter 9 (in which $s = 1$ and $d = 2$).

11.1 Quantum Billiards with $s \geq 2$ Nuclear *DOF*

In this section, we generalize some of the results of previous chapters to quantum billiards with $s \geq 2$ nuclear *dof*.

Suppose that ξ of the boundary constituents of a given quantum billiard are time-dependent and that the classical *dof* of the molecular Hamiltonian H can be decomposed as follows:

$$H(a_1, \cdots, a_\xi, P_1, \cdots, P_\xi; A_1, \cdots A_d) = \sum_{j=1}^{\xi} H_j(a_j, P_j; A_1, \cdots, A_d). \qquad (11.1)$$

For the classical *dof* of H to be decomposable, it is required that both the external potential $V(\mathbf{a})$ and the kinetic energy $K(\mathbf{a})$ can be decomposed in the same sense as the Hamiltonian. For some configurations, such as the vibrating rectangular parallelepiped billiard, the kinetic energy is decomposable. Others, however, are

*This chapter is based on reference [157].

not decomposable. For example, a spherical quantum billiard cannot be decomposed in the above sense if it undergoes both radial and angular oscillations, as its kinetic energy is $K(r,\theta,\phi) = K_1(r)K_2(\theta,\phi)$, which is not equal to $K_1 + K_2$.

If, for a given Galërkin expansion (5.20), there are no cross terms in the expectation obtained from Schrödinger's equation (5.1), the decomposable Hamiltonian H (11.1) decouples into ξ two-dimensional autonomous systems.[67, 114, 157, 159, 194] If either V or K is not decomposable, then H cannot be decomposed as in (11.1) and its associated dynamical system does not fully decouple.

Given a decomposable molecular Hamiltonian describing a vibrating quantum billiard on $D \subset \mathbb{R}^r$, a d-mode Galërkin expansion does not fully decouple if and only if the $(r-\xi)$ *fb* quantum numbers are the same for some pair of eigenstates (that is, the jth *fb* quantum number in one state must be the same as the jth *fb* quantum number in the other state of the pair, where j runs over all $(r-\xi)$ *fb* quantum numbers). This result, which is a generalization of the Quantum Number Symmetry Theorem, may be proven in an analogous manner.[157, 159]

11.2 The Rectangular Quantum Billiard

The rectangular quantum billiard describes the wavefunctions of a confined particle of mass m_0 undergoing perfectly elastic collisions inside a rectangular domain. The vertices of the rectangle are located at $(-\frac{a}{2}, -\frac{b}{2})$, $(-\frac{a}{2}, \frac{b}{2})$, $(\frac{a}{2}, -\frac{b}{2})$, and $(\frac{a}{2}, \frac{b}{2})$. If a and b are independent of time, a solution to the Schrödinger equation (5.1) with homogeneous Dirichlet boundary conditions is given by the following superposition of eigenstates:

$$\psi(x,y,t) = \sum_{n_x=1}^{\infty} \sum_{n_y=1}^{\infty} \alpha(a,b) A_{n_x n_y} \psi_{n_x n_y}(x,y) \exp\left[-\frac{iE_{n_x n_y} t}{\hbar}\right], \tag{11.2}$$

where $A_{n_x n_y}$ is the (complex) amplitude of the state with quantum numbers (n_x, n_y), $E_{n_x n_y} \equiv \epsilon_a(n_x) + \epsilon_b(n_y)$ is its eigenenergy, and $\psi_{n_x n_y}$ is its corresponding eigenstate.

This eigenstate is given by

$$\psi_{n_x n_y}(x,y) = \psi_{n_x}(x)\psi_{n_y}(y), \tag{11.3}$$

where

$$\psi_l(w) = \cos\left(\frac{\pi l w}{q}\right) \tag{11.4}$$

if l is even and

$$\psi_l(w) = \sin\left(\frac{\pi l w}{q}\right) \tag{11.5}$$

if l is odd. One absorbs the $n_x n_y$th (time-dependent) phase

$$\exp\left[-\frac{iE_{n_x n_y}t}{\hbar}\right] \tag{11.6}$$

into the coefficient $A_{n_x n_y}$.[157, 159] Note in equations (11.4,11.5) that $w = x$, $l = n_x$, $q = a$ for the length and $w = y$, $l = n_y$, $q = b$ for the width. Additionally,

$$\alpha(a,b) = \frac{2}{\sqrt{ab}} \tag{11.7}$$

is the normalization factor of the state with quantum numbers (n_x, n_y).

Allowing the walls to vibrate corresponds to a and b depending on time and $A_{n_x n_y}$ having a time-dependence other than the phase factor (11.6). All other parameters in the above equations remain constant with respect to time.

The time-dependent walls of the vibrating rectangular quantum billiard are described by its length $a(t)$ and width $b(t)$. The kinetic energy of the confined particle is given by

$$K = -\frac{\hbar^2}{2m_0}\nabla^2, \quad (x,y) \in \left[-\frac{a(t)}{2}, \frac{a(t)}{2}\right] \times \left[-\frac{b(t)}{2}, \frac{b(t)}{2}\right], \tag{11.8}$$

where the Laplacian ∇^2 is represented in Cartesian coordinates.

The molecular Hamiltonian is given by

$$H(a, P_a, b, P_b; A_1, \cdots, A_d) = K(a, b; A_1, \cdots A_d) + \frac{P_a^2}{2M_a} + \frac{P_b^2}{2M_b} + V(a,b), \tag{11.9}$$

where

$$P_a \equiv -i\hbar\frac{\partial}{\partial a} \tag{11.10}$$

is the momentum of the horizontal walls (which have mass $M_a \gg m_0$), and

$$P_b \equiv -i\hbar\frac{\partial}{\partial b} \tag{11.11}$$

is the momentum of the vertical walls (which have mass $M_b \gg m_0$). The external potential is $V(a,b)$. The molecular Hamiltonian (11.9) consists of a classical component ($P_a^2/2M_a + P_b^2/2M_b$) and a quantum one ($K+V$). We again apply the Born-Oppenheimer approximation[20, 22, 154] (see Chapter 2) in using only the quantum-mechanical component of the Hamiltonian in the Schrödinger equation. Additionally, the external potential V may be removed from the Schrödinger equation because it shifts all the eigenenergies by the same constant value.

11.3 Special Cases: Reduction to One Degree-of-Vibration

If either $a(t)$ or $b(t)$ (but not both) is independent of time, then the present problem has only one nuclear *dof.*[22, 23, 157] In this event, either P_a or P_b vanishes identically. If $a(t) = b(t)$ for all time, the rectangular quantum billiard is constrained to be a square, which again yields a configuration with one nuclear *dof.* This is discussed in greater detail in reference [157].

11.4 Equation of Motions

A two-mode Galërkin expansion of a quantum billiard with two nuclear *dof* is written

$$\psi(x,y,t) = A_1(t)\alpha\left(a(t),b(t)\right)\psi_{n_x n_y}(x,y,t) + A_2(t)\alpha\left(a(t),b(t)\right)\psi_{n'_x n'_y}(x,y,t) \tag{11.12}$$

and may be expressed using Dirac notation[174] as

$$|\psi\rangle = \psi_1 |n_x n_y\rangle + \psi_2 |n'_x n'_y\rangle . \tag{11.13}$$

The Schrödinger equation (5.1) is

$$i\hbar \frac{\partial \psi(x,y,t)}{\partial t} = -\frac{\hbar^2}{2m_0}\nabla^2 \psi(x,y,t), \quad (x,y) \in \left[-\frac{a(t)}{2}, \frac{a(t)}{2}\right] \times \left[-\frac{b(t)}{2}, \frac{b(t)}{2}\right], \tag{11.14}$$

The molecular Hamiltonian (11.9) is given by

$$H = K(a,b) + \frac{P_a^2}{2M_a} + \frac{P_b^2}{2M_b} + V(a,b), \tag{11.15}$$

where the walls of the quantum billiard have momenta P_a and P_b conjugate, respectively, to the length a and width b.

Inserting the superposition state (11.12) into the Schrödinger equation (11.14) and taking expectations gives

$$\begin{aligned} \left\langle \psi \left| -\frac{\hbar^2}{2m_0}\nabla^2 \psi \right. \right\rangle &= \frac{1}{a^2}\left(\epsilon_a^{(1)}|A_1|^2 + \epsilon_a^{(2)}|A_2|^2\right) + \frac{1}{b^2}\left(\epsilon_b^{(1)}|A_1|^2 + \epsilon_b^{(2)}|A_2|^2\right), \\ i\hbar \left\langle \psi \left| \frac{\partial \psi}{\partial t} \right. \right\rangle &= i\hbar \Big[\dot{A}_1 A_2^* + \dot{A}_2 A_1^* \\ &\quad + \nu_{11}|A_1|^2 + \nu_{22}|A_2|^2 + \nu_{12} A_1 A_2^* + \nu_{21} A_2 A_1^*\Big] , \end{aligned} \tag{11.16}$$

where ν_{ij} $(i,j \in \{1,2\})$ is a constant. In (11.16),

$$\begin{aligned} \epsilon_a^{(1)} &\equiv \frac{(n_x \pi \hbar)^2}{2m_0}, \\ \epsilon_a^{(2)} &\equiv \frac{(n'_x \pi \hbar)^2}{2m_0}, \\ \epsilon_b^{(1)} &\equiv \frac{(n_y \pi \hbar)^2}{2m_0}, \\ \epsilon_b^{(2)} &\equiv \frac{(n'_y \pi \hbar)^2}{2m_0}. \end{aligned} \tag{11.17}$$

Additionally, the enery $E_{n_x n_y}$ of the $n_x n_y$th eigenstate is given by[157]

$$E_{n_x n_y} = \epsilon_a^{(1)} + \epsilon_b^{(1)} \tag{11.18}$$

The choice of eigenstates in (11.12) determines the values of the coupling coefficients μ_{jk}, which are defined by

$$\nu_{jk} \equiv \mu_{jk} \frac{\dot{a}}{a} \tag{11.19}$$

or

$$\nu_{jk} \equiv \mu_{jk} \frac{\dot{b}}{b}. \tag{11.20}$$

The interaction coefficient $\mu_{jk} = -\mu_{kj}$, $(j \neq k)$ is nonzero only when either $n_x = n'_x$ or $n_y = n'_y$. (Exactly one of these equalities holds.) The diagonal coefficients μ_{jj} and μ_{kk} always vanish. Moreover, ν_{jk} is proportional to $\dot{a}/a$ if $n_y = n'_y$ and to $\dot{b}/b$ if $n_x = n'_x$. This proportionality constant, which is exactly the quantity μ_{jk}, is given by the same formula as in the one-dimensional vibrating quantum billard.[22, 23, 157] Using the indices n and n' to represent whichever pair of (n_x, n'_x) or (n_y, n'_y) has distinct values and also assuming $n < n'$ without loss of generality yields the expression

$$\mu_{jk} \equiv \mu_{nn'} = \frac{2nn'}{(n'+n)(n'-n)}. \tag{11.21}$$

If considering a superposition of more than two states, the results discussed in this paragraph apply to each pair of eigenstates. If the potential V is decomposable (as is the case with the harmonic potential), then the molecular Hamiltonian (11.9) decouples into two one-*dof* Hamiltonians.

A rectangular quantum billiard with two nuclear *dof* has only four types of two-term superpositions that give nonvanishing cross terms μ_{jk}. (This follows from the above results using trigonometric identities and the orthogonality relations of

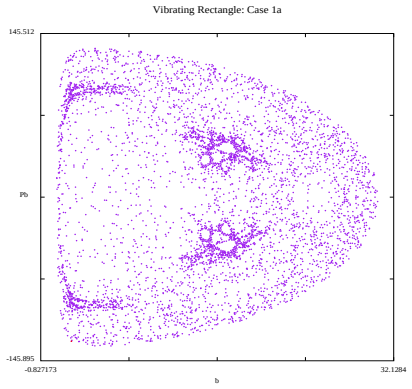

Figure 11.1: Poincaré section for the cut $P_a = 0$ in the (b, P_b)-plane with potential parameters $V_0 = 5$, $V_a = 10$, and $V_b = 2$

trigonometric functions.) These are

$$\begin{aligned}
\psi &= A_1\alpha \cos\left(\frac{n_x\pi x}{a}\right)\cos\left(\frac{n_y\pi y}{b}\right) + A_2\alpha \cos\left(\frac{n'_x\pi x}{a}\right)\cos\left(\frac{n'_y\pi y}{b}\right), \\
\psi &= A_1\alpha \cos\left(\frac{n_x\pi x}{a}\right)\sin\left(\frac{n_y\pi y}{b}\right) + A_2\alpha \cos\left(\frac{n'_x\pi x}{a}\right)\sin\left(\frac{n'_y\pi y}{b}\right), \\
\psi &= A_1\alpha \sin\left(\frac{n_x\pi x}{a}\right)\cos\left(\frac{n_y\pi y}{b}\right) + A_2\alpha \sin\left(\frac{n'_x\pi x}{a}\right)\cos\left(\frac{n'_y\pi y}{b}\right), \\
\psi &= A_1\alpha \sin\left(\frac{n_x\pi x}{a}\right)\sin\left(\frac{n_y\pi y}{b}\right) + A_2\alpha \sin\left(\frac{n'_x\pi x}{a}\right)\sin\left(\frac{n'_y\pi y}{b}\right),
\end{aligned} \tag{11.22}$$

where in each of the above equations, either $n_x = n'_x$ or $n_y = n'_y$ (but not both).

In addition to the symmetry requirements for *fb* quantum numbers discussed above, the *mb* quantum numbers in the vibrating rectangular quantum billiard must also satisfy some symmetry conditions for the coupling coefficients μ_{jk} to be nonzero. (There are no such requirements on *mb* quantum numbers in quantum billiards with one nuclear *dof.*) This is reflected in the superpositions (11.22), which are a subset of those that obey the symmetry requirements for the *fb* quantum numbers.

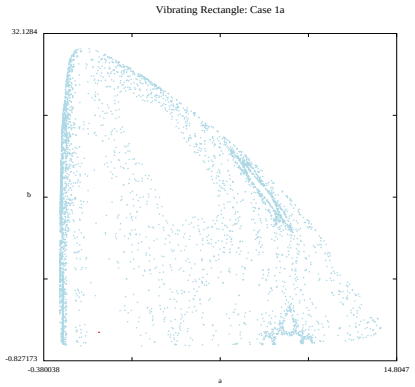

Figure 11.2: Poincaré section for the cut $P_a = 0$ in the (a, b)-plane with potential parameters $V_0 = 5$, $V_a = 10$, and $V_b = 2$

11.4.1 Case One: $\mu_{jk} = 0$

Suppose the interaction coefficients μ_{jk} vanish for all $j, k \in \{1, 2\}$. Equating coefficients in the quadratic forms (11.16) yields

$$i\dot{A}_j = \frac{1}{\hbar}\left(\frac{\epsilon_a^{(j)}}{a^2} + \frac{\epsilon_b^{(j)}}{b^2}\right), \quad j \in \{1, 2\}. \tag{11.23}$$

Integrating (11.23) gives

$$A_j = C_j \exp\left[-\frac{i}{\hbar}\int\left(\frac{\epsilon_a^{(j)}}{a^2} + \frac{\epsilon_b^{(j)}}{b^2}\right) dt\right], \tag{11.24}$$

where C_j is a constant. Since the only time-dependence of A_j is a phase, it follows that $|A_j|^2 = |C_j|^2$ is a constant. The dynamics of the present system are thus determined by the Hamiltonian

$$H(a, P_a, b, P_b) \equiv \frac{P_a^2}{2M_a} + \frac{P_b^2}{2M_b} + K(A_1, A_2, a, b) + V(a, b), \tag{11.25}$$

where the electronic kinetic energy $K(A_1, A_2, a, b)$ is decomposable in the sense that

$$K(A_1, A_2, a, b) = K_1(A_1, A_2, a) + K_2(A_1, A_2, b) \tag{11.26}$$

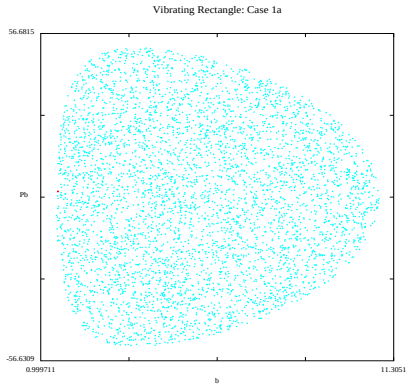

Figure 11.3: Poincaré section for the cut $P_a = 0$ in the (b, P_b)-plane with potential parameters $V_0 = 12$, $V_a = 1$, and $V_b = 3$

and is given by

$$\begin{aligned} K &= \left(\frac{\epsilon_a^{(1)}}{a^2} + \frac{\epsilon_b^{(1)}}{b^2}\right)|A_1|^2 + \left(\frac{\epsilon_a^{(2)}}{a^2} + \frac{\epsilon_b^{(2)}}{b^2}\right)|A_2|^2 \\ &= \frac{\epsilon_a^{(1)}|C_1|^2 + \epsilon_a^{(2)}|C_2|^2}{a^2} + \frac{\epsilon_b^{(1)}|C_1|^2 + \epsilon_b^{(2)}|C_2|^2}{b^2}. \end{aligned} \tag{11.27}$$

The equations of motion of (11.25) are

$$\begin{aligned} \dot{a} &= \frac{P_a}{M_a} \\ \dot{P}_a &= -\frac{\partial V}{\partial a} + \frac{2}{a^3}\left(\epsilon_a^{(1)}|C_1|^2 + \epsilon_a^{(2)}|C_2|^2\right) \\ \dot{b} &= \frac{P_b}{M_b} \\ \dot{P}_b &= -\frac{\partial V}{\partial b} + \frac{2}{b^3}\left(\epsilon_b^{(1)}|C_1|^2 + \epsilon_b^{(2)}|C_2|^2\right). \end{aligned} \tag{11.28}$$

Stationary points of (11.28) satisfy $P_a = P_b = 0$,

$$\frac{\partial V}{\partial a} = \frac{2}{a^3}\left(\epsilon_a^{(1)}|C_1|^2 + \epsilon_a^{(2)}|C_2|^2\right), \tag{11.29}$$

and

$$\frac{\partial V}{\partial b} = \frac{2}{b^3}\left(\epsilon_b^{(1)}|C_1|^2 + \epsilon_b^{(2)}|C_2|^2\right). \tag{11.30}$$

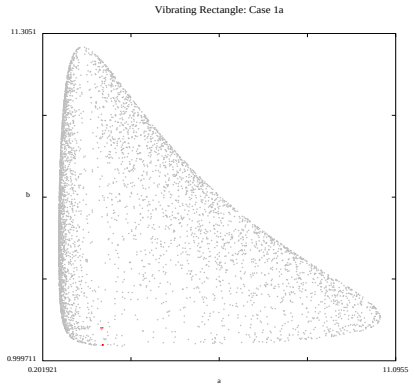

Figure 11.4: Poincaré section for the cut $P_a = 0$ in the (a, b)-plane with potential parameters $V_0 = 12$, $V_a = 1$, and $V_b = 3$

Define the quantities

$$\eta_a \equiv \epsilon_a^{(1)}|C_1|^2 + \epsilon_a^{(2)}|C_2|^2,$$
$$\eta_b \equiv \epsilon_b^{(1)}|C_1|^2 + \epsilon_b^{(2)}|C_2|^2. \tag{11.31}$$

The eigenvalues of any equilibrium point of (11.28) such that

$$\frac{\partial^2 V}{\partial a^2}(a_*, b_*)\frac{\partial^2 V}{\partial b^2}(a_*, b_*) - \left(\frac{\partial^2 V}{\partial a \partial b}(a_*, b_*)\right)^2 + \frac{6\eta_a}{a_*^4}\frac{\partial^2 V}{\partial b^2}(a_*, b_*) + \frac{6\eta_b}{b_*^4}\frac{\partial^2 V}{\partial a^2}(a_*, b_*) + \frac{36\eta_a\eta_b}{a_*^4 b_*^4} \geq 0, \tag{11.32}$$

where a_* and b_* denote equilibrium displacements, have zero real part. Such equilibria are hence elliptic (and linearly stable). In particular, if $V(a, b)$ has a single minimum, then every equilibrium point is elliptic.

The dynamical equations obtained in this section are analogous to those obtained if only a single eigenstate is considered.[157] If $K + V$ is not decomposable with respect to the nuclear *dof*, this yields chaotic dynamics. In the context of polyatomic molecules, this implies that a molecular system in which two or more

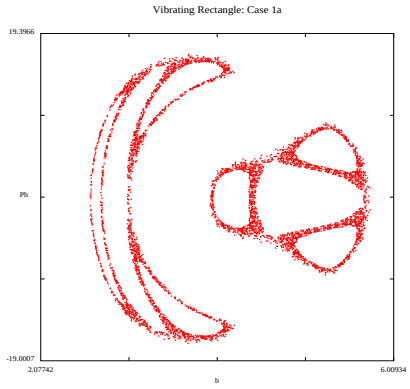

Figure 11.5: Poincaré section for the cut $P_a = 0$ in the (b, P_b)-plane with potential parameters $V_0 = 12$, $V_a = 1$, and $V_b = 3$

nuclear modes have been excited can behave chaotically even in the absence of electronic near-degeneracies. (When $K + V$ is decomposable, these modes act independently.) By contrast, as discussed in prior chapters, vibrations described by a single nuclear coordinate must be coupled to at least two of the molecule's electronic eigenstates to exhibit chaos.

If V can be decomposed as

$$V(a, b) = V_a(a) + V_b(b), \tag{11.33}$$

then $H(a, P_a, b, P_b)$ is also decomposable. That is,

$$H(a, P_a, b, P_b) = H_a(a, P_a) + H_b(b, P_b) \tag{11.34}$$

decouples into two one-*dof* Hamiltonian systems.[67, 114, 157, 194]

If, on the other hand, V cannot be decomposed as in (11.33), then the molecular Hamiltonian H is studied as a two *dof* system. Consider, for example, the anharmonic potential

$$V(a, b) = V_a(a - a_0)^2 + V_b b_0^2 (b - b_0)^2 + V_0(a - a_0)(b - b_0), \tag{11.35}$$

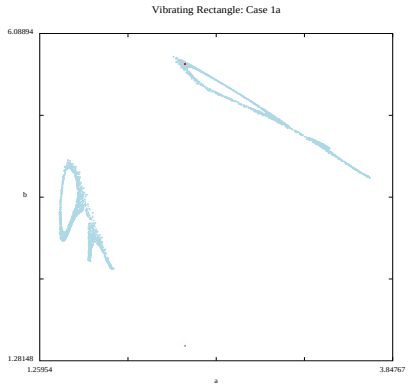

Figure 11.6: Poincaré section for the cut $P_a = 0$ in the (a, b)-plane with potential parameters $V_0 = 12$, $V_a = 1$, and $V_b = 3$

in which the last term measures the interaction between the two excited nuclear modes in the molecule of interest. In (11.35),

$$\begin{aligned} \frac{\partial^2 V}{\partial a^2} &= 2V_a, \\ \frac{\partial^2 V}{\partial b^2} &= 2V_b, \\ \frac{\partial^2 V}{\partial a \partial b} &= V_0, \end{aligned} \tag{11.36}$$

so an equilibrium point of (11.28) is elliptic if and only if

$$4V_aV_b - V_0^2 + \frac{12\eta_a V_b}{a_*^4} + \frac{12\eta_b V_a}{b_*^4} + \frac{36\eta_a\eta_b}{a_*^4 b_*^4} \geq 0. \tag{11.37}$$

Figures 11.1–11.6 show various Poincaré maps corresponding to the superposition state

$$\psi = \alpha(a,b)A_1 \cos\left(\frac{\pi x}{a}\right)\cos\left(\frac{3\pi y}{b}\right) + \alpha(a,b)A_2 \sin\left(\frac{2\pi x}{a}\right)\sin\left(\frac{4\pi y}{b}\right). \tag{11.38}$$

The parameter values in each figure are $\hbar = 1$, $m_0 = 1$, $\epsilon_a^{(1)} = \hbar^2\pi^2/2m_0 \approx 4.9348022$, $\epsilon_b^{(1)} = 9\hbar^2\pi^2/2m_0 \approx 44.4132198$, $\epsilon_a^{(2)} = 4\hbar^2\pi^2/2m_0 \approx 19.7392088$, $\epsilon_b^{(2)} =$

Figure 11.7: Poincaré section for the harmonic potential with the cut $x = 0$ projected into the (a, b)-plane

$15\hbar^2\pi^2/2m_0 \approx 78.9568352$, $a_0 = 1.25$, $b_0 = 0.75$, $|C_1|^2 = 4$, $|C_2|^2 = 8$, $M_a = 10$, and $M_b = 5$. Figure 11.1 shows the Poincaré map corresponding to the cut $P_a = 0$ projected into the (b, P_b)-plane for the parameter values $V_0 = 5$, $V_a = 10$, and $V_b = 2$. Figure 11.2 shows the corresponding projection in the (a, b)-plane.

Figures 11.3–11.6 depict Poincaré sections corresponding to the parameter values $V_0 = 12$, $V_a = 1$, and $V_b = 3$. Figures 11.3 and 11.5 depict Poincaré maps for $P_a = 0$ for different initial conditions projected into the (b, P_b)-plane. Figures 11.4 and 11.6 correspond, respectively, to Figures 11.3 and 11.5 and show projections of the Poincaré maps in the (a, b)-plane. Note that the plots are of the same form for any constant $c > 0$, where $|C_1|^2 + |C_2|^2 = |A_1|^2 + |A_2|^2 = c$, so only the relative sizes of $|C_1|^2$ and $|C_2|^2$ are relevant.

11.4.2 Case Two: $\mu_{jk} \neq 0$

Recall that a two-term superposition

$$|\psi\rangle = \psi_1 |n_x n_y\rangle + \psi_2 |n'_x n'_y\rangle \tag{11.39}$$

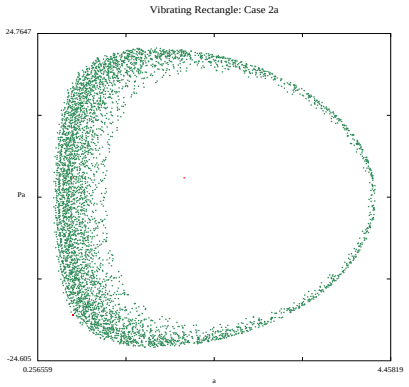

Figure 11.8: Poincaré section for the harmonic potential with the cut $x = 0$ projected into the (a, P_a)-plane

must satisfy either $n_x = n'_x$ or $n_y = n'_y$ to yield non-vanishing interaction coefficients μ_{jk}. Without loss of generality, consider the case in which $n_y = n'_y$. The equations of motion in the case $n_x = n'_x$ are obtained by reversing the roles of the vectors (a, P_a) and (b, P_b).

Taking expectations and equating coefficients gives

$$i\dot{A}_n = \sum_{j=1}^{2} D_{nj} A_j, \tag{11.40}$$

where

$$(D_{nj}) = \begin{pmatrix} \frac{1}{\hbar}\left(\frac{\epsilon_a^{(1)}}{a^2} + \frac{\epsilon_b^{(1)}}{b^2}\right) & -i\mu_{nn'}\frac{\dot{a}}{a} \\ i\mu_{nn'}\frac{\dot{a}}{a} & \frac{1}{\hbar}\left(\frac{\epsilon_a^{(2)}}{a^2} + \frac{\epsilon_b^{(2)}}{b^2}\right) \end{pmatrix} \tag{11.41}$$

and $\mu_{nn'}$ is the interaction coefficient corresponding to $A_n A^*_{n'}$ in (11.16).

Figure 11.9: Poincaré section for the harmonic potential with the cut $x = 0$ projected into the (b, P_b)-plane

Transforming to Bloch variables and noting that $\epsilon_b^{(1)} = \epsilon_b^{(2)}$ yields

$$\begin{aligned} \dot{x} &= -\frac{\omega_0^{(a)} y}{a^2} - \frac{2\mu_{nn'} P_a z}{M_a a}, \\ \dot{y} &= \frac{\omega_0^{(a)} x}{a^2}, \\ \dot{z} &= \frac{2\mu_{nn'} P x}{M_a a}, \end{aligned} \tag{11.42}$$

where

$$\omega_0^{(a)} \equiv \frac{\epsilon_a^{(2)} - \epsilon_a^{(1)}}{\hbar}. \tag{11.43}$$

Note additionally that the quantum subsystem (11.42) of the dynamical system of interest depends only on the displacement a and not on b. This follows from the fact that $n_y = n_y'$.

Using Bloch variables, one computes

$$K(A_1, A_2, a, b) = \frac{(\epsilon_a^+ + z\epsilon_a^-)}{a^2} + \frac{\epsilon_b^+}{b^2}, \tag{11.44}$$

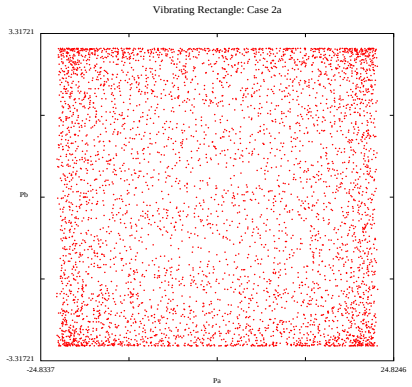

Figure 11.10: Poincaré section for the harmonic potential with the cut $x = 0$ projected into the (P_a, P_b)-plane

where

$$\epsilon_a^{\pm} \equiv \frac{\epsilon_a^{(2)} \pm \epsilon_a^{(1)}}{2},$$
$$\epsilon_b^{\pm} \equiv \frac{\epsilon_b^{(2)} \pm \epsilon_b^{(1)}}{2}. \tag{11.45}$$

Because $\epsilon_b^{(1)} = \epsilon_b^{(2)}$, the quantity ϵ_b^- vanishes for the superposition state (11.39) with $n_y = n_y'$.

The Hamiltonian corresponding to (11.39) is

$$H(a, P_a, b, P_b) = \frac{P_a^2}{2M_a} + \frac{P_b^2}{2M_b} + K(z; a, b) + V(a, b). \tag{11.46}$$

This leads to Hamilton's equations

$$\dot{a} = \frac{\partial H}{\partial P_a},$$
$$\dot{P}_a = -\frac{\partial H}{\partial a},$$
$$\dot{b} = \frac{\partial H}{\partial P_b},$$
$$\dot{P}_b = -\frac{\partial H}{\partial b}. \tag{11.47}$$

Figure 11.11: Poincaré section for the harmonic potential with the cut $P_a = 0$ projected into the (x, y)-plane

Consequently,

$$\begin{aligned} \dot{a} &= \frac{P_a}{M_a}, \\ \dot{b} &= \frac{P_b}{M_b}, \end{aligned} \tag{11.48}$$

and

$$\begin{aligned} \dot{P}_a &\equiv -\frac{\partial V}{\partial a} - \frac{\partial K}{\partial a} = -\frac{\partial V}{\partial a} + \frac{2}{a^3}[\epsilon_a^+ + \epsilon_a^-(z - \mu_{nn'}x)], \\ \dot{P}_b &\equiv -\frac{\partial V}{\partial b} - \frac{\partial K}{\partial b} = -\frac{\partial V}{\partial b} + \frac{2\epsilon_b^+}{b^3}. \end{aligned} \tag{11.49}$$

Stationary points of the dynamical system (11.42,11.48,11.49) satisfy $P_a = P_b = x = y = 0$, $z = \pm 1$, $a = a_\pm$, and $b = b_\pm$, where $a_\pm$ satisfies $\dot{P}_a = 0$ for $z = 1$ and $z = -1$, respectively, and $b_\pm$ does the same for $\dot{P}_b = 0$. That is, $a_\pm$ satisfies

$$\frac{2}{a_\pm^3}(\epsilon_a^+ \pm \epsilon_a^-) = \left.\frac{\partial V}{\partial a}\right|_{a=a_\pm} \tag{11.50}$$

and $b_\pm$ satisfies

$$\frac{2\epsilon_b^+}{b_\pm^3} = \left.\frac{\partial V}{\partial b}\right|_{b=b_\pm}. \tag{11.51}$$

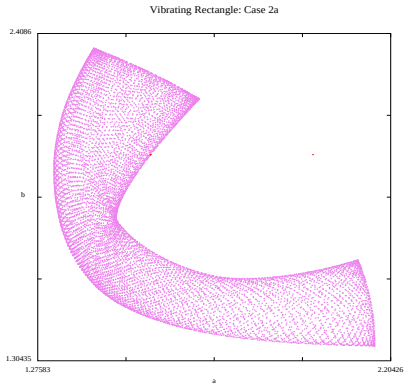

Figure 11.12: Poincaré section for the anharmonic potential with the cut $x = 0$ projected into the (a, b)-plane

As equations (11.50) and (11.51) correspond to those obtained previously for quantum billiards with one nuclear *dof*, it follows that every equilibrium in the vibrating rectangular quantum billiard corresponds to a pure state. In fact, this result holds for quantum billiards of any globally separable geometry with any number of nuclear *dof*. However, one may be able to obtain mixed-state equilibria for related systems (such as coupled vibrating quantum billiards) or upon the application of external forces (such as those due to magnetic fields).

As when $s = 1$, one may examine both decomposable and indecomposable potentials $V(a, b)$.[157] If V is decomposable, the dynamical system (11.42,11.48,11.49) decouples so that the time-evolutions of (x, y, z, a, P_a) and (b, P_b) are independent of each other. In this event, the analysis of (x, y, z, a, P_a) reduces to that for quantum billiards with one nuclear *dof*. Nevertheless, the integrable dynamics of (b, P_b) prove insightful when compared side-by-side with the potentially chaotic dynamics (a, P_a), as demonstrated by figures (11.7)–(11.11).

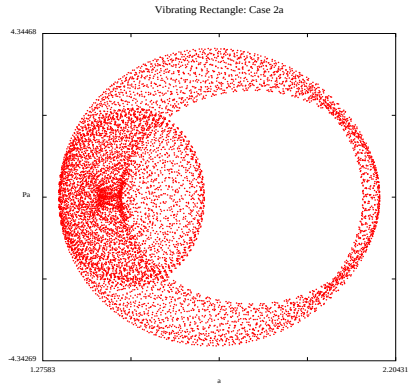

Figure 11.13: Poincaré section for the anharmonic potential with the cut $x = 0$ projected into the (a, P_a)-plane

In our numerical simulations, we utilized the superposition state

$$\psi = \alpha(a,b)A_1(t)\cos\left(\frac{\pi x}{a(t)}\right)\cos\left(\frac{\pi y}{b(t)}\right) + \alpha(a,b)A_2(t)\cos\left(\frac{3\pi x}{a(t)}\right)\cos\left(\frac{\pi y}{b(t)}\right), \tag{11.52}$$

for which $\mu_{12} = 3/4$. Recall that the roles of (a, P_a) and (b, P_b) are reversed if $n_x = n'_x$ rather than $n_y = n'_y$.

Consider first the harmonic potential

$$V(a,b) = V_a(a - a_0)^2 + V_b(b - b_0)^2, \tag{11.53}$$

which is decomposable. The (x, y, z, a, P_a) components of the equilibria correspond to those in the one-dimensional vibrating billiard.[157] These equilibria also satisfy

$$\frac{2\epsilon_b^+}{b_\pm^3} = 2V_b(b_\pm - b_0). \tag{11.54}$$

Poincaré sections for the harmonic potential are shown in Figures 11.7–11.11. These depict, respectively, the cut $x = 0$ projected into the (a, b)-plane, the cut $x = 0$ in the (a, P_a)-plane, the cut $x = 0$ in the (b, P_b)-plane, the cut $x = 0$ in

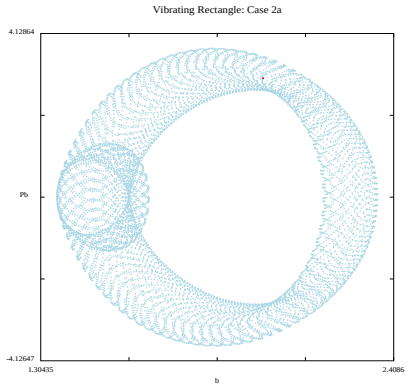

Figure 11.14: Poincaré section for the anharmonic potential with the cut $x = 0$ projected into the (b, P_b)-plane

the (P_a, P_b)-plane, and the cut $P_a = 0$ in the (x, y)-plane. In units of $\hbar = 1$, we used the paramter values $m_0 = 1$, $M_a = 10$, $\epsilon_a^{(1)} = \hbar^2\pi^2/2 \approx 4.9348022$, $\epsilon_a^{(2)} = 9\hbar^2\pi^2/2 \approx 44.4132198$, $\epsilon_b^{(1)} = \epsilon_b^{(2)} = \hbar^2\pi^2/2$, $V_a = 3$, $V_b = 2$, $a_0 = 1.25$, and $b_0 = 1.75$ with the initial conditions $x(0) = \sin(0.95\pi) \approx 0.156434$, $y(0) = 0$, $z(0) = \cos(0.95\pi) \approx -0.987688$, $a(0) \approx 0.6788079$, $P_a(0) \approx -17.6821192$, $b(0) = 2$, and $P_b(0) = 3$.

The dynamics depicted in Figures 11.8 and 11.11 correspond to that in quantum billiards with one nuclear *dof.*[159] Additionally, Figure 11.9 displays integrable motion in the (b, P_b) plane, which is necessarily the case in this decoupled situation. In contrast, the projection of the same motion in the (a, P_a)-plane is chaotic. This follows from the fact that the second term in the superposition state (11.52) was excited only with respect to the length $a(t)$ and the ensuing decoupling between the two nuclear *dof.*

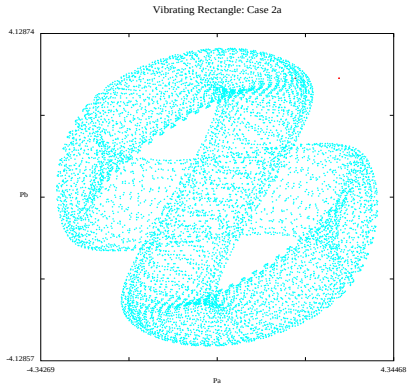

Figure 11.15: Poincaré section for the anharmonic potential with the cut $x = 0$ projected into the (P_a, P_b)-plane

As another example, consider the anharmonic potential

$$V(a,b) = V_a(a-a_0)^2 + V_b(b-b_0)^2 + V_0(a-a_0)(b-b_0), \tag{11.55}$$

which is indecomposable. Figures 11.12–11.19 depict, respectively, the Poincaré cut $x = 0$ projected into the (a,b)-plane, the cut $x = 0$ in the (a, P_a)-plane, the cut $x = 0$ in the (b, P_b)-plane, the cut $x = 0$ in the (P_a, P_b)-plane, the cut $P_a = 0$ in the (b, P_b)-plane, the cut $P_a = 0$ in the (x, y)-plane, the cut $P_a = 0$ in the (x, z)-plane, and the cut $P_a = 0$ in the (y, z)-plane. The parameter values in each figure are $\hbar = 1$, $m_0 = 1$, $M_a = 10$, $\epsilon_{a_1} = \hbar^2\pi^2/2m_0 \approx 4.9348022$, $\epsilon_{a_2} = 9\hbar^2\pi^2/2m \approx 44.4132198$, $\epsilon_{b_1} = \epsilon_{b_2} = \hbar^2\pi^2/2m_0$, $\mu_{12} = 0.75$, $V_0 = 5$, $a_0 = 1.25$, $b_0 = 1.75$, $M_b = 10$, $V_a = 3$, and $V_b = 2$. Additionally, the initial conditions for each plot are $x(0) = \sin(0.95\pi) \approx 0.156434$, $y(0) = 0$, and $z(0) = \cos(0.95\pi) \approx -0.987688$, $a(0) \approx 1.5728477$, $P_a(0) \approx 1.9205298$, $b(0) = 2$, and $P_b(0) = 3$. Each plot except Figure 11.14 exhibits chaotic behavior. (In general, the regions in parameter space in which the projection of the motion in the (b, P_b)-plane is integrable are larger

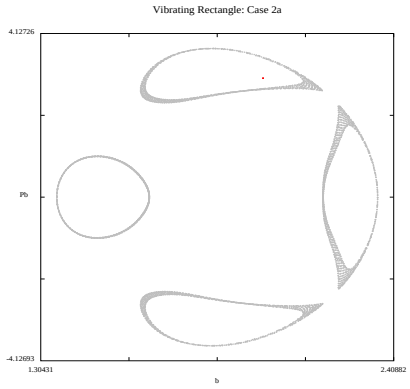

Figure 11.16: Poincaré section for the anharmonic potential with the cut $P_a = 0$ projected into the (b, P_b)-plane

than those in any other two-dimensional projection. Recall that for decomposable potentials such as the harmonic potential, the projection of the motion in this plane is always integrable.)

Unlike when V is harmonic, the behavior of the vibrating rectangular quantum billiard in anharmonic potentials is clearly distinguishable from the dynamics of quantum billiards with one nuclear *dof.*[157] The indecomposability of the anharmonic potential leads to coupling between the billiard's two nuclear *dof.*

In Figures 11.13 and 11.14, both the (a, P_a)-plane and the (b, P_b)-plane include two distinct elliptical regions. Additionally, the behavior in the (b, P_b)-plane is (as expected) more complicated in this situation than it was in the harmonic case. In Figure 11.14, the behavior in the (b, P_b) plot appears to be integrable, but that is no longer guaranteed to be the case a priori. For the anharmonic potential (or any other indecomposable potential), Poincaré maps *can* exhibit chaos when projected into the (b, P_b)-plane. Note additionally that the depicted double-ellipse structure is not present for all initial conditions.

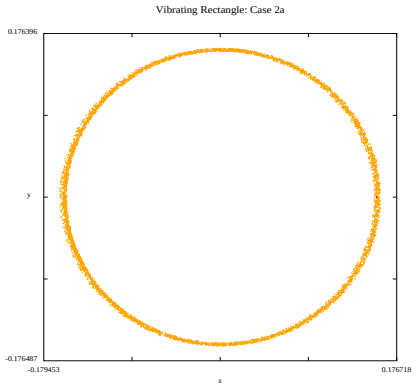

Figure 11.17: Poincaré section for the anharmonic potential with the cut $P_a = 0$ projected into the (x, y)-plane

Just as we found for vibrating quantum billiards with $s = 1$ nuclear *dof*, Poincaré sections commonly indicate that trajectories of (11.42,11.48,11.49) spend more time in regions of low $a(t)$ than in those of high $a(t)$. This follows from the $1/a^2$ dependence of the electronic kinetic energy K. We consider the physical context of this behavior in some detail, in particular with reference to Figure 11.8, which is similar to many plots obtained when studying the radially vibrating spherical quantum billiard.[112, 155, 157, 158] A low value of $a(t)$ leads to a larger kinetic energy, as the frequency of the confined particle's wavefunctions increases as a result of the smaller enclosure. The derivative of K with respect to a (which is proportional to $1/a^3$) becomes very large as well, so $|\dot{P}_a|$ also becomes large. This often leads to a sign change in P_a and consquently a change in direction of the motion of that constituent of the wall. One thus often observes a large range of momenta P_a for small a. For large a, the potential $V(a, b)$ (and its derivative with respect to a) often becomes large, leading to a sign change in P_a in that region as well. (More complicated behavior can also occur, but the present description

Figure 11.18: Poincaré section for the anharmonic potential with the cut $P_a = 0$ projected into the (x, z)-plane

pertains to the standard chaotic configuration that is depicted in Figure 11.8.) The potential $V(a, b) \propto a^2$, so

$$\frac{\partial V(a,b)}{\partial a} \propto a. \tag{11.56}$$

On the other hand,

$$\frac{\partial K}{\partial a} \propto a^3. \tag{11.57}$$

Consequently, the range of momenta P_a is larger for small a than it is for large a. For a quartic potential, however, one computes that

$$\frac{\partial V(a,b)}{\partial a} \propto a^3, \tag{11.58}$$

so the analogous configuration has an equally large range for P_a for both the upper and lower regions of $a(t)$.[155, 157] For intermediate values of a, the terms from the potential energy V (whether or not it includes quartic terms) and the kinetic energy K compete with each other, so $|\dot{P}_a|$ is not very large and the momentum P_a does not change signs. For small a, moreover, one often observes a higher density

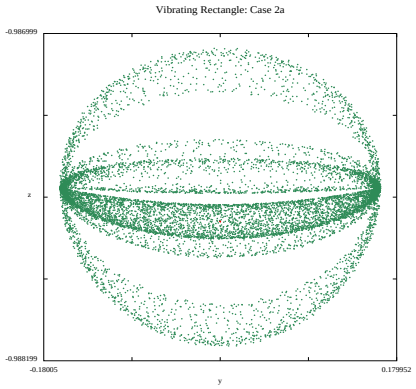

Figure 11.19: Poincaré section for the anharmonic potential with the cut $P_a = 0$ projected into the (y, z)-plane

of points in the Poincaré map (for the cut $x = 0$). Indeed, the Bloch variable x often changes sign as a result of a change in sign of P_a, so such behavior is expected to occur for many initial conditions.

The significance of the dynamical behavior at small, intermediate, and large values of a discussed above may be interpreted in a molecular context in light of the physical interpretations of K and V. The influence of K is increased as one considers increasingly excited electronic states, and the influence of V becomes larger as the interatomic bonds become stiffer. We note, in particular, that the above analysis indicates a preference for small interatomic displacements.[159]

CHAPTER 12

HOMOCLINIC TANGLES AND ARNOLD DIFFUSION

To examine vibrating quantum billiards in the context of Jahn-Teller theory, it is necessary to express their quantum *dof* using action-angle variables. In the present chapter, we do this with an adiabatic basis.[137, 154, 189] We also apply Melnikov's method to prove that vibrating quantum billiards exhibit homoclinic tangles and provide a plausibility argument that Galërkin expansions (i.e., superposition states) with at least three states also exhibit a priori unstable Arnold diffusion.

12.1 Adiabatic Action-Angle Formulation

To obtain action-angle variables, one applies a polar decomposition.[189] Define actions (real amplitudes) $n_k \in (0, 1)$ and angles (phases) θ_j from the complex amplitudes A_k in a Galërkin expansion via the relation[78, 137, 154, 189]

$$A_k \equiv \sqrt{n_k} e^{i\theta_k}. \tag{12.1}$$

The quantum actions satisfy

$$\sum_{k=1}^{d} n_k = 1, \tag{12.2}$$

by conservation of probability, so only $(d-1)$ of them are independent. There are also only $(d-1)$ independent phases, as quantum systems are invariant under global phase shifts. Consequently, a d-mode Galërkin expansion yields $(d-1)$ quantum-mechanical *dof*.[160]

The adiabatic Hamiltonian for a d-term superposition state of a quantum billiard with s vibrational modes is given by

$$H(\mathbf{a},\mathbf{P},\mathbf{n},\theta) = \sum_{l=1}^{s} \frac{P_l^2}{2M_l} + \sum_{l=1}^{s} \frac{1}{M_l} P_l W_l(\mathbf{n},\theta;\mathbf{a}) + \sum_{l=1}^{s} \frac{1}{2M_l} W_l^2 + K(\mathbf{n};\mathbf{a}) + V(\mathbf{a}), \tag{12.3}$$

where $\mathbf{a} \equiv (a_1, \cdots, a_s)$ is the vector of nuclear displacements, $\mathbf{P} \equiv (P_1, \cdots, P_s)$ is the vector of (non-kinetic) conjugate momenta, $\mathbf{n} \equiv (n_1, \cdots, n_d)$ is the vector of actions, $\theta \equiv (\theta_1, \cdots, \theta_d)$ is the vector of conjugate angles, and M_l is the mass of the lth (time-dependent) boundary constituent of the quantum billiard.

The electronic kinetic energy K can be decomposed as

$$K(\mathbf{n};\mathbf{a}) = \sum_{l=1}^{s} K_l\left(\mathbf{n};a_l\right), \tag{12.4}$$

where

$$K_l = \frac{1}{a_l^2} \sum_{c=1}^{d} n_c \epsilon_l^{(c)} \tag{12.5}$$

is the kinetic energy due to the interaction of the confined particle with the lth portion of the boundary. The quantity $\epsilon_l^{(c)}$, which is larger for increasingly excited eigenstates, is an energy parameter reflecting the interaction between the cth eigenstate and the lth boundary constituent.

The lth *harmonic coupling function* W_l is given by

$$W_l \equiv -i\hbar \sum_{j,k=1}^{d} \sqrt{n_j n_k} \exp\left[i(\theta_k - \theta_j)\right] T_{jk}^{(l)}(\mathbf{a}), \tag{12.6}$$

where

$$T_{kj}^{(l)}(\mathbf{a}) = \left\langle \psi_k \left| \frac{\partial \psi_j}{\partial a_l} \right. \right\rangle = -T_{jk}^{(l)}(\mathbf{a}) \tag{12.7}$$

is the lth adiabatic coupling element. The condition $T_{kk} = 0$ yields an implicit choice of gauge.[35, 137, 203]

Using Hamilton's equations[67, 70, 114, 194], one obtains

$$\begin{aligned}
\dot{a}_\zeta &= \frac{P_\zeta + W_\zeta}{M_\zeta} \equiv \frac{\partial H}{\partial P_\zeta}, \\
\dot{P}_\zeta &= -\frac{\partial V}{\partial a_\zeta} - \frac{\partial K}{\partial a_\zeta} - \left(\sum_{l=1}^{s} \frac{P_l + W_l}{M_l} \frac{\partial W_l}{\partial a_\zeta} \right) \equiv -\frac{\partial H}{\partial a_\zeta}, \\
\dot{n}_\eta &= -\left(\sum_{l=1}^{s} \frac{P_l + W_l}{M_l} \frac{\partial W_l}{\partial \theta_\eta} \right) \equiv -\frac{\partial H}{\partial \theta_\eta}, \\
\dot{\theta}_\eta &= \frac{\partial K}{\partial n_\eta} + \left(\sum_{l=1}^{s} \frac{P_l + W_l}{M_l} \frac{\partial W_l}{\partial n_\eta} \right) \equiv \frac{\partial H}{\partial n_\eta}.
\end{aligned} \tag{12.8}$$

In (12.8), the index $\zeta \in \{1, \cdots, s\}$ runs over all nuclear *dof*, and $\eta \in \{1, \cdots, d-1\}$ runs over all electronic *dof*. (The $(d-1)$ quantum actions are labeled $n_2, \cdots, n_d$ because $n_1 = 1 - \sum_{j=2}^{d} n_j$.)

If every time-dependent boundary constituent of a vibrating quantum billiard has the same mass M, then (12.3) may be expressed as

$$\begin{aligned}
H &= \frac{\|\mathbf{P}\|^2}{2M} + \frac{\mathbf{P} \cdot \mathbf{W}(\mathbf{n}, \theta; \mathbf{a})}{M} + \frac{\|\mathbf{W}(\mathbf{n}, \theta; \mathbf{a})\|^2}{2M} + K + V, \\
\mathbf{W} &= -i\hbar \sum_{j,k=1}^{d} \sqrt{n_j n_k} \exp\left[i(\theta_k - \theta_j)\right] \vec{T}_{jk}(\mathbf{a}), \\
\vec{T}_{kj}(\mathbf{a}) &= \left\langle \psi_k \left| \frac{\partial \psi_j}{\partial \mathbf{a}} \right. \right\rangle = -\vec{T}_{jk}(\mathbf{a}),
\end{aligned} \tag{12.9}$$

where $\frac{\partial}{\partial \mathbf{a}} \equiv \nabla_a$ is the gradient with respect to the nuclear displacements.[137] The quantum angles are constrained by the invariance of quantum systems under global phase shifts, so only the relative phases between eigenstates are important. We thus define $\theta_{jk} \equiv \theta_k - \theta_j$.

For quantum billiards with $s = 1$ nuclear *dof*, the adiabatic molecular Hamiltonian (12.9) becomes

$$H(a, P, \mathbf{n}, \theta) = \frac{P^2}{2M} + \frac{P \cdot W(\mathbf{n}, \theta; a)}{M} + \frac{|W(\mathbf{n}, \theta; a)|^2}{2M} + K + V, \tag{12.10}$$

where the harmonic coupling function

$$W(\mathbf{n},\theta;a) = -i\hbar \sum_{j,k=1}^{d} \sqrt{n_j n_k}\exp\left[i(\theta_k-\theta_j)\right] T_{jk}(a) \tag{12.11}$$

and the adiabatic coupling element

$$T_{jk}(a) = \left\langle \psi_j \left| \frac{\partial \psi_k}{\partial a} \right\rangle = \frac{\hbar \mu_{jk}}{a}. \right. \tag{12.12}$$

The harmonic coupling function is then

$$W = -\frac{i\hbar}{a} \sum_{j,k=1}^{d} \mu_{jk}\sqrt{n_j n_k}\exp\left[i(\theta_k-\theta_j)\right]. \tag{12.13}$$

The (non-kinetic) momentum in the adiabatic basis is

$$P = M\dot{a} + \hbar P_1 = M\dot{a} - W, \tag{12.14}$$

where $M\dot{a}$ is the kinetic term and $\hbar P_1 = -W$ is a momentum shift. The presence of an $\mathcal{O}(\hbar)$ non-kinetic term in the momentum P is a direct consequence of using an adiabatic basis rather than a diabatic one.

When $d = 2$, the harmonic coupling function (12.13) becomes

$$W(n,\theta,a) = \frac{2\hbar\mu_{12}\sqrt{n(1-n)}}{a}\sin\theta. \tag{12.15}$$

The adiabatic Hamiltonian (12.10) for $s = 1$ and $d = 2$ is consequently given by

$$\begin{aligned} H &= \frac{P^2}{2M} + V(a) + K + \frac{2\hbar\mu_{12}P}{Ma}\sqrt{n(1-n)}\sin\theta + \frac{2\hbar^2\mu_{12}^2 n(1-n)}{Ma^2}\sin^2(\theta) \\ &\equiv H_0 + \hbar H_1 + \hbar^2 H_2 \equiv H_0 + \bar{H}_1, \end{aligned} \tag{12.16}$$

where

$$H_0(a,P;n) = \frac{P^2}{2M} + V(a) + K(a;n) \tag{12.17}$$

is the integrable component of the Hamiltonian (12.16).

Hamilton's equations applied to (12.16) yield

$$\begin{aligned}
\dot{a} &= \frac{P+W}{M} = \frac{P}{M} + \frac{2\hbar\mu_{12}\sqrt{n(1-n)}}{Ma}\sin(\theta),\\
\dot{P} &= -\frac{\partial V}{\partial a} - \frac{\partial K}{\partial a} - \frac{\partial W}{\partial a}\frac{P+W}{M} = -\frac{\partial V}{\partial a}\\
&\quad + \frac{2}{a^3}[(1-n)\epsilon_1 + n\epsilon_2] + \frac{2\hbar\mu_{12}P}{Ma^2}\sqrt{n(1-n)}\sin(\theta) + \frac{4\hbar^2\mu_{12}^2}{Ma^3}n(1-n)\sin^2(\theta),\\
\dot{n} &= -\frac{\partial W}{\partial\theta}\frac{P+W}{M} = -\frac{2\hbar\mu_{12}P}{Ma}\sqrt{n(1-n)}\cos(\theta) - \frac{2\hbar^2\mu_{12}^2}{Ma^2}n(1-n)\sin(2\theta),\\
\dot{\theta} &= \frac{\partial K}{\partial n} + \frac{\partial W}{\partial n}\frac{P+W}{M}\\
&= \frac{\epsilon_2-\epsilon_1}{a^2} + \frac{\hbar\mu_{12}P}{Ma}\frac{(1-2n)}{\sqrt{n(1-n)}}\sin(\theta) + \frac{2\hbar^2\mu_{12}^2}{Ma^2}(1-2n)\sin^2(\theta).
\end{aligned} \tag{12.18}$$

We remark that we will not be applying the so-called "Langer modification" to (12.18).[78, 137, 189]

When $d = 3$, define

$$\begin{aligned}
n_\alpha &\equiv n_2,\\
n_\beta &\equiv n_3,
\end{aligned} \tag{12.19}$$

so that

$$n_1 = 1 - n_\alpha - n_\beta. \tag{12.20}$$

The conjugate angles of n_α and n_β are

$$\begin{aligned}
\theta_\alpha &\equiv \theta_2 - \theta_1,\\
\theta_\beta &\equiv \theta_3 - \theta_1.
\end{aligned} \tag{12.21}$$

The harmonic coupling function (12.11) then becomes

$$\begin{aligned}
W &= \frac{2\hbar}{a}\mu_{12}\sqrt{n_\alpha(1-n_\alpha-n_\beta)}\sin(\theta_\alpha)\\
&\quad + \frac{2\hbar}{a}\mu_{13}\sqrt{n_\beta(1-n_\alpha-n_\beta)}\sin(\theta_\beta) + \frac{2\hbar}{a}\mu_{23}\sqrt{n_\alpha n_\beta}\sin(\theta_\beta-\theta_\alpha).
\end{aligned} \tag{12.22}$$

Additionally, the electronic kinetic energy is given by

$$K = \frac{1}{a^2}\left[\epsilon_1(1-n_\alpha-n_\beta)+\epsilon_2 n_\alpha+\epsilon_3 n_\beta\right]. \tag{12.23}$$

The adiabatic Hamiltonian (12.10) is consequently given by

$$H(a,P,n_\alpha,n_\beta,\theta_\alpha,\theta_\beta) = \frac{P^2}{2M}+K+V+\frac{PW}{M}+\frac{W^2}{2M}, \tag{12.24}$$

where

$$\begin{aligned}\frac{PW}{M} &= \frac{2\hbar P}{Ma}\mu_{12}\sqrt{n_\alpha(1-n_\alpha-n_\beta)}\sin(\theta_\alpha)\\ &\quad+\frac{2\hbar P}{Ma}\mu_{13}\sqrt{n_\beta(1-n_\alpha-n_\beta)}\sin(\theta_\beta)+\frac{2\hbar P}{Ma}\mu_{23}\sqrt{n_\alpha n_\beta}\sin(\theta_\beta-\theta_\alpha)\end{aligned} \tag{12.25}$$

and

$$\begin{aligned}\frac{W^2}{2M} &= \frac{2\hbar^2}{Ma^2}\mu_{12}^2 n_\alpha(1-n_\alpha-n_\beta)\sin^2(\theta_\alpha)\\ &\quad+\frac{2\hbar^2}{Ma^2}\mu_{13}^2 n_\beta(1-n_\alpha-n_\beta)\sin^2(\theta_\beta)+\frac{2\hbar^2}{Ma^2}\mu_{23}^2 n_\alpha n_\beta\sin^2(\theta_\beta-\theta_\alpha)\\ &\quad+\frac{4\hbar^2}{Ma^2}\mu_{12}\mu_{13}(1-n_\alpha-n_\beta)\sqrt{n_\alpha n_\beta}\sin(\theta_\alpha)\sin(\theta_\beta)\\ &\quad+\frac{4\hbar^2}{Ma^2}\mu_{12}\mu_{23}n_\alpha\sqrt{n_\beta(1-n_\alpha-n_\beta)}\sin(\theta_\alpha)\sin(\theta_\beta-\theta_\alpha)\\ &\quad+\frac{4\hbar^2}{Ma^2}\mu_{13}\mu_{23}n_\beta\sqrt{n_\alpha(1-n_\alpha-n_\beta)}\sin(\theta_\beta)\sin(\theta_\beta-\theta_\alpha).\end{aligned} \tag{12.26}$$

The Hamiltonian (12.24) has terms with a sinusoidal dependence on θ_1, θ_2, and $(\theta_2-\theta_1)$. The prefactors of these terms include, respectively, the coupling coefficients μ_{12}, μ_{13}, and μ_{23}. Each coefficient represents a different type of excitation and appears as a prefactor in one of the terms in the harmonic coupling function W. As discussed in Chapter 9,[160] their sizes indicate the interaction strengths of pairs of eigenstates.

12.1.1 Equivalence to Bloch Formulation

Using the case $s=1$, $d=2$ as an example, we demonstrate the equivalence of the adiabatic action-angle formulation of vibrating quantum billiards introduced above

with the Bloch-variable formulation derived directly from Schrödinger's equation (5.1) in Chapter 5. Essentially the same argument holds for arbitrary s and d.

Defining the (kinetic) momentum

$$P' \equiv P + W = P + \frac{2\hbar\mu_{12}}{a}\sqrt{n(1-n)}\sin(\theta') = M\dot{a}, \tag{12.27}$$

shifting the angle by defining

$$\theta' \equiv \theta - \frac{\pi}{2}, \tag{12.28}$$

and dropping the primes from the new momentum and angle yields the following equations of motion:

$$\begin{aligned}
\dot{a} &= \frac{P}{M} \\
\dot{P} &= -\frac{\partial V}{\partial a} - \frac{\partial K}{\partial a} \\
&= -\frac{\partial V}{\partial a} + \frac{2}{a^3}\left[\epsilon_1(1-n) + \epsilon_2 n\right] - \frac{(\epsilon_2 - \epsilon_1)2\hbar\mu_{12}}{a^3}\sqrt{n(1-n)}\sin(\theta) \\
\dot{\theta} &= \frac{(\epsilon_2 - \epsilon_1)}{a^2} + \frac{\hbar\mu P}{Ma}\frac{(1-2n)}{\sqrt{n(1-n)}}\cos(\theta), \\
\dot{n} &= \frac{2\hbar\mu_{12}P}{Ma}\sqrt{n(1-n)}\sin(\theta).
\end{aligned} \tag{12.29}$$

For general d, one must shift $(d-1)$ angles exactly in the manner just discussed. Furthermore, the harmonic coupling function W (and hence the momentum shift) is given by a more complicated expression. For general s, one simply shifts each of the momenta as described above. The essence of the argument is the same for any s and d.

When $d = 2$, one obtains action-angle variables from the complex amplitudes in equation (8.4) by defining

$$\begin{aligned}
A_1 &\equiv \sqrt{(1-n)}e^{i\theta}, \\
A_2 &\equiv \sqrt{n}.
\end{aligned} \tag{12.30}$$

In terms of action-angle coordinates, Bloch variables are given by

$$\begin{aligned} x &= 2\sqrt{n(1-n)}\cos(\theta), \\ y &= 2\sqrt{n(1-n)}\sin(\theta), \\ z &= 2n-1. \end{aligned} \tag{12.31}$$

Inserting the relations (12.31) into the quantum subsystem of (8.9), rescaling time with

$$\tau \equiv \frac{t}{\hbar}, \tag{12.32}$$

shifting the angle θ, and renaming the new time and angle as t and θ, respectively, for notational consistency yields the quantum subsystem of (12.29) and thereby demonstrates the equivalence of (8.9) and (12.18). Moreover, this calculation shows by construction that a two-mode Galërkin expansion of a vibrating quantum billiard with $s = 1$ nuclear *dof* yields a two *dof* Hamiltonian system.

12.2 Melnikov Analysis for the Case $s = 1$, $d = 2$

In this section, we construct a leading-order Melnikov function to show analytically that two-mode Galërkin expansions of vibrating quantum billiards with one nuclear *dof* exhibit homoclinic tangles.

The molecular Hamiltonian (12.16) is of the form

$$H(a, P, n, \theta) = F(a, P) + g(a, P)G(n) + \bar{H}_1(a, P, n, \theta), \tag{12.33}$$

where

$$\begin{aligned} F(a,P) &= \frac{P^2}{2M} + V(a), \\ g(a,P) &\equiv g(a) = \frac{1}{a^2}, \\ G(n) &= (1-n)\epsilon_1 + n\epsilon_2, \\ \bar{H}_1(a,P,n,\theta) &= \frac{2\hbar\mu_{12}P}{Ma}\sqrt{n(1-n)}\sin\theta + \frac{2\hbar^2\mu_{12}^2 n(1-n)}{Ma^2}\sin^2(\theta) \\ &\equiv \hbar H_1 + \hbar^2 H_2 = \hbar H_1 + \mathcal{O}(\hbar^2). \end{aligned} \tag{12.34}$$

The first integrals of the uncoupled Hamiltonian (12.17) are $H_0 \equiv F + gG$ and n, as θ is *ignorable*. Note that we will drop the $\mathcal{O}(\hbar^2)$ term in (12.16) from the Melnikov calculation. We discuss the validity of this procedure in a subsequent section.

The angular frequency of the orbit with action n is

$$\Omega(n;a) = \frac{d(gG)}{dn} = g(a)G'(n) = \frac{1}{a^2}(\epsilon_2 - \epsilon_1), \tag{12.35}$$

which is positive since $\epsilon_2 > \epsilon_1$. Had we been studying fully degenerate electronic energy levels (for which $\epsilon_1 = \epsilon_2$) rather than nearly degenerate ones, the frequency $\Omega(n;a)$ would have vanished.

To apply Melnikov's method, define the perturbation strength ϵ as

$$\epsilon \equiv \hbar. \tag{12.36}$$

(We show that this choice is permissible in a subsequent section.) For small ϵ, the equation $H = E_H$ is invertible and can be solved for the action n:[67, 194]

$$n \equiv L(a,P,\theta;E_H) = L_0(a,P;E_H) + \epsilon L_1(a,P,\theta;E_H) + \mathcal{O}(\epsilon^2), \tag{12.37}$$

where

$$\begin{aligned} L_0 &= G^{-1}\left(\frac{1}{g(a,P)}[E_H - F(a,P)]\right), \\ L_1 &= -\frac{H_1\left(a,P,\theta,L_0(a,p,\theta;E_H)\right)}{\Omega(L_0(a,P;E_H),a,P)} = -\frac{H_1\left(a,P,\theta,L_0(a,p,\theta;E_H)\right)}{g(a,P)G'\left(L_0(a,P;E_H)\right)}. \end{aligned} \tag{12.38}$$

One consequently obtains

$$\dot{a} = -\frac{\partial L_0}{\partial P}(a, P; E_H) - \epsilon \frac{\partial L_1}{\partial P}(a, P, \theta; E_H) + \mathcal{O}(\epsilon^2),$$
$$\dot{P} = \frac{\partial L_0}{\partial a}(a, P; E_H) + \epsilon \frac{\partial L_1}{\partial q}(a, P, \theta; E_H) + \mathcal{O}(\epsilon^2). \tag{12.39}$$

The equations of motion for the unperturbed system (12.17) are then expressed as

$$\dot{a} = -\frac{\partial L_0}{\partial P}(a, P; E_H),$$
$$\dot{P} = \frac{\partial L_0}{\partial a}(a, P; E_H). \tag{12.40}$$

The smallness of the term $G(n)$ for small ϵ_j is expressed formally as

$$g(a, P)G(n) = \mathcal{O}(\lambda), \tag{12.41}$$

where

$$\lambda \propto \frac{1}{a^2}\left[\sum_{j=1}^{d} \epsilon_j n_j\right] \leq \frac{\epsilon_d}{a^2} \tag{12.42}$$

for a d-mode Galërkin expansion (5.20) with $s = 1$. The quantity ϵ_d is the largest energy parameter, as it corresponds to the most excited state under consideration. The size of the perturbation parameter λ is therefore determined by the energy of this state:

$$\mathcal{O}(\lambda) = \mathcal{O}\left(\frac{\epsilon_d}{a^2}\right). \tag{12.43}$$

The quantity λ is small when the electronic kinetic energy K is small. This energy becomes larger as one considers increasingly excited states. It is also larger for confined particles with smaller masses m_0 and for billiards with larger spatial dimensions. As λ represents an energy, homoclinic orbits are more likely to exist when it is small. (This was shown in Chapter 7.[155]) Consequently, the Melnikov calculation in this section has an energy threshold (encoded in the electronic kinetic energy K) above which it is not valid.

The unperturbed Hamiltonian (12.17) is given by

$$H_0(a, P; n) = F(a, P) + \mathcal{O}(\lambda). \tag{12.44}$$

For sufficiently small λ, the unperturbed dynamical system (12.40) has a homoclinic orbit provided F does. This latter homoclinic orbit $F(a, P) = \bar{E}_F$ is expressed analytically as a function of time as

$$(a, P) = \left(\hat{a}(t), \hat{P}(t)\right). \tag{12.45}$$

One uses (12.45) to approximate the homoclinic orbit $H_0(a, P; \lambda) = E_0$ in a Melnikov integral $\mathfrak{M}$. This homoclinic orbit is parametrized by

$$(a, P) = \left(\tilde{a}(t), \tilde{P}(t)\right). \tag{12.46}$$

Homoclinic orbits in (12.40) are determined from the relation

$$l_0 = G^{-1}\left(\frac{1}{g(a, P)}\left[E_H + \mathcal{O}(\lambda)\right]\right). \tag{12.47}$$

Expanding (12.47) in a Taylor series in λ, the homoclinic orbit of (12.40) is given by

$$n = l_0 = G^{-1}\left(\frac{1}{g(a, P)} E_H\right) + \mathcal{O}(\lambda). \tag{12.48}$$

Consider perturbations of a homoclinic orbit in the unperturbed system (12.40). The upper subharmonic Melnikov function is given by[67, 194]

$$\mathfrak{M}(\theta_0) = \int_{-\infty}^{\infty} \left\{ L_0\left(\tilde{a}(\theta), \tilde{P}(\theta); E_H\right), L_1\left(\tilde{a}(\theta), \tilde{P}(\theta), \theta_\omega + \theta_0; E_H\right)\right\} d\theta, \tag{12.49}$$

where $\{Y_1, Y_2\}$ is the (canonical) Poisson bracket of Y_1 and Y_2 and $\theta = \theta_\omega + \theta_0 \equiv \Omega(l_0)t + \theta_0$.

In terms of the original Hamiltonian H, the Melnikov integral (12.49) is

$$\mathfrak{M}(\theta_0) = \int_{-\infty}^{\infty} \left[\frac{g\{F, H_1\} + H_1\{F, g\} + E_H\{H_1, g\} + F\{g, H_1\}}{g^3[G'(n)]^2}\right] dt, \tag{12.50}$$

where the Hamiltonian F is evaluated at $(\tilde{a}(t), \tilde{P}(t))$ and H_1 is evaluated at $\left(\tilde{a}(t), \tilde{P}(t), \Omega(l_0)t + \theta_0; l_0\right)$.

As $g(a, P) \equiv g(a)$, the Melnikov integral (12.50) reduces to

$$\mathfrak{M}(\theta_0) = \int_{-\infty}^{\infty} \left[\frac{g\{F, H_1\} + \frac{\partial g}{\partial a}\left([F - E_H]\frac{\partial H_1}{\partial P} - H_1 \frac{\partial F}{\partial P}\right)}{g^3 [G'(n)]^2} \right] dt. \tag{12.51}$$

The homoclinic orbit $\left(\tilde{a}(t), \tilde{P}(t)\right)$ cannot be expressed in closed form, but one can write the nearby orbit $\left(\hat{a}(t), \hat{P}(t)\right)$ associated with the Hamiltonian $F(a, P)$ in this manner. When $g(a)G(n)$ is sufficiently small, $\bar{E}_F = F(a, P)$ is *almost* a constant of the motion of $H_0(a, P; n)$.

The true energy of $\left(\hat{a}(t), \hat{P}(t)\right)$ is $F(a, P) = E_0 - \mathcal{O}(\lambda)$, so by inserting this orbit into (12.50), one obtains an expression $\mathfrak{M}_0(\theta_0)$ that is accurate to leading order. That is,

$$\mathfrak{M}(\theta_0) = \mathfrak{M}_0(\theta_0) + \mathfrak{o}(\lambda^0). \tag{12.52}$$

We demonstrated in Chapter 8 that quartic potentials $V(a)$ can yield homoclinic tangles in vibrating quantum billiards,[155] so consider a potential of the form

$$\begin{aligned} V(a) &= V_4 a^4 + V_2 a^2 \\ &\equiv \tilde{V}_4 (a - a_0)^4 + \tilde{V}_3 (a - a_0)^3 + \tilde{V}_2 (a - a_0)^2 + \tilde{V}_1 (a - a_0) + \tilde{V}_0. \end{aligned} \tag{12.53}$$

When $V_2 < 0$ and $V_4 > 0$, the Hamiltonian $F(a, P)$ describes a Duffing oscillator.[67, 164] For sufficiently small ϵ_j/a^2 (and hence for sufficiently small ϵ_j), the right-hand Duffing homoclinic orbit is a good approximation of the right-hand homoclinic orbit for unperturbed vibrating quantum billiards (which have Hamiltonian H_0). The parameter V_2 is assumed to be sufficiently negative so that the local maximum of the potential $V(a)$ is large enough for (12.17) to possess a homoclinic orbit.[155] In particular, the Hamiltonian H_0 has a homoclinic orbit for sufficiently small ϵ_j when $V_2 = -V_4 < 0$.[155]

The perturbation of $F(a,P)$ to $H_0(a,P;n)$ is singular, as the term $K(n;a)$ contains powers of the displacement a in the denominator. Nevertheless, we observed numerically in Chapter 7 that the dynamical system with Hamiltonian H_0 has homoclinic orbits near those in Duffing oscillators.[155] For sufficiently small ϵ_j, the homoclinic connection corresponding to positive a in the Hamiltonian $F(a,P)$ is well-approximated by that corresponding to the Hamiltonian $H_0(a,P;n)$, as is shown in Figure 12.1. Because of the singular nature of the perturbation from F to H_0, however, the left homoclinic connection in the Hamiltonian $F(a,P)$ is *not* similarly well-approximated.

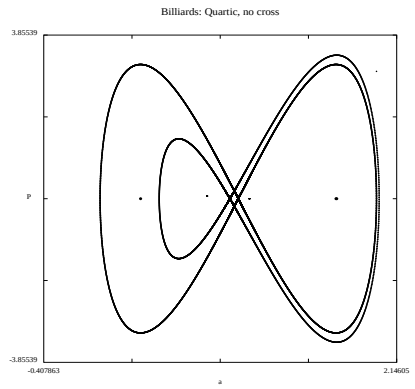

Figure 12.1: This plot shows homoclinic orbits for the Duffing Hamiltonian F and nearby ones for the integrable vibrating billiard Hamiltonian H_0. Because the perturbation from F to H_0 is singular, only the right-hand homoclinic connection is well-approximated. These two homoclinic orbits are especially close together when $t \in [-T,T]$ for sufficiently small T.

The approximate (Duffing) homoclinic orbit, whose energy is $\bar{E}_F = 0$, is expressed parametrically as

$$\begin{aligned}&\left(\hat{a}(t),\hat{P}(t)\right) = \\ &= \left(\sqrt{-\frac{V_2}{V_4}}\operatorname{sech}\left(\sqrt{-2\frac{V_2}{M}}t\right), V_2\sqrt{\frac{2M}{V_4}}\operatorname{sech}\left(\sqrt{-2\frac{V_2}{M}}t\right)\tanh\left(\sqrt{-2\frac{V_2}{M}}t\right)\right).\end{aligned} \tag{12.54}$$

The approximate energy

$$E_F = \bar{E}_F + \mathcal{O}(\lambda) = 0 + \mathcal{O}(\lambda) \tag{12.55}$$

is then inserted into the Melnikov integral (12.51).

The quantity $\bar{E}_F$ denotes the energy of the exact homoclinic orbit corresponding to the system with Hamiltonian F, whereas E_F denotes the energy of the approximate homoclinic orbit obtained by using only the F term in the Hamiltonian H_0. (Although $\bar{E}_F$ and E_F both "equal" $F(a,P)$, we use different symbols to explicitly recognize their distinct meanings.) This latter quantity is defined by the relation

$$E_F \equiv E_0 - \frac{G(n)}{\hat{a}^2}, \tag{12.56}$$

so it is only approximately constant. (By contrast, $\bar{E}_F$ is exactly constant.) The energy E_0 of the Hamiltonian H_0 is comparably close to both $\bar{E}_F$ and E_F:

$$H_0(\hat{a},\hat{P};n) = E_0 = F(\hat{a},\hat{P}) + \frac{1}{\hat{a}^2}G(n) = \bar{E}_F + \mathcal{O}(\lambda) = 0 + \mathcal{O}(\lambda) = E_F + \mathcal{O}(\lambda). \tag{12.57}$$

The angle θ is given by

$$\theta(t) = \Omega\left(L_0(\hat{a},\hat{P};E_H)\right)t + \theta_0 \equiv \Omega(l_0)t + \theta_0 \equiv \omega t + \theta_0, \tag{12.58}$$

where

$$l_0 = G^{-1}\left(\hat{a}^2[E_H - E_F]\right) = \frac{1}{\omega}(E_H - E_F) + \mathcal{O}(\lambda) = \frac{E_H}{\omega} + \mathcal{O}(\lambda), \tag{12.59}$$

and $H = E_H$ is the energy manifold. The leading-order Melnikov integral is then

$$\begin{aligned}\mathfrak{M}_0 &= \int_{-\infty}^{\infty}\left[\frac{4\mu_{12}\sqrt{n(1-n)}\hat{a}^2\hat{P}^2}{M^2(\epsilon_2-\epsilon_1)^2}\sin(\theta) + \frac{4\mu_{12}V_4\sqrt{n(1-n)}\hat{a}^6}{M(\epsilon_2-\epsilon_1)^2}\sin(\theta)\right.\\ &\quad\left. + \frac{4\mu_{12}E_H\sqrt{n(1-n)}\hat{a}^2}{M(\epsilon_2-\epsilon_1)^2}\sin(\theta)\right]dt\\ &= \int_{-\infty}^{\infty}\frac{4\mu_{12}\sqrt{n(1-n)}}{M(\epsilon_2-\epsilon_1)^2}\left[\frac{1}{M}\hat{a}^2\hat{P}^2\sin(\theta) + V_4\hat{a}^6\sin(\theta) + E_H\hat{a}^2\sin(\theta)\right]dt.\end{aligned} \tag{12.60}$$

Along the homoclinic orbit $(a, P) = \left(\tilde{a}(t), \tilde{P}(t)\right)$, the action is

$$n = l_0 = \frac{E_H}{\omega} + \mathcal{O}(\lambda). \tag{12.61}$$

Therefore,

$$\sqrt{n(1-n)} = \sqrt{\frac{E_H}{\omega}\left(1 - \frac{E_H}{\omega}\right)} + \mathcal{O}(\sqrt{\lambda}). \tag{12.62}$$

Defining the quantity

$$\gamma = 4\frac{\mu_{12} V_2 \sqrt{\frac{E_H}{\omega}\left(1 - \frac{E_H}{\omega}\right)}}{V_4 M(\epsilon_2 - \epsilon_1)^2} \tag{12.63}$$

and inserting the time-dependence of the approximate homoclinic orbit (12.54) into (12.60) yields

$$\mathfrak{M} = \mathfrak{M}_0 + \mathcal{O}(\sqrt{\lambda}) = \gamma \sum_{j=1}^{6} I_j + \mathcal{O}(\sqrt{\lambda}), \tag{12.64}$$

where

$$\begin{aligned}
I_1 &= \int_{-\infty}^{\infty} \frac{V_2^2}{V_4} \mathrm{sech}^6\left(\sqrt{\frac{-2V_2}{M}}t\right) \cos(\theta_0)\sin(\omega t)dt, \\
I_2 &= -2\int_{-\infty}^{\infty} \frac{V_2^2}{V_4} \mathrm{sech}^4\left(\sqrt{\frac{-2V_2}{M}}t\right) \cos(\theta_0)\sin(\omega t)dt, \\
I_3 &= -\int_{-\infty}^{\infty} E_H \mathrm{sech}^2\left(\sqrt{\frac{-2V_2}{M}}t\right) \cos(\theta_0)\sin(\omega t)dt, \\
I_4 &= \int_{-\infty}^{\infty} \frac{V_2^2}{V_4} \mathrm{sech}^6\left(\sqrt{\frac{-2V_2}{M}}t\right) \sin(\theta_0)\cos(\omega t)dt, \\
I_5 &= -2\int_{-\infty}^{\infty} \frac{V_2^2}{V_4} \mathrm{sech}^4\left(\sqrt{\frac{-2V_2}{M}}t\right) \sin(\theta_0)\cos(\omega t)dt, \\
I_6 &= -\int_{-\infty}^{\infty} E_H \mathrm{sech}^2\left(\sqrt{\frac{-2V_2}{M}}t\right) \sin(\theta_0)\cos(\omega t)dt.
\end{aligned} \tag{12.65}$$

The first three integrals I_1, I_2, and I_3 vanish because their integrands are odd and their intervals of integration are symmetric.

Computing the other three integrals yields

$$I_4 = -\frac{M^3\omega\pi\left(\omega^2 - \frac{8V_2}{M}\right)\left(\omega^2 - \frac{32V_2}{M}\right)}{960V_2V_4}\text{csch}\left(\sqrt{-\frac{M}{2V_2}}\frac{\omega\pi}{2}\right)\sin(\theta_0),$$

$$I_5 = -\frac{M^2\omega\pi\left(\omega^2 - \frac{8V_2}{M}\right)}{12V_4}\text{csch}\left(\sqrt{-\frac{M}{2V_2}}\frac{\omega\pi}{2}\right)\sin(\theta_0),$$

$$I_6 = \frac{ME_H\omega\pi}{2V_2}\text{csch}\left(\sqrt{-\frac{M}{2V_2}}\frac{\omega\pi}{2}\right)\sin(\theta_0). \tag{12.66}$$

Defining B_j with the relation

$$I_j \equiv B_j \sin(\theta_0), \tag{12.67}$$

one obtains

$$\mathfrak{M} = \beta(B_1 + B_2 + B_3)\sin(\theta_0) + \mathcal{O}(\sqrt{\lambda}), \tag{12.68}$$

which has simple zeroes for $\theta_0 = k\pi$ (where k is an integer) when $\lambda = 0$. For sufficiently small λ, there exist points near $k\pi$ that are simple zeroes of $\mathfrak{M}$ to all orders (as the coefficient of the term of order $\mathcal{O}(\sqrt{\lambda})$ is finite).

Consequently, homoclinic tangles occur in vibrating quantum billiards when $V(a)$ is a quartic, double-well potential.

12.3 Melnikov Analysis for the Case $s = 1$, $d = 3$

One can generalize the scalar Melnikov method discussed above to a vectorial method[82] and thereby provide a plausibility argument for a priori unstable Arnold diffusion in the Hamiltonian (12.24) with a Duffing potential $V(a)$. (This calculation can likely be extended to a proof by overcoming the so-called *gap problem*,[74, 114, 115] whose recent resolution has not yet been published.[130])

Melnikov calculations establish the existence of individual homoclinic connections to invariant KAM tori, but they are not sufficient to construct a chain of such connections (which must exist if diffusion is to occur). Resonances on invariant

manifolds in Hamiltonian systems $H = H_0 + \epsilon H_1$ lead to gaps of order $\mathcal{O}(\sqrt{\epsilon})$ in the surviving tori,[74, 82, 114, 115] so one may not be able to construct finite heteroclinic chains (*transition chains*) between them. The variation in actions along perturbed homoclinic and heteroclinic orbits is of order $\mathcal{O}(\epsilon)$, so these orbits cannot connect tori on opposite sides of $\mathcal{O}(\sqrt{\epsilon})$ gaps. This gap problem is generic, as any smooth path of tori contains a dense set of resonant tori. Consequently, the gaps necessarily occur on any fixed diffusion route.[74]

Moreover, KAM theory must be invoked, as one otherwise demonstrates only the existence of homoclinic tangles.[74, 82, 114, 115] The simultaneous existence of a horseshoe structure and invariant KAM tori allow for the possibility of Hamiltonian diffusion. A vectorial Melnikov technique provides a mechanism to examine a priori unstable Arnold diffusion at the perturbation strength $\mathcal{O}(\epsilon)$. Overcoming the gap problem involves the application of additional estimates to account for the fact that the perturbation strength is smaller than the gap size.

To ensure isoenergetic nondegeneracy,[67, 82] one calculates that KAM theory can be applied whenever

$$\begin{aligned}
&4\left[2V_4a^2 + V_2\right]\left[\frac{P^2}{2M} + V_4a^4 + V_2a^2\right]\left[(1-n_\alpha)\epsilon_1 + n_\alpha\epsilon_2\right] \\
&\quad - 4a^4\left[2V_4a^2 + V_2\right]^2\left[\frac{P^2}{2M} + V_4a^4 + V_2a^2\right] - a^6\left[2V_4a^2 + V_2\right]^3 \\
&\quad + a^2\left[2V_4a^4 + V_2\right]^2\left[(1-n_\alpha)\epsilon_1 + n_\alpha\epsilon_2\right] \\
&\quad - 4\left[3V_4a^2 + V_2\right]\left[\frac{P^2}{2M} + V_4a^4 + V_2a^2\right]\left[(1-n_\alpha)\epsilon_1 + n_\alpha\epsilon_2\right] \neq 0, \quad (12.69)
\end{aligned}$$

where $V(a) = V_4a^4 + V_2a^2$ is the Duffing potential (12.53). (Only n_α appears in (12.69) because we have "reduced" the Hamiltonian (12.24) by the action n_β. The reduction procedure that has been applied is discussed in reference [82].)

We now summarize the results of a vectorial Melnikov analysis, the details of which have been omitted from this work. The procedure is analogous to the scalar

Melnikov method outlined above.

The Hamiltonian (12.24) is of the form

$$H = F(a,P) + g(a,P)\left[G_\alpha(n_\alpha) + G_\beta(n_\beta)\right] + \bar{H}_1(a,P,n_\alpha,\theta_\alpha,n_\beta,\theta_\beta), \qquad (12.70)$$

where

$$\begin{aligned} F(a,P) &= \frac{P^2}{2M} + V(a), \\ g(a) \equiv g(a,P) &= \frac{1}{a^2}, \\ G_\alpha(n_\alpha) &= (1-n_\alpha)\epsilon_1 + n_\alpha\epsilon_2, \\ G_\beta(n_\beta) &= (\epsilon_3 - \epsilon_1)n_\beta, \\ \bar{H}_1(a,P,n_\alpha,\theta_\alpha,n_\beta,\theta_\beta) &= \frac{PW}{M} + \frac{W^2}{2M} \equiv \hbar H_1 + \hbar^2 H_2 = \hbar H_1 + \mathcal{O}(\hbar^2), \end{aligned} \qquad (12.71)$$

where W is given by equation (12.22).

The kth frequency ($k \in \{\alpha,\beta\}$) in (12.24) is given by

$$\Omega_k(n_k;a) = \frac{\partial\left[g(a)G_k(n_k)\right]}{\partial n_k} = g(a)G_k'(n_k), \qquad (12.72)$$

so the kth phase is

$$\theta_k(t) = \Omega_k t + \theta_0^k, \qquad (12.73)$$

where θ_0^k is the kth reference angle. The quantity E_H represents the energy of the full Hamiltonian, $E_\alpha \equiv H - G_\beta$ is the energy contribution of the αth action-angle pair, and $E_\beta \equiv H - G_\alpha$ is the contribution of the βth action-angle pair.

One derives a two-dimensional Melnikov vector $(\mathfrak{M}_1, \mathfrak{M}_2)$, where

$$\begin{aligned} \mathfrak{M}_1(\theta_0^\alpha,\theta_0^\beta,E_H,E_\alpha) &= -\int_{-\infty}^{\infty} \frac{\partial H_1/\partial\theta_\alpha}{\Omega_\beta(n_\beta;a,P)}dt \\ &= \int_{-\infty}^{\infty} \frac{\{n_\alpha,H_1\}}{\Omega_\beta}dt, \\ \mathfrak{M}_2(\theta_0^\alpha,\theta_0^\beta,E_H,E_\alpha) &= \int_{-\infty}^{\infty} \left[\frac{g\{F,H_1\} + H_1\{F,g\} + E_H\{H_1,g\} + F\{g,H_1\}}{g^3[G_\beta'(n_\beta)]^2}\right]dt. \end{aligned} \qquad (12.74)$$

Computing (12.74) yields

$$\begin{aligned}
\mathfrak{M}_1 &= c_{12}L_{12}\sin(\theta_0^\alpha) + c_{23}L_{23}\sin(\theta_0^\alpha - \theta_0^\beta) + \mathcal{O}(\sqrt{\lambda}),\\
\mathfrak{M}_2 &= (-C_1\Gamma_6^\alpha - C_4\Gamma_4^\alpha + C_7\Gamma_2^\alpha)\sin(\theta_0^\alpha) + (-C_2\Gamma_6^\beta - C_5\Gamma_4^\beta + C_8\Gamma_2^\beta)\sin(\theta_0^\beta)\\
&\quad + (C_3\Gamma_6^{\alpha\beta} + C_6\Gamma_4^{\alpha\beta} - C_9\Gamma_2^{\alpha\beta})\sin(\theta_0^\alpha - \theta_0^\beta) + \mathcal{O}(\sqrt{\lambda}),
\end{aligned} \tag{12.75}$$

where

$$\begin{aligned}
c_{12} &\equiv 4\frac{V_2}{V_4}\sqrt{-2MV_2}\frac{\mu_{12}}{(\epsilon_3-\epsilon_1)}\sqrt{\frac{E_\alpha}{\omega_\alpha}\left(1-\frac{E_\alpha}{\omega_\alpha}-\frac{E_\beta}{\omega_\beta}\right)},\\
c_{23} &\equiv 4\frac{V_2}{V_4}\sqrt{-2MV_2}\frac{\mu_{23}}{(\epsilon_3-\epsilon_1)}\sqrt{\frac{E_\alpha E_\beta}{\omega_\alpha\omega_\beta}},\\
L_{12} &\equiv \frac{\pi\omega_\alpha^2}{4\sqrt{2}}\left(\frac{-M}{V_2}\right)^{\frac{3}{2}}\operatorname{csch}\left(\frac{\pi\omega_\alpha}{2\sqrt{2}}\sqrt{\frac{-M}{V_2}}\right),\\
L_{23} &\equiv \frac{\pi[\omega_\alpha-\omega_\beta]^2}{4\sqrt{2}}\left(\frac{-M}{V_2}\right)^{\frac{3}{2}}\operatorname{csch}\left(\frac{\pi\omega_\alpha}{2\sqrt{2}}\sqrt{\frac{-M}{V_2}}\right).
\end{aligned} \tag{12.76}$$

Additionally,

$$\begin{aligned}
C_1 &\equiv \frac{4\mu_{12}}{M(\epsilon_3-\epsilon_1)^2}\frac{V_2^3}{V_4^2}\sqrt{\frac{E_\alpha}{\omega_\alpha}\left(1-\frac{E_\alpha}{\omega_\alpha}-\frac{E_\beta}{\omega_\beta}\right)},\\
C_2 &\equiv \frac{4\mu_{13}}{M(\epsilon_3-\epsilon_1)^2}\frac{V_2^3}{V_4^2}\sqrt{\frac{E_\beta}{\omega_\beta}\left(1-\frac{E_\alpha}{\omega_\alpha}-\frac{E_\beta}{\omega_\beta}\right)},\\
C_3 &\equiv \frac{4\mu_{23}}{M(\epsilon_3-\epsilon_1)^2}\frac{V_2^3}{V_4^2}\sqrt{\frac{E_\alpha E_\beta}{\omega_\alpha\omega_\beta}},\\
C_4 &\equiv \frac{4\mu_{12}E_H}{M(\epsilon_3-\epsilon_1)^2}\frac{V_2}{V_4}\sqrt{\frac{E_\alpha}{\omega_\alpha}\left(1-\frac{E_\alpha}{\omega_\alpha}-\frac{E_\beta}{\omega_\beta}\right)},\\
C_5 &\equiv \frac{4\mu_{13}E_H}{M(\epsilon_3-\epsilon_1)^2}\frac{V_2}{V_4}\sqrt{\frac{E_\beta}{\omega_\beta}\left(1-\frac{E_\alpha}{\omega_\alpha}-\frac{E_\beta}{\omega_\beta}\right)},\\
C_6 &\equiv \frac{4\mu_{23}E_H}{M(\epsilon_3-\epsilon_1)^2}\frac{V_2}{V_4}\sqrt{\frac{E_\alpha E_\beta}{\omega_\alpha\omega_\beta}},\\
C_7 &\equiv 2C_1,\quad C_8 \equiv 2C_2,\quad C_9 \equiv 2C_3.
\end{aligned} \tag{12.77}$$

Finally,

$$\Gamma_2^k \equiv -\frac{M\omega_k\pi}{2V_2}\mathrm{csch}\left(\frac{\omega_k\pi}{2}\sqrt{-\frac{M}{2V_2}}\right),$$
$$\Gamma_4^k \equiv \frac{M^2\omega_k\pi}{24V_2^2}\left(\omega_k^2-\frac{8V_2}{M}\right)\mathrm{csch}\left(\frac{\omega_k\pi}{2}\sqrt{-\frac{M}{2V_2}}\right),$$
$$\Gamma_6^k \equiv -\frac{M^3\omega_k\pi}{960V_2^3}\left(\omega_k^2-\frac{8V_2}{M}\right)\left(\omega_k^2-\frac{32V_2}{M}\right)\mathrm{csch}\left(\frac{\omega_k\pi}{2}\sqrt{-\frac{M}{2V_2}}\right), \qquad (12.78)$$

where $k \in \{\alpha, \beta, \alpha\beta\}$ and the *interaction frequency* $\omega_{\alpha\beta}$ is defined as

$$\omega_{\alpha\beta} \equiv \omega_\alpha - \omega_\beta. \qquad (12.79)$$

To leading order, points $(b_\alpha\pi, b_\beta\pi)$, where b_α and b_β are integers, are simple zeroes of $(\mathfrak{M}_1, \mathfrak{M}_2)$. One thereby obtains transversal intersections of stable and unstable manifolds in a positive measure of two dimensional invariant tori, which–by invoking KAM theory–yields a plausibility argument for a priori unstable Arnold diffusion. Equation (12.75) represents the leading order computation of $(\mathfrak{M}_1, \mathfrak{M}_2)$. For sufficiently small λ, there exist points near $(b_\alpha\pi, b_\beta\pi)$ that are simple zeroes of the Melnikov vector $(\mathfrak{M}_1, \mathfrak{M}_2)$ to all orders.

12.4 The Role of $\hbar$

In the analyses above, we used $\hbar$ as a perturbation parameter when applying Melnikov's method. Although it is a constant of nature, perturbation parameters in quantum systems are often expressed as ratios of $\hbar$ divided by some other action.

To examine this dichotomy, we consider the sizes of the nuclear and electronic energies in the adiabatic Hamiltonian (12.16). Recall that the perturbation term in (12.16) is

$$H_\hbar \equiv \frac{1}{\hbar}\bar{H}_1 = \frac{1}{\hbar}(\hbar H_1 + \hbar^2 H_2) = \frac{2\mu_{12}P}{Ma}\sqrt{n(1-n)}\sin(\theta) + \frac{2\hbar\mu_{12}^2 n(1-n)}{Ma^2}\sin^2(\theta)$$
$$= \frac{2\mu_{12}P}{Ma}\sqrt{n(1-n)}\sin(\theta) + \mathcal{O}(\hbar). \qquad (12.80)$$

We will examine the relative sizes of the terms in (12.80) and show that they are independent of $\hbar$. We will also show that the term of order $\mathcal{O}(\hbar^2)$ is smaller than that of order $\mathcal{O}(\hbar)$, which–in turn–is smaller than those of order $\mathcal{O}(\hbar^0)$ and thereby justify the choice of $\hbar$ as the perturbation parameter in Melnikov's method.

Recall from Chapter 2 that the nuclear kinetic energy $P^2/2M$ varies as the zero-point nuclear energy, which for a harmonic potential is proportional to $1/\sqrt{m_0 M}$. Additionally, the electronic kinetic energy K is proportional to $1/m_0$, which is larger than $1/\sqrt{m_0 M}$ by a factor of $\sqrt{M/m_0}$. Hence, the nuclear mass M is typically about 10000 times larger than the electronic mass m_0, so the electronic kinetic energy K is about 100 times larger for molecular systems than is the nuclear kinetic energy $P^2/2M$.

The size of the electronic kinetic energy K is

$$K \sim \frac{\Upsilon \hbar^2 n}{m_0 a^2} \tag{12.81}$$

where the constant Υ depends on the choice of electronic eigenstates in (5.20) and is larger for increasingly excited states. The size of the smallest perturbation term in (12.16) is

$$\frac{\hbar \mu_{12} P}{Ma} \sqrt{n(1-n)}, \tag{12.82}$$

so it is required that

$$\frac{\hbar \mu_{12} P}{Ma} \sqrt{n(1-n)} \ll \frac{\Upsilon \hbar^2 n}{m_0 a^2} \tag{12.83}$$

and hence that

$$\frac{\mu_{12} P}{M} \sqrt{n(1-n)} \ll \frac{\Upsilon \hbar n}{m_0 a} \tag{12.84}$$

for this term to be much smaller than K. As n ranges over $(0,1)$, it follows that

$$n \sim \sqrt{n(1-n)} \tag{12.85}$$

on average, so it is necessary that

$$\frac{\mu_{12} P}{M} \ll \frac{\Upsilon \hbar}{m_0 a}. \tag{12.86}$$

The nuclear velocity in molecular systems is roughly[154]

$$v_N = \frac{P}{M} \sim \left(\frac{m_0}{M}\right)^{\frac{3}{4}} \frac{\hbar}{m_0 a}. \tag{12.87}$$

Inserting (12.87) into (12.86) yields the condition

$$\mu_{12} \kappa^3 \ll \Upsilon, \tag{12.88}$$

where

$$\kappa \equiv \left(\frac{m_0}{M}\right)^{\frac{3}{4}}, \tag{12.89}$$

the ratio of nuclear vibrational displacement to the spacing between nuclei, is the expansion parameter in the Born-Oppenheimer approximation. Its cube is the expansion parameter in the adiabatic approximation.[7, 19, 20, 154] (We discussed this in Chapter 2.)

For typical nuclear masses, $M \sim 10^4 m_0$, so equation (12.88) implies that

$$10^{-3} \mu_{12} \ll \Upsilon. \tag{12.90}$$

The electronic interaction strength μ_{12} is typically of order $\mathcal{O}(1)$ and the excitation parameter Υ is typically *at least* of order $\mathcal{O}(1)$.[112, 157, 159, 160] Hence, the $\mathcal{O}(\hbar)$ term in (12.16) is much smaller than the $\mathcal{O}(\hbar^0)$ terms. (Because of the 10^{-3} difference in the order of magnitude in the left-hand and right-hand sides of equation (12.90), there are almost never any problems with this estimate even when n ranges only over a small subset of $(0, 1)$. More precisely, one needs $n \lesssim 10^{-6}$ for almost all time for this estimate to fail.)

When applying Melnikov's method, we dropped the $\mathcal{O}(\hbar^2)$ term in $\bar{H}_1$ and showed that perturbing H_0 by terms of order $\mathcal{O}(\hbar)$ leads to homoclinic tangles.

Numerical simulations reveal chaotic dynamics regardless of whether one drops the terms of order $\mathcal{O}(\hbar^2)$. Those simulations, in which $\hbar = 1$, suggest that the $\mathcal{O}(\hbar^2)$ terms in (12.16) are smaller than the $\mathcal{O}(\hbar)$ terms regardless of the size of $\hbar$.

To examine the actual sizes of the $\mathcal{O}(\hbar)$ and $\mathcal{O}(\hbar^2)$ terms in (12.16), one removes common factors from both terms and compares the size of P with that of

$$\frac{\hbar\mu_{12}\sqrt{n(1-n)}}{a}\sin(\theta). \tag{12.91}$$

The quantities μ_{12}, $\sqrt{n(1-n)}$, and $\sin(\theta)$ are all of order $\mathcal{O}(1)$, so one need only examine the relative sizes of P and $\hbar/a$. These are the only remaining factors of the $\mathcal{O}(\hbar)$ and $\mathcal{O}(\hbar^2)$ terms, respectively, in (12.16).

In Chapter 2, we estimated the zero-point momentum in a harmonic potential to be[7, 154]

$$P \approx \left(\frac{M}{m_0}\right)^{\frac{1}{4}}\frac{\hbar}{a}, \tag{12.92}$$

so the term of order $\mathcal{O}(\hbar^2)$ term is smaller than that of order $\mathcal{O}(\hbar)$ by roughly a factor of $\kappa \approx 1/10$. Note that although κ is an appropriate unitless parameter to use in Melnikov calculations, it is not as mathematically convenient as $\hbar$. The present discussion shows that this latter choice is a valid one.

In light of the size of $\hbar H_1$, the Melnikov calculation above implies that the dynamical system (12.18) describing two-mode Galërkin expansions of vibrating quantum billiards with one nuclear *dof* has transverse homoclinic orbits and hence Smale horseshoes at every energy level $E_H > 0 + \mathcal{O}(\lambda)$ as long as κ^3 is sufficiently small.

CHAPTER 13

CHAOTIC ONSET IN CLASSICAL AND QUANTUM *DOF*

The interaction terms in the molecular Hamiltonian (12.16) describe faster fluctuations than those that arise from diagonal terms in the quadratic form (5.21). This phenomenon, which is a consequence of the Born-Oppenheimer approximation,[7, 19, 20, 154, 189] implies that when perturbing from integrable configurations, a vibrating quantum billiard's quantum *dof* become chaotic far sooner than do its classical *dof*.

We note, moreover, that this is true in general for systems derived via the Born-Oppenheimer approximation. Consequently, this phenomenon is a signature of semiquantum chaos. Moreover, one expects to frequently encounter configurations in which the quantum *dof* are globally chaotic but the classical *dof* are only locally so.

13.1 Introduction

In this thesis, we have observed numerous configurations for which the quantum probabilities (represented by the actions n_j) in vibrating quantum billiards behave more erratically (are "more chaotic") than the system's classical variables.[160] (See, for example, Chapter 9.)

Consider, for example, a nearly integrable configuration in a two-mode Galërkin expansion of a quantum billiard with $s = 1$ nuclear *dof*. Empirical observations suggest that it takes a smaller perturbation for $n(t)$ to develop chaotic behavior

than it does for $a(t)$ and $P(t)$ to do so.[160] As one increases this perturbation, one often observes situations for which $n(t)$ is completely erratic while $a(t)$ and $P(t)$ are only mildly so. This is intuitively reasonable because the system's quantum dynamics evolve at a faster timescale than do its classical dynamics.[154]

In the context of diatomic molecules, the analysis in this chapter indicates that for a typical initial configuration, one expects the quantum probabilities of the eigenstates to fluctuate more violently than the interatomic distance a, which we recall defines the lengthscale of the eigenstates ψ_j.

To explore chaotic onset in (12.16) systematically, we simulate the associated dynamical system (12.18) numerically and perform some simple calculations.

13.2 Analysis

As discussed in prior chapters, the dynamical system (12.18) has dynamics on multiple timescales even when $\hbar = 1$. As $\hbar = 1$ in our simulations, the size of Planck's constant also does not affect our numerical results. The disparity of scales we seek to describe is due to the difference in size between the nuclear mass M and the electronic mass m_0. Consequently, we let $\hbar = 1$ without loss of generality.

In our numerical simulations, $M = 10m_0$. However, typical molecular systems have mass ratios M/m_0 of roughly 10^4 or 10^5,[7, 154] as an electron's rest mass is $m_e \approx 9.1094 \times 10^{-31}$ kg and the mass of a single neutron is about $M_n \approx 1.675 \times 10^{-27}$ kg.[105] Thus, by using more realistic values for the nuclear and electronic masses, the difference in ease of chaotic onset in the classical and quantum *dof* becomes even more pronounced than what we observed numerically.

We derived in Chapter 2 the following estimate for the frequency (and energy, since $\hbar = 1$) of nuclear oscillations:[7, 154]

$$\omega_N \approx \frac{1}{m_0 a^2}\sqrt{\frac{m_0}{M}}. \tag{13.1}$$

The energy of the electronic excitation is about

$$\omega_e \approx \frac{1}{2m_0 a^2}, \tag{13.2}$$

which is larger by a factor of

$$\mathcal{O}\left(\sqrt{\frac{M}{m_0}}\right) \sim \sqrt{10000} = 100. \tag{13.3}$$

As this division of speeds is built into the Born-Oppenheimer approximation, the phenomenon discussed in this chapter pertains to any system derived from such a scheme (and hence to most semiquantum systems).

More generally, this signature of semiquantum chaos represents a particular facet of nonadiabatic dynamics, so any system that exhibits coupling between *dof* that evolve on different timescales is expected to exhibit different facilities of chaotic onset in its fast and slow *dof* (assuming it is not constrained to be integrable).

The nuclear dynamics of vibrating quantum billiards are determined by $\dot{a}_j$ and $\dot{P}_j$ (where j represents the jth nuclear *dof*), whereas the electronic dynamics are described by the dynamical equations for the quantum phase and action or via Bloch variables.[154, 160, 189] To illustrate the phenomenon of interest, consider a two-term superposition of a quantum billiard with $s = 1$ nuclear *dof*.

With $\hbar = 1$, the equations of motion (12.18) become

$$\begin{aligned}
\dot{a} &= \frac{P}{M} + \frac{2\mu_{12}\sqrt{n(1-n)}}{Ma}\sin(\theta), \\
\dot{P} &= -\frac{\partial V}{\partial a} + \frac{2}{a^3}[(1-n)\epsilon_1 + n\epsilon_2] \\
&\quad + \frac{2\mu_{12}P}{Ma^2}\sqrt{n(1-n)}\sin(\theta) + \frac{4\mu_{12}^2}{Ma^3}n(1-n)\sin^2(\theta), \\
\dot{n} &= -\frac{2\mu_{12}P}{Ma}\sqrt{n(1-n)}\cos(\theta) - \frac{2\mu_{12}^2}{Ma^2}n(1-n)\sin(2\theta), \\
\dot{\theta} &= \frac{\epsilon_2 - \epsilon_1}{a^2} + \frac{\mu_{12}P}{Ma}\frac{(1-2n)}{\sqrt{n(1-n)}}\sin(\theta) + \frac{2\mu_{12}^2}{Ma^2}(1-2n)\sin^2(\theta).
\end{aligned} \tag{13.4}$$

When the interaction strength μ_{12} is small, the largest terms in the right-hand-sides of $\dot{a}$ and $\dot{P}$ are those present in the integrable configuration (when $\mu_{12} = 0$). In this event, the classical dynamics of (13.4) are influenced significantly more by the nuclear *dof* than by the electronic *dof*. However, every term in the right-hand-side of $\dot{n}$ is proportional to at least one power of μ_{12}, so small coupling *cannot* be neglected in the quantum dynamics even when its contribution to the classical dynamics is negligible. Thus, a smaller coupling strength is required to significantly influence the quantum dynamics of (13.4) than is necessary to influence its classical dynamics substantially. In particular, this implies that if one perturbs the coupling strength μ_{12} from zero–$\mu_{12} = 0$ guarantees integrable dynamics–it follows that chaotic onset in the quantum *dof* requires weaker interactions than chaotic onset in the classical *dof*.

To examine this phenomenon, one compares the interaction terms to P/M in the $\dot{a}$ equation of motion in (13.4) and to $\partial V/\partial a$ and $\partial K/\partial a$ in the $\dot{P}$ equation. Thus, the nuclear displacement a is most affected by an increase in electronic coupling when the conjugate momentum P is small. More precisely, it is requisite that

$$\mathcal{O}(P) \lesssim \mathcal{O}\left(\frac{1}{a}\right) \tag{13.5}$$

for an $\mathcal{O}(1)$ electronic coupling μ_{12} to significantly influence the classical displacement (provided the phase θ is not too small). For an $\mathcal{O}(1)$ electronic coupling to heavily influence the nuclear momentum (again assuming that θ is not too small), either

$$\mathcal{O}\left(-\frac{\partial V}{\partial a} - \frac{\partial K}{\partial a}\right) \lesssim \mathcal{O}\left(\frac{P}{Ma^2}\right) \tag{13.6}$$

or

$$\mathcal{O}\left(-\frac{\partial V}{\partial a} - \frac{\partial K}{\partial a}\right) \lesssim \mathcal{O}\left(\frac{1}{Ma^3}\right) \tag{13.7}$$

must hold. The interaction terms in the $\dot{P}$ equation of (13.4) are proportional to $1/M$, whereas the other terms are independent of M. Condition (13.6) is ordinarily more restrictive than (13.7) when the nuclear displacement a is small (especially if P is also small), and the reverse is the case when a is large (especially if the momentum P is also large).

One decomposes the adiabatic Hamiltonian (12.16) into (integrable) diagonal terms and (perturbative) cross terms as follows:

$$\begin{aligned} H &= H_0 + \bar{H}_1, \\ H_0 &= \frac{P^2}{2M} + V(a) + K, \\ \bar{H}_1 &= \frac{2\hbar\mu_{12}P}{Ma}\sqrt{n(1-n)}\sin\theta + \frac{2\hbar^2\mu_{12}^2 n(1-n)}{Ma^2}\sin^2(\theta). \end{aligned} \tag{13.8}$$

The electronic kinetic energy K and the nuclear kinetic energy $P^2/2M$ are non-negative. The external potential $V(a)$ is also non-negative if it is a polynomial in $(a-a_0)^2$, as is the case with the symmetric harmonic potential discussed in several previous chapters.[112, 155, 157–160] When $V \geq 0$, it is also true that $H_0 \geq 0$, so associated with the energy manifold $H = E_H$ is a condition guaranteeing boundedness of the perturbation term $\bar{H}_1$:

$$\bar{H}_1 \leq E_H. \tag{13.9}$$

As the time-evolution of the quantum action n is due entirely to the interaction terms (i.e., $\bar{H}_1$), it follows that the fast dynamics of (12.16) are bounded in magnitude. Thus, every trajectory visits only regions of phase space in which the perturbation $\bar{H}_1$ is at most some finite value. In particular, one cannot reach the entirety of phase space for any given energy E_H (no matter how large).

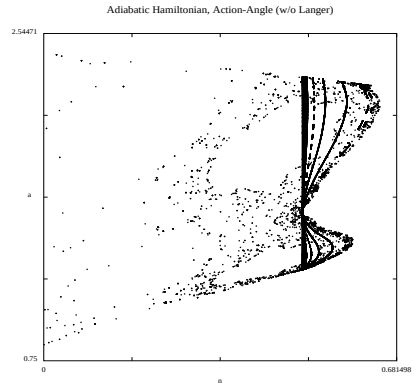

Figure 13.1: This plot depicts several $\theta = 0$ Poincaré cuts projected into the (n, a)-plane. They correspond to the interaction strengths $\mu_{12} = 0$, 0.01, 0.02, 0.05, 0.1, 0.25, 0.5, 1, 1.5, 1.6, and 1.75.

13.3 Numerical Simulations

To study chaotic onset numerically, we utilize $\theta = 0$ Poincaré sections. The perturbation term $\bar{H}_1$ vanishes when $\theta = 0$, so

$$H(\theta = 0) = H_0(\theta = 0) = E_H. \tag{13.10}$$

As the energy E_H is independent of the cross terms, it is also independent of the coupling strength μ_{12}. Hence, it is convenient for the present discussion to tune μ_{12} by gradually increasing its value from zero in examining the departure of (12.16) from integrability.

In general, coupling constants μ_{jk} are determined by the geometry of quantum billiards as well as which eigenstates are included in the superposition state (5.20).[159, 160] Thus, although we manipulate μ_{12} mathematically, a given coupling coefficient is actually a physical constant. The parameter μ_{jk} measures the strength of the interaction between the jth and kth eigenstates.

We show numerically that as μ_{12} is increased, the quantum *dof* become globally chaotic significantly sooner than do the classical *dof*. One can also show

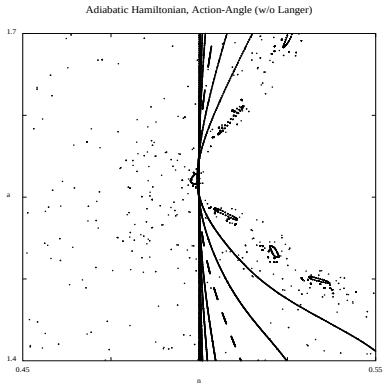

Figure 13.2: This plot shows a magnification of Figure 13.1.

this by making the electronic coupling increasingly negative, although because the term of order $\mathcal{O}(\mu_{12}^2)$ is proportional to $\sin^2(\theta)$, it is more difficult to examine the phenomenon of interest in this manner using the Hamiltonian (12.16). Note additionally that by KAM theory, even the classical *dof* become locally chaotic as soon as μ_{12} is increased from zero.[67, 70, 114, 194]

Solving for the momentum, one obtains

$$P = \pm\sqrt{2M\left[E_H - V(a) - K\right]}. \tag{13.11}$$

To find real values for P, it is necessary that the energy $E_H \geq E > 0$. In our simulations, we use $M = 10$, $\hbar = 1$, $V_0 = 5$, $a_0 = 1.25$, $\epsilon_1 = \pi^2/2$, and $\epsilon_2 = 2\pi^2$. With these values,

$$P(t=0) = \pm 2\sqrt{5\left(E_H - 5\left[a(0) - 1.25\right]^2 - \frac{\pi^2}{2\left[a(0)\right]^2}\left[1 + 2n(0)\right]\right)}. \tag{13.12}$$

To determine $P(t=0)$, one needs to specify $a(0)$ and $n(0)$. Let $\theta(0) = 0$ in order to compute the energy E_H independently of μ_{12}. For simplicity, also let $a(0) = 1.25 = a_0$. This yields

$$P(0) = \pm\frac{2}{5}\sqrt{125E_H - 8\pi^2\left[1 + 2n(0)\right]}. \tag{13.13}$$

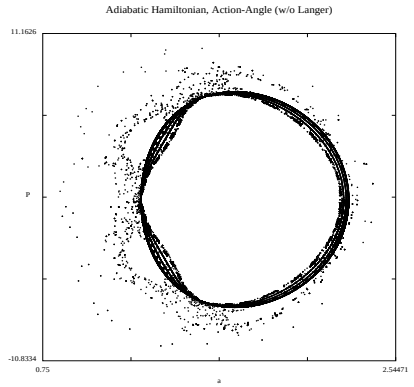

Figure 13.3: This plot depicts the $\theta = 0$ Poincaré sections from Figure 13.1 projected into the (a, P)-plane.

If the initial superposition contains an equal probability of the two states under consideration (i.e., if $n(0) = 0.5$), the equation (13.13) simplifies to

$$P(0) = \pm\frac{2}{5}\sqrt{125E_H - 16\pi^2}. \tag{13.14}$$

If the initial momentum $P(0) = 0$, then the energy is $E_H = 16\pi^2/125 \approx 1.2633094$. Consequently,

$$H(t=0) = H_0(t=0) = \frac{8(\epsilon_1 + \epsilon_2)}{25} = \frac{16\pi^2}{125} = E_H. \tag{13.15}$$

Increasing E_H corresponds to increasing the magnitude of the initial momentum.

Figure 13.1 displays $\theta = 0$ Poincaré sections projected into the (n, a)-plane for trajectories corresponding to interaction strengths $\mu_{12} = 0$, 0.01, 0.02, 0.05, 0.1, 0.25, 0.5, 1, 1.5, 1.6, and 1.75. The $\mu_{12} = 0$ trajectory yields integrable dynamics. As one increases the coupling strength, however, the trajectories become increasingly bowed, which indicates that the quantum action n encompasses a wider range of values. The behavior of the displacement, however, does not change very much. Figure 13.2 shows a magnification of a portion of Figure 13.1. Figure 13.3 shows the same Poincaré section projected into the (a, P)-plane. As μ_{12}

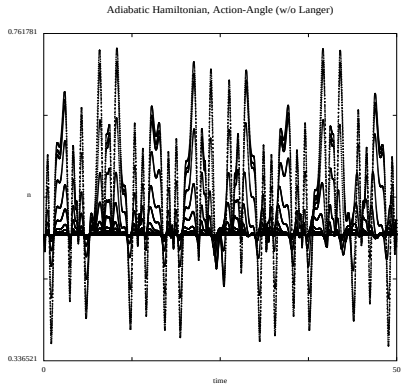

Figure 13.4: This plot shows time series up to $t = 50$ of the quantum action $n(t)$ for the initial conditions and interaction strengths used in Figure 13.1.

increases, the classical dynamics change slowly from integrable to near-integrable until finally reaching a state of global chaos. The only globally chaotic trajectory that is depicted corresponds to the parameter value $\mu_{12} = 1.75$. The local chaos becomes increasingly evident as one increases μ_{12}. It is extremely difficult or impossible to observe for very small μ_{12}, but by KAM theory it is present for any nonzero coupling.[67, 163, 194]

To accentuate our point, we examine time series for $n(t)$ (see Figure 13.4) and $a(t)$ (see Figure 13.5) for each interaction strength depicted in prior plots. The time series for the quantum action (and hence for the quantum probabilities) is extremely erratic for all nonzero couplings. For smaller μ_{12}, this chaotic behavior–though quite evident–occurs over a smaller range of n. That is, the quantum dynamics are not necessarily more chaotic for larger electronic coupling; rather, the range of quantum probabilities that can be achieved is larger. The story is rather different for the nuclear displacement $a(t)$, however, as there are no substantial changes in the dynamics until the coupling strength becomes of order $\mathcal{O}(1)$. Even then, the chaotic behavior in a is not evident in the time series. One must examine

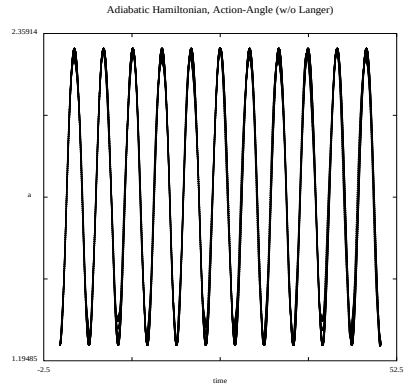

Figure 13.5: This plot shows time series up to $t = 50$ of the nuclear displacement $a(t)$ for the initial conditions and interaction strengths used in Figure 13.1.

stroboscopic maps of phase space to observe it clearly.

One can generalize the analysis in this chapter to superpositions with $d \geq 3$ states. In this situation, each pair of eigenstates has a corresponding interaction coefficient (see Chapter 9).[160] Thus, one can separately examine increases in coupling strength between any pair of eigenstates. One can thereby examine individually the various modes of excitation corresponding to these interactions.

APPENDIX A

GENERALIZED BLOCH COORDINATES*

One way to transform the quantum-mechanical subsystem of a d-mode Galërkin expansion to real variables is to use *generalized Bloch coordinates.* For $k < l$, define

$$\begin{aligned} x_{kl} &\equiv \rho_{kl} + \rho_{lk}, \\ y_{kl} &\equiv i(\rho_{lk} - \rho_{kl}), \\ z_{kl} &\equiv \rho_{ll} - \rho_{kk}, \end{aligned} \tag{A.1}$$

where $\rho_{kj} = A_k^* A_j$. This yields $3\binom{d}{2} = 3d!/(2 \cdot (d-2)!)$ variables, of which $[2(d-1)]$ are independent. (This corresponds to the $(d-1)$ quantum-mechanical *dof* obtained from a d-mode Galërkin expansion.)

Equations (A.1) satisfy the constraint

$$\sum_{k,l=1,k<l}^{d} \left[\alpha \left(x_{kl}^2 + y_{kl}^2\right) + z_{kl}^2\right] = \beta, \tag{A.2}$$

where $\alpha = d/2$ and $\beta = d - 1$. Additionally,

$$z_{kl} \equiv \rho_{ll} - \rho_{kk} = (\rho_{ll} - \rho_{jj}) + (\rho_{jj} - \rho_{kk}) \equiv z_{kj} + z_{jl}. \tag{A.3}$$

Applying (A.3) recursively then implies that

$$z_{k,k+s} = z_{k,k+1} + \cdots z_{k+s-1,k+s}. \tag{A.4}$$

It is easier to derive the additional constraints after d has been specified. When $d = 4$, for example, the final six constraints are derived from the six equations

$$x_{ij}^2 + y_{ij}^2 + z_{ij}^2 = \left[1 - |A_k|^2 - |A_l|^2\right]^2, \tag{A.5}$$

*This chapter is based on portions of reference [160].

where i, j, k, and l are distinct indices in $\{1,2,3,4\}$. Three of these equations take the form

$$\sqrt{x_{ij}^2+y_{ij}^2+z_{ij}^2}+\sqrt{x_{kl}^2+y_{kl}^2+z_{kl}^2}=1, \tag{A.6}$$

where all the indices are again distinct. (One then applies equation (A.4).) The other three equations are

$$\begin{aligned}
-\sqrt{x_{12}^2+y_{12}^2+z_{12}^2}+\sqrt{x_{34}^2+y_{34}^2+z_{34}^2} &= z_{14}+z_{23}=z_{12}+2z_{23}+z_{34},\\
-\sqrt{x_{13}^2+y_{13}^2+z_{13}^2}+\sqrt{x_{24}^2+y_{24}^2+z_{24}^2} &= z_{12}+z_{34},\\
-\sqrt{x_{14}^2+y_{14}^2+z_{14}^2}+\sqrt{x_{23}^2+y_{23}^2+z_{23}^2} &= z_{12}-z_{34},
\end{aligned} \tag{A.7}$$

where one again utilizes equation (A.4).

Bloch variables can also be defined using a Lie group formulation.[160, 199] With this procedure, one can show that $d=2$ yields Pauli spin matrices and $d=3$ yields Gell-Mann matrices.[38, 150] The special cases $d=2$ and $d=3$ are considered, respectively, in Chapters 7 and Chapter 8. The case $d=1$, which is discussed in Chapter 6, yields zero quantum-mechanical *dof*.

REFERENCES

[1] Ralph Abraham, Jerrold E. Marsden, and Tudor Ratiu. *Manifolds, Tensor Analysis, and Applications*. Number 75 in Applied Mathematical Sciences. Springer-Verlag, New York, NY, 2nd edition, 1988.

[2] L. Allen and J. H. Eberly. *Optical Resonance and Two-Level Atoms*. Dover Publications, Inc., New York, NY, 1987.

[3] Vladimir I. Arnold. *Geometrical Methods in the Theory of Ordinary Differential Equations*. Number 250 in A Series of Comprehensive Studies in Mathematics. Springer-Verlag, New York, NY, 2nd edition, 1988.

[4] R. Badrinarayanan and Jorge V. José. Spectral properties of a Fermi accelerating disk. *Physica D*, 83:1–29, 1995.

[5] Leslie E. Ballentine. Is semiquantum chaos real? *Physical Review E*, 63(056204):1–7, April 2001.

[6] Armelle Barelli, Jean Bellissard, Philippe Jacquod, and Dima L. Shepelyanksy. Two interacting Hofstadter butterflies. *Physical Review B*, 55(15):9524–9533, April 1997.

[7] Gordon Baym. *Lectures on Quantum Mechanics*. Lecture Notes and Supplements in Physics. Perseus Books, Reading, Massachusetts, 1990.

[8] Carl M. Bender and Steven A. Orszag. *Advanced Mathematical Methods for Scientists and Engineers*. McGraw-Hill, New York, NY, 1978.

[9] Sergio Benenti. Separability structures on Riemannian manifolds. In *Differential Geometrical Methods in Mathematical Physics: Proceedings, Aix-en-Provence and Salamanca 1979*, number 836 in Lecture Notes in Mathematics, pages 512–538, New York, NY, 1980. Springer-Verlag.

[10] Francesco Benvenuto, Giulio Casati, and Dima L. Shepelyansky. Chaos in a quasiclassical hadronic atom. *Physical Review A*, 53(2):737–743, February 1996.

[11] G. P. Berman, E. N. Bulgakov, and G. M. Zaslavsky. Quantum chaos of atoms in a resonant cavity. *Chaos*, 2(2):257–265, 1992.

[12] M. J. Berry, J. A. Katine, R. M. Westervelt, and A. C. Gossard. Influence of shape on electron transport in ballistic quantum dots. *Physical Review B*, 50(23):17721–17724, December 1994.

[13] Michael V. Berry. Quantizing a classically ergodic system: Sinai's billiard and the KKR method. *Annals of Physics*, 131(1):163–216, January 1981.

[14] Michael V. Berry. Regularity and chaos in classical mechanics, illustrated by three deformations of a circular billiard. *European Journal of Physics*, 2:91–102, 1981.

[15] Michael V. Berry. Quantal phase factors accompanying adiabatic changes. *Procedures of the Royal Society of London A*, 392:45–57, 1984.

[16] Michael V. Berry and J. P. Keating. The Riemann zeros and eigenvalue asymptotics. *SIAM Review*, 41(2):236–266, 1999.

[17] Michael V. Berry and J. M. Robbins. Chaotic classical and half-classical adiabatic reactions: geometric magnetism and deterministic friction. *Procedures of the Royal Society of London A*, 442:659–672, 1993.

[18] Michael V. Berry and M. Wilkinson. Diabolical points in the spectra of triangles. *Procedures of the Royal Society of London A*, 392:15–43, 1984.

[19] Isaac B. Bersuker. Modern aspects of the Jahn-Teller effect theory and applications to molecular problems. *Chemical Reviews*, 101:1067–1114, 2001.

[20] Isaac B. Bersuker and Victor Z. Polinger. *Vibronic Interactions in Molecules and Crystals*. Number 49 in Springer Series in Chemical Physics. Springer-Verlag, New York, NY, 1989.

[21] Misha Bialy. Convex billiards and a theorem by E. Hopf. *Mathematische Zeitschrift*, 214(1):147–154, 1993.

[22] Reinhold Blümel and B. Esser. Quantum chaos in the Born-Oppenheimer approximation. *Physical Review Letters*, 72(23):3658–3661, 1994.

[23] Reinhold Blümel and W. P. Reinhardt. *Chaos in Atomic Physics*. Cambridge University Press, Cambridge, England, 1997.

[24] Fausto Borgonovi and Dima L. Shepelyansky. Particle propogation in a random and quasi-periodic potential. *Physica D*, 109:24–31, 1997.

[25] Aurel Bulgac. Level crossings, adiabatic approximation, and beyond. *Physical Review Letters*, 67(8):965–967, August 1991.

[26] Leonid A. Bunimovich and Jan Rehacek. Nowhere dispersing 3d billiards with non-vanishing Lyapunov exponents. *Communications in Mathematical Physics*, 189:729–757, March 1997.

[27] Eugene Butkov. *Mathematical Physics*. Addison-Wesley Publishing Company, Reading, MA, 1968.

[28] Giulio Casati and Boris Chirikov. *Quantum Chaos*. Cambridge, New York, NY, 1995.

[29] Giulio Casati, Italo Guarneri, and Dima L. Shepelyanksy. Anderson transition in a one-dimensional system with three incommensurate frequencies. *Physical Review Letters*, 62(4):345–348, January 1989.

[30] Giulio Casati and Tomaž Prosen. Mixing property of triangular billiards. *Physical Review Letters*, 83(23):4729–4732, December 1999.

[31] Giulio Casati (Ed.). *Chaotic Behavior in Quantum Systems*. Plenum, New York, NY, 1985.

[32] Alan R. Champneys, Yuri A. Kuznetsov, and Björn Sandstede. A numerical toolbox for homoclinic bifurcation analysis. *International Journal of Bifurcation and Chaos*, 6(5):867–887, 1996.

[33] Alan R. Champneys and Yuri A. Kuznetsov. Numerical detection and continuation of codimension-two homoclinic bifurcations. *International Journal of Bifurcation and Chaos*, 4(4):785–822, 1994.

[34] Boris V. Chirikov, Felix M. Izrailev, and Dima L. Shepelyanksy. Quantum chaos - localization vs ergodicity. *Physica D*, 33:77–88, October-November 1988.

[35] Doron Cohen. Chaos and energy spreading for time-dependent Hamiltonians, and the various regimes in the theory of quantum dissipation. *Annals of Physics*, 283:175–231, 2000.

[36] D. F. Coker and L. Xiao. Methods for molecular dynamics with nonadiabatic transitions. *Journal of Chemical Physics*, 102(1):496–510, January 1995.

[37] Eli Comay. Interrelations between the neutron's magnetic interactions and the magnetic Aharonov-Bohm effect. *Physical Review A*, 62(042102), 2000.

[38] J. F. Cornwell. *Group Theory in Physics*, volume 2. Harcourt Brace Jovanovich, Publishers, London, England, 1984.

[39] Richard Courant and David Hilbert. *Methods of Mathematical Physics*, volume 1. Interscience Publishers, Inc., New York, NY, 1953.

[40] Michael C. Cross and Pierre C. Hohenberg. Pattern formation outside equilibrium. *Reviews of Modern Physics*, 65(3):851–1112, July 1993.

[41] Predrag Cvitanović, Roberto Artuso, Ronnie Mainieri, Gregor Tanner, and Gábor Vattay. *Classical and Quantum Chaos*, volume Version 7.0.1. Niels Bohr Institute, August 2000. *www.nbi.dk/ChaosBook/*.

[42] Robert L. Devaney. *An Introduction to Chaotic Dynamical Systems.* Addison-Wesley, Redwood City, CA, 2nd edition, 1989.

[43] Florin Diacu and Philip Holmes. *Celestial Encounters: The Origins of Chaos and Stability.* Princeton University Press, Princeton, NJ, 1996.

[44] Joseph Diggins, J. F. Ralph, T. P. Spiller, T. D. Clark, H. Prance, and R. J. Prance. Chaotic dynamics in the rf superconducting quantum-interference-device magnetometer: A coupled quantum-classical system. *Physical Review E*, 49(3):1854–1859, March 1994.

[45] Manfredo P. do Carmo. *Differential Geometry of Curves and Surfaces.* Prentice-Hall, Englewood Cliffs, NJ, 1976.

[46] Manfredo P. do Carmo. *Riemannian Geometry.* Birkhäuser, Boston, MA, 1992.

[47] Eusebius J. Doedel, Alan R. Champneys, Thomas F. Fairgrieve, Yuri A. Kuznetsov, Björn Sandstede, and Xianjun Wang. *AUTO 97: Continuation and Bifurcation Software for Ordinary Differential Equations (with HomCont)*, March 1998.

[48] Eusebius J. Doedel, Mark J. Friedman, and Anand C. Monteiro. On locating homoclinic and heteroclinic orbits. Technical report, Center for Applied Mathematics, Cornell University, June 1993.

[49] Holger R. Dullin, Peter H. Richter, and Andreas Wittek. A two-parameter study of the extent of chaos in a billiard system. *Chaos*, 6(1):43–58, 1996.

[50] David S. Dummit and Richard M. Foote. *Abstract Algebra*. Prentice Hall, Englewood Cliffs, NJ, 1991.

[51] J.-P. Eckmann and David Ruelle. Ergodic theory of chaos and strange attractors. *Reviews of Modern Physics*, 57(3):617–656, July 1985.

[52] Robert Eisberg and Robert Resnick. *Quantum Physics of Atoms, Molecules, Solids, Nuclei, and Particles*. John Wiley and Sons, New York, NY, 2nd edition, 1985.

[53] Richard P. Feynman. Forces in molecules. *Physical Review*, 56:340–343, August 1939.

[54] Richard P. Feynman, Robert B. Leighton, and Matthew Sands. *The Feynman Lectures on Physics*, volume I. Addison-Wesley Publishing Company, Reading, MA, 1964.

[55] Richard P. Feynman, Robert B. Leighton, and Matthew Sands. *The Feynman Lectures on Physics*, volume III. Addison-Wesley Publishing Company, Reading, MA, 1964.

[56] Richard P. Feynman, Robert B. Leighton, and Matthew Sands. *The Feynman Lectures on Physics*, volume II. Addison-Wesley Publishing Company, Reading, MA, 1964.

[57] Joseph Ford and Matthias Ilg. Eigenfunctions, eigenvalues, and time evolution of finite, bounded, undriven, quantum systems are not chaotic. *Physical Review A*, 45(9):6165–6173, May 1992.

[58] Joseph Ford and Giorgio Mantica. Does quantum mechanics obey the correspondence principle? Is it complete? *American Journal of Physics*, 60(12):1086–1098, December 1992.

[59] E. Freire, L. Pizarro, and Alejandro J. Rodríguez-Luis. Numerical continuation of homoclinic orbits to non-hyperbolic equilibria in planar systems. Preprint, 1999.

[60] Avner Friedman. Free boundary problems in science and technology. *Notices of the American Mathematical Society*, 47(8):854–861, September 2000.

[61] A. Fuhrer, S. Lüscher, T. Ihn, T. Heinzel, K. Ensslin, W. Wegscheider, and M. Bichler. Energy spectra of quantum rings. *Nature*, 413:822–825, October 2001.

[62] William Fulton. *Algebraic Topology: A First Course*. Number 153 in Graduate Texts in Mathematics. Springer-Verlag, New York, NY, 1995.

[63] James Gleick. *Chaos: Making a New Science*. Penguin USA, New York, NY, 1988.

[64] Herbert Goldstein. *Classical Mechanics*. Addison-Wesley Publishing Company, Reading, MA, 2nd edition, 1980.

[65] A. Góngora-T, Jorge V. José, S. Schaffner, and P. H. E. Tiesinga. Quantum and classical solutions for a free particle in wedge billiards. *Physics Letters A*, 274:117–122, September 2000.

[66] Kurt Gottfried. *Quantum Mechanics*, volume I: Fundamentals of *Advanced Book Classics*. Addison-Wesley Publishing Company, Reading, Massachusetts, 1966.

[67] John Guckenheimer and Philip Holmes. *Nonlinear Oscillations, Dynamical Systems, and Bifurcations of Vector Fields*. Number 42 in Applied Mathematical Sciences. Springer-Verlag, New York, NY, 1983.

[68] John Guckenheimer, B. A. Meloon, M. R. Myers, F. J. Wicklin, and P. A. Worfolk. *DsTool: A Dynamical Systems Toolkit with an Interactive Graphical Interface: User's Manual*. Center for Applied Mathematics, Cornell University, Ithaca, NY, December 1997. Version Tk Draft.

[69] Martin C. Gutzwiller. Periodic orbits and classical quantization conditions. *Journal of Mathematical Physics*, 12:343–358, 1971.

[70] Martin C. Gutzwiller. *Chaos in Classical and Quantum Mechanics*. Number 1 in Interdisciplinary Applied Mathematics. Springer-Verlag, New York, NY, 1990.

[71] Fritz Haake. *Quantum Signatures of Chaos*. Springer Series in Synergetics. Springer-Verlag, Berlin, Germany, 2nd edition, 2001.

[72] Jack Hale and Hüseyin Koçak. *Dynamics and Bifurcation*. Number 3 in Texts in Applied Mathematics. Springer-Verlag, New York, NY, 1991.

[73] Rachel W. Hall and Krešimir Josić. The mathematics of musical instruments. *The American Mathematical Monthly*, 108(4):347–357, April 2001.

[74] György Haller. *Chaos Near Resonance*. Number 138 in Applied Mathematical Sciences. Springer-Verlag, New York, NY, 1999.

[75] Serge Haroche. Cavity quantum electrodynamics. In J. Dalibard, J.-M. Raimond, and J. Zinn-Justin, editors, *Fundamental Systems in Quantum Optics*, pages 767–940. Elsevier Science Publishers B. V., 1992.

[76] Eric J. Heller. The many faces of tunneling. *Journal of Physical Chemistry A*, 103:10433–10444, November 1999.

[77] Eric J. Heller. Quantum physics: Air juggling and other tricks. *Nature*, 412:33–34, July 5th, 2001.

[78] Michael F. Herman and Robert Currier. A justification for the use of the Langer modification in Miller's classic analog method of non-adiabatic scattering. *Chemical Physics Letters*, 114(4):411–414, March 1985.

[79] G. Herzberg and H. C. Longuet-Higgins. Intersection of potential energy surfaces in polyatomic molecules. *Discussions of the Faraday Society*, 35:77–82, 1963.

[80] Arthur Hobson. Ergodic properties of a particle moving elastically inside a polygon. *Journal of Mathematical Physics*, 16(11):2210–2214, November 1975.

[81] Mark H. Holmes. *Introduction to Perturbation Methods*. Number 20 in Texts in Applied Mathematics. Springer-Verlag, New York, NY, 1995.

[82] Philip J. Holmes and Jerrold E. Marsden. Melnikov's method and Arnold diffusion for perturbations of integrable Hamiltonian systems. *Journal of Mathematical Physics*, 23(4):669–675, April 1982.

[83] Edward Lindsay Ince. *Ordinary Differential Equations*. Dover Publications, Inc., New York, NY, 1956.

[84] Teturo Inui, Yukito Tanabe, and Yositaka Onodera. *Group Theory and Its Applications in Physics*. Number 78 in Solid-State Sciences. Springer-Verlag, Berlin, Germany, 1990.

[85] Christopher Jarzynski. Thermalization of a brownian particle via coupling to low-dimensional chaos. *Physical Review Letters*, 74(15):2937–2940, April 1995.

[86] Fritz John. *Partial Differential Equations*. Number 1 in Applied Mathematical Sciences. Springer-Verlag, New York, NY, 4th edition, 1982.

[87] Claes Johnson. *Numerical Solution of Partial Differential Equations by the Finite Element Method*. Cambridge University Press, Cambridge, England, 1987.

[88] Anatole Katok and Boris Hasselblatt. *Introduction to the Modern Theory of Dynamical Systems*. Cambridge University Press, New York, NY, 1995.

[89] Charles Kittel and Herbert Kroemer. *Thermal Physics*. W. H. Freeman and Company, New York, NY, 2nd edition, 1980.

[90] Leo Kouwenhoven. Bouncing a C_{60} ball. *Nature*, 407:35–36, September 2000.

[91] Leo Kouwenhoven and Charles Marcus. Quantum dots. *Physics World*, pages 35–39, June 1998.

[92] H. A. Kramers. über das modell des helium atoms. *Z. Phys.*, 13:312–341, 1923.

[93] A. Kudrolli and S. Sridhar. Experiments on quantum chaos using microwave cavities: Results for the pseudo-integrable L-billiard. *Pramana - Journal of Physics*, 48(2):459–467, February 1997.

[94] David M. Leitner and Peter G. Wolynes. Many-dimensional quantum energy flow at low energy. *Physical Review Letters*, 76(2):216–219, January 1996.

[95] David M. Leitner and Peter G. Wolynes. Vibrational relxation and energy localization in polyatomics: Effects of high-order resonances on flow rates and the quantum ergodicity transition. *Journal of Chemical Physics*, 105(24):11226–11236, December 1996.

[96] David M. Leitner and Peter G. Wolynes. Predictions of local random matrix theory for vibrational mixing and energy flow in polyatomics. *ACH-Models in Chemistry*, 134(5):663–677, 1997.

[97] David M. Leitner and Peter G. Wolynes. Quantization of the stochastic pump model of Arnold diffusion. *Physical Review Letters*, 79(1):55–58, July 1997.

[98] Wenjie Liang, Marc Bockrath, Dolores Bozovic, Jason H. Hafner, M. Tinkham, and Hongkun Park. Fabry-Perot interference in a nanotube electron waveguide. *Nature*, 411:665–669, June 7th 2001.

[99] Richard L. Liboff. Bohr correspondence principle for large quantum numbers. *Foundations of Physics*, 5(2):271–293, 1975.

[100] Richard L. Liboff. The correspondence principle revisited. *Physics Today*, 37(2):50–55, 1984.

[101] Richard L. Liboff. Circular-sector quantum-billiard and allied configurations. *Journal of Mathematical Physics*, 35(5):2218–2228, May 1994.

[102] Richard L. Liboff. The polygon quantum-billiard problem. *Journal of Mathematical Physics*, 35(2):596–607, February 1994.

[103] Richard L. Liboff. Function mixing hypothesis and quantum chaos. *Physica D*, pages 137–142, 1996.

[104] Richard L. Liboff. Maxwell's demon and the second law of thermodynamics. *Foundations of Physics Letters*, 10(1):89–92, 1997.

[105] Richard L. Liboff. *Introductory Quantum Mechanics*. Addison-Wesley, San Francisco, CA, 3rd edition, 1998.

[106] Richard L. Liboff. *Kinetic Theory: Classical, Quantum, and Relativistic Descriptions*. Wiley, New York, NY, 2nd edition, 1998.

[107] Richard L. Liboff. Many faces of the Helmholtz equation. *Physics Essays*, 12:1–8, 1999.

[108] Richard L. Liboff. Quantum billiard chaos. *Physics Letters*, A269:230–233, 2000.

[109] Richard L. Liboff and Joseph Greenberg. The hexagon quantum billiard. *Journal of Statistical Physics*, 105(1/2):389–402, October 2001.

[110] Richard L. Liboff and Jack Liu. The Sinai billiard, square torus, and field chaos. *Chaos*, 10(4):756–759, December 2000.

[111] Richard L. Liboff, Isaiah Nebenzahl, and Hans H. Fleischmann. On the radial momentum operator. *American Journal of Physics*, 41:976–979, August 1973.

[112] Richard L. Liboff and Mason A. Porter. Quantum chaos for the radially vibrating spherical billiard. *Chaos*, 10(2):366–370, 2000.

[113] Richard L. Liboff and Michael Wong. Quasi-chaotic property of the prime-number sequence. *International Journal of Theoretical Physics*, 37:3109–3117, 1998.

[114] Allan J. Lichtenberg and M. A. Lieberman. *Regular and Chaotic Dynamics*. Number 38 in Applied Mathematical Sciences. Springer-Verlag, New York, NY, 2nd edition, 1992.

[115] Pierre Lochak. Arnold diffusion; a compendium of remarks and questions. In Carles Simó, editor, *Hamiltonian Systems with Three or More Degrees of Freedom*, number 533 in NATO ASI Series C: Mathematical and Physical Sciences, pages 168–183, Dordrecht, The Netherlands, 1999. Kluwer Academic Publishers. S'Agaró, Spain: June 19-30, 1995.

[116] V. Lopac, I. Mrkonjić, and D. Radić. Chaotic behavior in lemon-shaped billiards with elliptical and hyperbolic boundary arcs. *Physical Review E*, 64(016214):1–8, June 2001.

[117] A. Loskutov, A. B. Ryabov, and L. G. Akinshin. Properties of some chaotic billiards with time-dependent boundaries. *Journal of Physics A: Math and General*, 33:7972–7986, 2000.

[118] J Lucan. *Quantum Dots*. Springer, New York, NY, 1998.

[119] Steven W. MacDonald and Allan N. Kaufman. Spectrum and eigenfunctions for a Hamiltonian with stochastic trajectories. *Physical Review Letters*, 42(18):1189–1191, April 1979.

[120] Steven W. MacDonald and Allan N. Kaufman. Wave chaos in the stadium: Statistical properties of short-wave solutions of the Helmholtz equation. *Physical Review A*, 37:3067, 1988.

[121] Lawrence E. Malvern. *Introduction to the Mechanics of a Continuous Medium*. Series in Engineering of the Physical Sciences. Prentice-Hall, Inc., Englewood Cliffs, New Jersey, 1969.

[122] Paul Manneville. *Dissipative Structures and Weak Turbulence*. Perspectives in Physics. Academic Press, Inc., San Diego, CA, 1990.

[123] Robert S. Manning. *Semiclassical Propagation for Non-Cartesian Variables*. PhD thesis, Cornell University, 1994. Center for Applied Mathematics.

[124] Giorgio Mantica. Quantum algorithmic integrability: The metaphor of classical polygonal billiards. *Physical Review E*, 61(6):6434–6443, June 2000.

[125] Charles M. Marcus, S. R. Patel, A. G. Huibers, S. M. Cronenwett, M. Switkes, I. H. Chan, R. M. Clarke, J. A. Folk, S. F. Godijn, K. Campman, and A. C. Gossard. Quantum chaos in open versus closed quantum dots: Signatures of interacting particles. *Chaos, Solitons, and Fractals*, 8(7-8):1261–1279, July/August 1997.

[126] Robert S. Markiewicz. Chaos in a Jahn-Teller molecule. *Physical Review E*, 64(026216):1–5, August 2001.

[127] Jerrold E. Marsden and Michael J. Hoffman. *Elementary Classical Analysis*. W. H. Freeman and Company, New York, NY, 2nd edition, 1993.

[128] Jerrold E. Marsden and Tudor S. Ratiu. *Introduction to Mechanics and Symmetry*. Number 17 in Texts in Applied Mathematics. Springer-Verlag, New York, NY, second edition, 1999.

[129] Craig C. Martens and Arnaldo Donoso. Semiclassical multistate Liouville dynamics in the adiabatic representation. *Journal of Chemical Physics*, 112(9):3980–3989, March 2000.

[130] Teresa Martínez-Seara Alonso, 2001. Private Communication.

[131] William S. Massey. *Algebraic Topology: An Introduction*. Number 56 in Graduate Texts in Mathematics. Springer-Verlag, New York, NY, 1967.

[132] Carver A. Mead. Electronic spin-orbit interaction and the molecular Aharonov-Bohm effect. *Chemical Physics*, 49(1):33–38, 1980.

[133] Carver A. Mead. The molecular Aharonov-Bohm effect in bound-states. *Chemical Physics*, 49(1):23–32, 1980.

[134] Carver Alden Mead. The geometric phase in molecular systems. *Reviews of Modern Physics*, 64(1):51–85, January 1992.

[135] Madhu Menon, Ernst Richter, and K. R. Subbaswamy. Structural and vibrational properties of fullerenes and nanotubes in a nonorthogonal tight-binding scheme. *Journal of Chemical Physics*, 104(15):5875–5882, April 1996.

[136] Eugen Merzbacher. *Quantum Mechanics*. John Wiley and Sons, Inc., New York, NY, 3rd edition, 1998.

[137] Hans-Dieter Meyer and William H. Miller. A classical analog for electronic degrees of freedom in nonadiabatic collision processes. *Journal of Chemical Physics*, 70(7):3214–3223, April 1979.

[138] William H. Miller. Classical-limit quantum mechanics and the theory of molecular collisions. *Advances in Chemical Physics*, 25:69–177, 1974.

[139] William H. Miller. Classical S-matrix in molecular collisions. *Advances in Chemical Physics*, 30:77–136, 1975.

[140] Nicolai Minorsky. *Nonlinear Oscillations*. Krieger Pub., Malabar, FL, 1983.

[141] B. Mirbach and Giulio Casati. Transition from quantum ergodicity to adiabaticity: Dynamical localization in an amplitude modulated pendulum. *Physical Review Letters*, 83(7):1327–1330, August 1999.

[142] Parry Moon and Domina Eberle Spencer. *Field Theory Handbook*. Springer-Verlag, Berlin, Germany, 2nd edition, 1988.

[143] F. L. Moore, J. C. Robinson, C. F. Bharucha, Bala Sundaram, and M. G. Raizen. Atom optics realization of the quantum δ-kicked rotor. *Physical Review Letters*, 75(25):4598–4601, December 1995.

[144] Thomas Papenbrock. Numerical study of a three-dimensional generalized stadium billiard. *Physical Review E*, 61(4):4626–4628, April 2000.

[145] Hongkun Park, Jiwoong Park, Andrew K. Lim, Erik H. Anderson, A. Paul Alivisatos, and Paul L. McEuen. Nanomechanical oscillations in a single C_{60} transistor. *Nature*, 407:57–60, September 2000.

[146] M. Hossein Partovi. Absence of sensitivity to initial conditions in quantum dynamics. *Physical Review A*, 45(2):R555–R558, January 1992.

[147] Philip Pechukas. Time-dependent semiclassical scattering theory. i. potential scattering. *Physical Review*, 181(1):166–174, May 1969.

[148] Philip Pechukas. Time-dependent semiclassical scattering theory. ii. atomic collisions. *Physical Review*, 181(1):174–184, May 1969.

[149] Asher Peres. Chaotic evolution in quantum mechanics. *Physical Review E*, 53(5):4524–4527, May 1996.

[150] Michael E. Peskin and Daniel V. Schroeder. *An Introduction to Quantum Field Theory*. Perseus Books, Cambridge, Massachusetts, 1995.

[151] Pierre M. Petroff, Axel Lorke, and Atac Imamoglu. Epitaxially self-assembled quantum dots. *Physics Today*, 54(5):46–52, May 2001.

[152] Mark A. Pinsky. The eigenvalues of an equilateral triangle. *SIAM Journal on Mathematical Analysis*, 5:819–827, September 1980.

[153] Brendan B. Plapp, David A. Egolf, and Eberhard Bodenschatz. Dynamics and selection of giant spirals in Rayleigh-Bénard convection. *Physical Review Letters*, 81(24):5334–5337, December 1998.

[154] Mason A. Porter. Nonadiabatic dynamics in semiquantal physics. *Reports on Progress in Physics*, 64(9):1165–1190, September 2001.

[155] Mason A. Porter and Richard L. Liboff. Bifurcations in one degree-of-vibration quantum billiards. *International Journal of Bifurcation and Chaos*, 11(4):903–911, April 2001.

[156] Mason A. Porter and Richard L. Liboff. Chaos on the quantum scale. *American Scientist*, 89(6):532–537, November-December 2001.

[157] Mason A. Porter and Richard L. Liboff. Quantum chaos for the vibrating rectangular billiard. *International Journal of Bifurcation and Chaos*, 11(9):2317–2337, September 2001.

[158] Mason A. Porter and Richard L. Liboff. The radially vibrating spherical quantum billiard. *Discrete and Continuous Dynamical Systems*, pages 310–318, 2001. Proceedings of the Third International Conference: "Dynamical Systems and Differential Equations", Kennesaw State University: Georgia, May 2000.

[159] Mason A. Porter and Richard L. Liboff. Vibrating quantum billiards on Riemannian manifolds. *International Journal of Bifurcation and Chaos*, 11(9):2305–2315, September 2001.

[160] Mason A. Porter and Richard L. Liboff. A Galërkin approach to electronic near-degeneracies in molecular systems. *Physica D*, 2002. To Appear.

[161] William H. Press, Brian P. Flannery, Saul A. Teukolsky, and William T. Vetterling. *Numerical Recipes: The Art of Scientific Computing.* Cambridge University Press, New York, NY, 1986.

[162] Edward W. Purcell. *Electricity and Magnetism*, volume 2 of *Berkeley Physics Course.* McGraw-Hill, Inc., New York, NY, 2nd edition, 1985.

[163] Richard H. Rand. *Topics in Nonlinear Dynamics with Computer Algebra*, volume 1 of *Computation in Education: Mathematics, Science and Engineering.* Gordon and Breach Science Publishers, USA, 1994.

[164] Richard H. Rand. Lecture notes on nonlinear vibrations. Unpublished, Version 34, 2000.

[165] Richard H. Rand and W. L. Keith. Dynamics of a system exhibiting the global bifurcation of a limit-cycle at infinity. *International Journal of Non-Linear Mechanics*, 20(4):325–338, 1985.

[166] Suhan Ree and Linda E. Reichl. Classical and quantum chaos in a circular billiard with a straight cut. *Physical Review E*, 60(2):1607–1615, August 1999.

[167] P. J. Richens and Michael V. Berry. Pseudointegrable systems in classical and quantum mechanics. *Physica*, 2D:495–512, 1981.

[168] Richard W. Robinett. Periodic orbit theory analysis of a continuous family of quasi-circular billiards. *Journal of Mathematical Physics*, 39(1):278–298, January 1998.

[169] Richard W. Robinett. Isolated versus nonisolated periodic orbits in variants of the two-dimensional square and circular billiards. *Journal of Mathematical Physics*, 40(1):101–122, January 1999.

[170] Richard W. Robinett. Periodic orbit theory analysis of the circular disk or annular billiard: Nonclassical effects and the distribution of energy eigenvalues. *American Journal of Physics*, 67(1):67–77, January 1999.

[171] Joseph Rotman. *An Introduction to Algebraic Topology.* Number 119 in Graduate Texts in Mathematics. Springer-Verlag, New York, NY, 1988.

[172] Walter Rudin. *Real & Complex Analysis.* McGraw-Hill, Inc., New York, NY, 3rd edition, 1987.

[173] Walter Rudin. *Functional Analysis.* International Series in Pure and Applied Mathematics. McGraw-Hill, Inc., Boston Massachusetts, second edition, 1991.

[174] Jun John Sakurai. *Modern Quantum Mechanics.* Addison-Wesley Publishing Company, Reading, MA, Revised edition, 1994.

[175] Manfred Schroeder. *Fractals, Chaos, Power Laws: Minutes from an Infinite Paradise.* W. H. Freeman and Company, New York, NY, 1991.

[176] Dima L. Shepelyanksy and A. Douglas Stone. Chaotic Landau level mixing in classical and quantum wells. *Physical Review Letters*, 74(11):2098–2101, March 1995.

[177] F. Simmel and M. Eckert. Statistical measures for eigenfunctions of nonseparable quantum billiard systems. *Physica D*, 97:517–530, 1996.

[178] George F. Simmons. *Differential Equations with Applications and Historical Notes*. McGraw-Hill, Inc., New York, NY, 2nd edition, 1991.

[179] B. Space and D. F. Coker. Nonadiabatic dynamics of excited excess electrons in simple fluids. *Journal of Chemical Physics*, 94(3):1976–1984, February 1991.

[180] B. Space and D. F. Coker. Dynamics of trapping and localization of excess electrons in simple fluids. *Journal of Chemical Physics*, 96(1):652–663, January 1992.

[181] Michael Spivak. *A Comprehensive Introduction to Differential Geometry*, volume One. Publish or Perish, Inc., Houston, Texas, third edition, 1999.

[182] Gilbert Strang. *Linear Algebra and its Applications*. Harcourt Brace Jovanovich College Publishers, Orlando, FL, 3rd edition, 1988.

[183] Steven H. Strogatz. *Nonlinear Dynamics and Chaos*. Addison-Wesley, Reading, MA, 1994.

[184] Catherine Sulem and Pierre-Louis Sulem. *The Nonlinear Schrödinger Equation: Self-Focusing and Wave Collapse*. Number 139 in Applied Mathematical Sciences. Springer-Verlag, New York, NY, 1999.

[185] Bobby G. Sumpter and Donald W. Noid. The onset of instability in nanostructures: The role of nonlinear resonance. *Journal of Chemical Physics*, 102(16):6619–6622, April 1995.

[186] Roger Temam. *Infinite-Dimensional Dynamical Systems in Mechanics and Physics*. Number 68 in Applied Mathematical Sciences. Springer-Verlag, New York, NY, 2nd edition, 1997.

[187] Daniel Walgraef. *Spatio-Temporal Pattern Formation*. Partially Ordered Systems. Springer-Verlag, New York, NY, 1997.

[188] Frank W. Warner. *Foundations of Differentiable Manifolds and Lie Groups*. Number 94 in Graduate Texts in Mathematics. Springer-Verlag, New York, NY, 1983.

[189] Rober L. Whetten, Gregory S. Ezra, and Edward R. Grant. Molecular dynamics beyond the adiabatic approximation: New experiments and theory. *Annual Reviews of Physical Chemistry*, 36:277–320, 1985.

[190] Carter T. White and Tchavdar N. Todorov. Quantum electronics: Nanotubes go ballistic. *Nature*, 411:649–651, June 7th 2001.

[191] Gerald B. Whitham. *Linear and Nonlinear Waves*. Pure and Applied Mathematics. Wiley-Interscience, New York, NY, 1974.

[192] Jan Wiersig. Singular continuous spectra in a pseudointegrable billiard. *Physical Review E*, 62(1):R21–R24, July 2000.

[193] Jan Wiersig. Quantum-classical correspondence in polygonal billiards. *Physical Review E*, 64(026212):1–8, July 2001.

[194] Stephen Wiggins. *Introduction to Applied Nonlinear Dynamical Systems and Chaos*. Number 2 in Texts in Applied Mathematics. Springer-Verlag, New York, NY, 1990.

[195] Alan Wolf, J. B. Swift, Harry L. Swinney, and J. A. Vastano. Determining Lyapunov exponents from a time series. *Physica D*, 16:285–317, 1985.

[196] S Wong. *Introductory Nuclear Physics*. Prentice Hall, Englewood Cliffs, NJ, 1990.

[197] Boris I. Yakobson and Richard E. Smalley. Fullerene nanotubes: $C_{1,000,000}$ and beyond. *American Scientist*, 85(4):324–337, July-August 1997.

[198] Oleg Zaitsev, R. Narevich, and R. E. Prange. Quasiclassical Born-Oppenheimer approximations. *Foundations of Physics*, 31(1):7–26, 2001.

[199] Paolo Zanardi. Quantum cloning in d dimensions. *Physical Review A*, 58(5):3484–3490, November 1998.

[200] H Zaren, K Vahala, and A Yariv. Gain spectra of quantum wires with inhomogeneous broadening. *IEEE Journal of Quantum Electronics*, 25:705, 1989.

[201] Wojciech Hubert Zurek. Sub-Planck structure in phase space and its relevance for quantum decoherence. *Nature*, 412:712–717, August 16 2001.

[202] Josef W. Zwanziger, Edward R. Grant, and Gregory S. Ezra. Semiclassical quantization of a classical analog for the Jahn-Teller E $\times$ e system. *Journal of Chemical Physics*, 85(4):2089–2098, August 1986.

[203] Josef W. Zwanziger, M. Koenig, and A. Pines. Berry's phase. *Annual Reviews of Physical Chemistry*, 41:601–646, 1990.

[204] Daniel Zwillinger (Ed.). *Handbook of Differential Equations*. Academic Press, San Diego, CA, 2nd edition, 1992.

[205] Daniel Zwillinger (Ed.). *Standard Mathematical Tables and Formulae*. CRC Press, Inc., Boca Raton, FL, 30th edition, 1996.